PHYSIOLOGICAL CONSEQUENCES OF COMPARTMENTALIZED GLYCEROLIPID SYNTHESIS

Daniel Earl Cooper

A dissertation submitted to the faculty of the University of North Carolina at Chapel Hill in partial fulfillment of the requirements for the degree of Doctor of Philosophy in the Department of Nutrition in the Gillings School of Global Public Health.

Chapel Hill
2015

Approved by:

Rosalind A. Coleman

Eric L. Klett

Liza Makowski Hayes

P. Kay Lund

Stephen D. Hursting

ABSTRACT

Daniel Earl Cooper: Physiological Consequences of Compartmentalized Glycerolipid Synthesis
(Under the direction of Rosalind A. Coleman)

The metabolic derangements present in type 2 diabetes are associated with the accumulation of triacylglycerol (TAG) in adipose and non-adipose tissues. However, the mechanisms whereby TAG accumulation drives pathogenesis remain obscure. The synthesis of TAG and other glycerolipids is initiated by the rate-limiting enzyme, glycerol-3-phosphate acyltransferase (GPAT), which catalyzes the esterification of an acyl-CoA to the sn-1 position of the glycerol-3-phosphate backbone. Four mammalian GPAT isoforms, each the product of a separate gene, have been discovered and recent evidence suggests that each GPAT isoform performs a unique function in directing glycerolipid synthesis. To test this hypothesis, we investigated the role of different GPAT isoforms in liver and brown adipose lipid metabolism, and adipocyte differentiation. First, we compared the unique functions of the major hepatic GPAT isoforms, GPAT1 and GPAT4. Although these isoforms contribute a similar amount of total GPAT activity in liver, GPAT1, but not GPAT4, was required for the incorporation of *de novo* synthesized fatty acids (FA) into TAG and to divert FA away from β-oxidation. Next, we elucidated the mechanism whereby mice lacking GPAT4 are protected from diet-induced obesity. GPAT4 is a major GPAT isoform in BAT, comprising approximately 65% of the total GPAT activity. In primary brown adipocytes lacking

GPAT4 exogenous oleate was oxidized at a 46% higher rate than controls, suggesting that *Gpat4*$^{-/-}$ mice are protected from diet-induced obesity because GPAT4 in brown adipose tissue is required to limit the oxidation of exogenous FA. Finally, we provide evidence that the lipodystrophy-associated protein Seipin is an evolutionarily conserved regulator of GPAT activity. Seipin and its yeast ortholog, Fld1, physically interacted with GPAT and the loss of Seipin was associated with increased GPAT activity because GPAT had a higher affinity for one of its substrates, glycerol-3-phosphate. Seipin deficiency impairs adipogenesis and alters lipid droplet morphology and in 3T3L1 preadipocytes, GPAT overexpression recapitulated these effects, suggesting that increased GPAT activity is the underlying cause of the impaired adipogenesis and altered lipid droplet morphology. Taken together, these results suggest that the functions of each GPAT isoform are linked to specific physiological processes and that glycerolipid synthesis is highly compartmentalized.

To Mom, Ashley, and Clark: Thank you for always being there to help me loosen up and providing a good laugh. I couldn't have done this without you. Knowing that I had so much support from you allowed me to push forward even when I might not have wanted to. I love you all.

To my love, Jessye Brick: You have been so patient with me throughout this entire process. I cannot thank you enough. I appreciate how much you have done to help me remain positive throughout everything. Thank you for continuing to help me grow and never tiring of my scientific conversations.

ACKNOWLEDGEMENTS

To my mentor, Rosalind: Thank you for all of your time, effort, and support. I am forever grateful for the lessons you shared. Thank you for always pushing me to get better.

PREFACE

In addition to the work conducted as a part of this dissertation, I have co-authored a total of 7 published papers, which are included here:

1. Wendel AA*, **Cooper DE***, Ilkayeva OR, Muoio DM, Coleman RA. Glycerol-3-phosphate acyltransferase (GPAT)-1, but not GPAT4, incorporates newly synthesized fatty acids into triacylglycerol and diminishes fatty acid oxidation. *J Biol Chem*. 2013 Sep 20; 288(38): 27299-306. *co-first authors. PMID: 23908354

2. Zhang C, **Cooper DE**, Grevengoed T, Li LO, Klett EL, Eaton JM, Harris TE, Coleman RA. Glycerol-3-phosphate acyltransferase-4 deficient mice are protected from diet-induced insulin resistance by the enhanced association of mTOR and rictor. *Am J Physiol-Endoc M*. 2014 Aug 1; 307(3): E305-15. PMID: 24939733

3. Zhang C, Hwarng G, **Cooper DE**, Grevengoed TJ, Eaton JM, Natarajan V, Harris TE, and Coleman RA. Inhibited insulin signaling in mouse hepatocytes is associated with increased phosphatidic acid but not diacylglycerol. *J Biol Chem.* 2015 Feb 6; 290(6): 3519-28. PMID: 25512376

4. Schisler JC, Grevengoed TJ, Pascual F, **Cooper DE**, Ellis JM, Paul DS, Willis MS, Patterson C, Jia W, Coleman RA. Cardiac energy dependence on glucose increases metabolites related to glutathione and activates metabolic genes controlled by mTOR. *J Am Heart Assoc.* 2015 Feb 24; 4(2)

5. **Cooper DE**, Grevengoed T, Klett EL, and Coleman, RA. Glycerol-3-phosphate acyltransferase (GPAT)-4 regulates fatty acid-induced thermogenesis in brown adipose tissue. *J Biol Chem*. Submitted March 4, 2015. Accepted with revision.

6. Grevengoed TJ, **Cooper DE**, Ellis JM, and Coleman RA. Loss of ACSL1 impairs mitochondrial dynamics by changing cardiac metabolism. *FASEB J.* Submitted March 18, 2015. Accepted with revision.

7. Grevengoed TJ, Martin SM, Katunga L, **Cooper DE**, Anderson EJ, Murphy RC, Coleman RA. ACSL1 activates fatty acids for phospholipid formation and remodeling in heart. *J Lipid Res*. Submitted April 8th, 2015.

TABLE OF CONTENTS

LIST OF TABLES

LIST OF FIGURES

LIST OF ABBREVIATIONS

TAG	Triacylglycerol
PL	Phospholipid
GPAT	Glycerol-3-phosphate acyltransferase
BAT	Brown adipose tissue
LPA	Lysophosphatidic acid
PA	Phosphatidic acid
DAG	Diacylglycerol
AGPAT	1-acylglycerol-3-phosphate acyltransferase
PAP	Phosphatidic acid phosphohydrolase
DGAT	Diacylglycerol acyltransferase
ACSL	Acyl-CoA synthetase, long-chain
CPT	CDP-choline:diacylglycerol choline phosphotransferase
EPT	CDP-ethanolamine:diacylglycerol ethanolamine phosphotransferase
ER	Endoplasmic reticulum
SREBP1c	Sterol regulatory element binding protein 1c
NEM	*N*-ethylmaleimide
LD	Lipid droplet
OMM	Outer mitochondrial membrane
PPAR	Peroxisome proliferator-activated receptor
MGAT	Monoacylglycerol acyltransferase
C/EBP	CCAAT/enhancer binding protein
PKC	Protein kinase C

mTORC	Mammalian target of rapamycin
IRS1/2	Insulin receptor substrate 1/2
FA	Fatty acid
Ser	Serine
Thr	Threonine
DIO	Diet-induced obesity
CGL	Congenital generalized lipodystrophy
FPL	Familial partial lipodystrophy
BSCL2	Berardinelli-Seip congenital lipodystrophy-2
CAV1	Caveolin-1
ANOVA	Analysis of variance
mRNA	messenger ribonucleic acid
ASM	Acid soluble metabolites
CPT1	Carnitine-palmitoyl transferase-1
PGC1α	Peroxisome proliferator-activated receptor gamma co-activator 1
CTE1	Cytosolic thioesterase-1
UCP1	Uncoupling protein-1
AMPK	Adenosine monophosphate-activated kinase
LXR	Liver X receptor
VLDL	Very low density lipoprotein
cDNA	complimentary deoxyribonucleic acid
RT-PCR	Real-time polymerase chain reaction
RT	Room temperature

TCA	Tricarboxylic acid
DPM	Disintegrations per minute
PBS	Phosphate-buffered saline
BSA	Bovine serum albumin
DMEM	Dulbecco’s modified eagle medium
FBS	Fetal bovine serum
NCS	Newborn calf serum
WT	Wild type

CHAPTER I: INTRODUCTION

The worldwide prevalence of obesity has reached epidemic proportions and in the US alone, the treatment costs of obesity-associated co-morbidities comprise 10% of total health care expenditures (1-3). The metabolic syndrome, encompassing a set of conditions including obesity, insulin resistance, cardiovascular disease, and hyperlipidemia, is highly associated with the accumulation of excess triacylglycerol (TAG) in liver, skeletal muscle, and adipose tissue (4). Despite this association, little is known about the regulation of TAG synthesis in response to changes in dietary composition or nutritional status. Thus, understanding the basic mechanisms of TAG synthesis under different physiological conditions may provide insight into the relationship between metabolic disease and TAG accumulation.

The initial and rate-limiting step in the synthesis of TAG and phospholipids is catalyzed by glycerol-3-phosphate acyltransferase (GPAT; EC 2.3.1.15). GPAT esterifies a fatty acyl-CoA to the sn-1 position of a glycerol-3-phosphate backbone to produce lysophosphatidic acid. Four mammalian GPAT isoforms, each the product of a separate gene, have been discovered and differ in their subcellular location, response to nutritional stimuli, substrate preference, and tissue expression pattern. Although the presence of four distinct enzymes that catalyze the same biochemical reaction appears redundant, a growing body of evidence supports the hypothesis that each GPAT isoform performs a unique function in glycerolipid synthesis.

Consistent with this hypothesis, mice with deleted GPATs express vastly different phenotypes. GPAT1-deficient mice are protected from diet-induced hepatic steatosis and insulin resistance, have increased hepatic fatty acid oxidation, and are protected from diethylnitrosamine-induced hepatocellular carcinoma (5-8). Although a mouse model deficient in GPAT2 has not been reported, its expression in testis suggests a function for GPAT2 in that tissue (9). GPAT3 is highly expressed in adipose tissue, comprising approximately 80% of the total GPAT activity in that tissue, however, *Gpat3*$^{-/-}$ mice are not lipodystrophic and, when fed a high-fat diet, gain weight normally (10,11). GPAT4 is highly expressed in liver and BAT, comprising approximately 45% and 65% of the total GPAT activity, respectively (12). GPAT4 is also highly expressed in mammary gland, where its deficiency prevents normal mammary gland development and decreases milk TAG and DAG content (13). Mice lacking GPAT4 are protected from diet-induced obesity and insulin resistance (14). In addition, *Gpat4*$^{-/-}$ mice lack a subdermal adipose tissue layer, and their metabolic rate was 5% higher than controls (15). Vergnes et al. attributed the metabolic phenotype to the lack of subdermal adipose tissue; however, it remains unclear whether the lack of subdermal adipose tissue was the cause of or an adaptation to a higher metabolic rate. Because each GPAT isoform catalyzes the same enzymatic reaction, it is likely that many of the phenotypic differences in GPAT-null animals are due to differences in subcellular location, nutritional regulation, or tissue expression patterns.

The focus of this dissertation is to investigate how these differences in GPAT isozymes result in unique functions within a physiological context. In chapter III, we

investigate the unique functions of the major hepatic GPAT isoforms, GPAT1 and GPAT4. Results from this study provide evidence that GPAT1, but not GPAT4, is required for the incorporation of *de novo* synthesized fatty acids into TAG and to divert fatty acids away from β-oxidation. The purpose of Chapter IV is to elucidate the mechanism whereby mice lacking GPAT4 are protected from diet-induced obesity. Findings from this study suggest that *Gpat4*$^{-/-}$ mice are protected from diet-induced obesity because GPAT4 in brown adipose tissue is required to limit the oxidation of exogenous fatty acids. Preliminary findings in Chapter V suggest that the microsomal GPATs are regulated by an ER-protein, Seipin, and that this interaction is conserved from yeast to mammalian tissues. The loss of Seipin increased GPAT activity because in the absence of Seipin, GPAT had a higher affinity for one of its substrates, glycerol-3-phosphate. This study is the first to identify a protein that directly interacts with GPAT to alter its activity. Taken together, these results provide indirect evidence suggesting that pathways of glycerolipid synthesis are highly compartmentalized and that this compartmentalization is an important mechanism for responding to physiological stimuli.

CHAPTER II: BACKGROUND

The compartmentalized metabolism hypothesis

Meeting the complex physiological demands of mammalian life requires strict control of fatty acyl-CoA metabolism. Acyl-CoA synthetases must activate fatty acids to form acyl-CoAs before they can be used for energy production in mitochondria and peroxisomes, stored as triacylglycerol, cholesterol esters, and retinol esters in lipid droplets, esterified to form membrane phospholipids, or activate transcription factors and signaling pathways. Indirect evidence suggests that acyl-CoAs do not wander freely within cells, but instead, are channeled into specific downstream pathways.

Intracellular signaling cascades are typically depicted as a series of protein-protein interactions that act as scaffolds to bridge two intracellular compartments or span across membrane bilayers. In contrast, metabolic pathways are presented as a linear sequence of steps occurring in a virtually empty cytosolic space. In reality, the cytosol is a dense non-homogeneous network of proteins and metabolites fighting for space (16). Considered in this view, several potential mechanisms might mediate the flux of metabolites among and between intracellular compartments. First, metabolic enzymes are likely found in complexes; either arranged very close together or directly interacting. Second, in response to various physiological stimuli membrane-organelles might reorganize to permit interaction of enzymes from different organelles. Third, selective movement of enzymes from one membrane to another, similar to that of TAG

synthetic enzymes moving from the ER to the leaflet of lipid droplets, may aid in compartmentalization. Before we can investigate these mechanisms, further work is required to understand the relationship between various metabolic enzymes and the physiological processes they mediate. The focus of this dissertation is to understand the physiological consequences of compartmentalized glycerolipid synthesis.

The Kennedy Pathway for glycerolipid synthesis

One predominant pathway whereby acyl-CoAs are metabolized is in the synthesis of complex lipids. Although initially thought to be a random process, recent evidence suggests that glycerolipid synthetic enzymes influence the flux of acyl-CoAs to specific fates within the cell. During the early 1950s and 60s, Eugene Kennedy and colleagues identified a series of enzymatic steps required for the synthesis of glycerol-containing lipids, including triacylglycerol and phospholipids (PL). The initial and rate-limiting step in the synthesis of TAG and PL is performed by glycerol-3-phosphate acyltransferase (GPAT), and this enzyme catalyzes the addition of an acyl-CoA to the *sn*-1 position of glycerol-3-phosphate to form lysophosphatidic acid (LPA) (17). The esterification of a second acyl-CoA at the *sn*-2 position of LPA, catalyzed by acylglycerol-3-phosphate acyltransferase (AGPAT), results in the formation of phosphatidic acid (PA). Subsequent dephosphorylation of PA by Lipin/phosphatidic acid phosphohydrolase (PAP) and the esterification of a third acyl-CoA by diacylglycerol acyltransferase (DGAT) culminates in the formation of TAG. Alternatively, diacylglycerol can be used in the formation of phosphatidylethanolamine and

phosphatidylcholine by the enzymes CDP-ethanolamine phosphotransferase and CDP-choline phosphotransferase, respectively (**Fig 2.1**) (18).

Since these initial discoveries, further work has elucidated a number of distinct isozymes for each step in the Kennedy Pathway. Thus, the number of enzymes and diverse set of glycerolipid products suggests the need for a complex regulatory network to meet the demands of individual cells, tissues, and whole organisms. Because it possesses the lowest enzymatic activity of Kennedy Pathway enzymes, GPAT is positioned at a key regulatory point in the flux of acyl-CoAs and glycerol-3-phosphate toward glycerolipids.

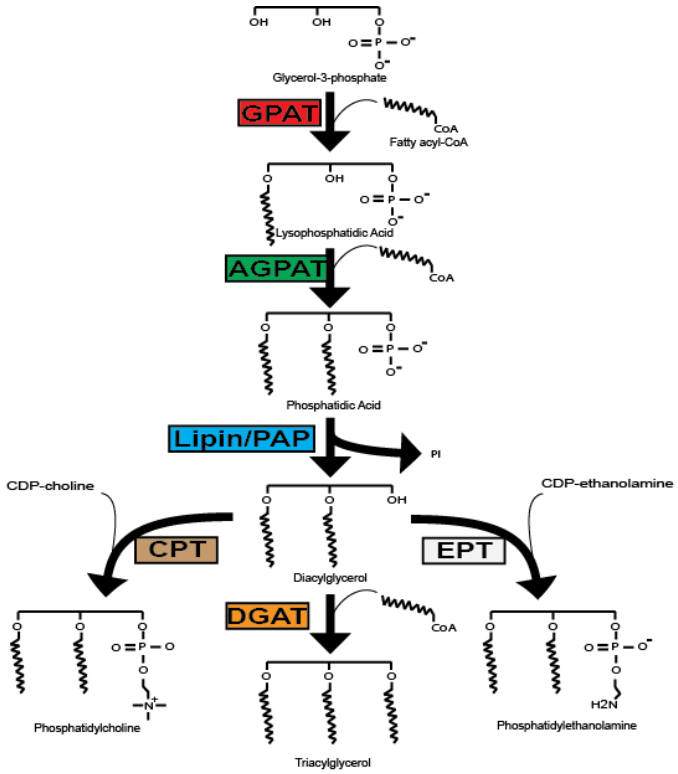

Figure 2.1 The Kennedy Pathway for glycerolipid synthesis. GPAT, glycerol-3-phosphate acyltransferase; AGPAT, 1-acylglycerol-3-phosphate acyltransferase; PAP, phosphatidic acid phosphohydrolase; DGAT, diacylglycerol acyltransferase; CPT, CDP-Choline:diacylglycerol cholinephosphotransferase; EPT, CDP-Ethanolamine:diacylglycerol ethanolaminephosphotransferase.

GPATs are members of the acyltransferase family of enzymes

Four mammalian GPAT isoforms, each the product of a separate gene, have been discovered and identified as members of the pfam 01553 family of glycerolipid acyltransferases. The GPAT proteins possess two transmembrane domains, four conserved acyltransferase motifs, and their active sites face the cytosol (19) (**Fig 2.2**). The mutagenesis of invariant residues within these motifs confirmed that these regions are required for the activity of *Escherichia coli* (*E. Coli*) GPAT and mouse GPAT1 (20,21). In *E. coli*, the invariant histidine and aspartate in motif I, glycine in motif III, and proline in motif IV are essential for catalysis. The invariant phenylalanine and arginine in motif II and glutamate and serine in motif III are essential for glycerol-3-phosphate binding (**Table 2.1**). In murine GPAT1, Arg-318 is required for maximal GPAT catalysis (21). Leading to their initial identification as AGPAT isoforms, both microsomal GPAT isoforms, GPAT3 and GPAT4, possess a fifth motif, similar to that in AGPAT1 and -2. However, subsequent studies confirmed that GPAT3 and 4 possess GPAT activity and, thus, were reclassified as GPATs (10,12,22).

Figure 2.2: Acyltransferase motifs, active site, and predicted transmembrane domains of murine GPAT isoforms. Black bars indicate active site. Yellow bars represent acyltransferase motifs. Dark blue illustrates the transmembrane domains.

Although these acyltransferase motifs are highly conserved from *E. coli* to rodents, the presence of four distinct GPAT isoforms is only observed in vertebrates (23). Comparative genomic and phylogenetic analyses have suggested that small-scale duplication events in vertebrates are responsible for the divergence of GPAT1 and GPAT2 as well as splits for GPAT3 and GPAT4 (23). In support of the hypothesis that GPAT isozymes perform distinct functions, previous work in genetics suggests that compared to whole-genome duplications, small-scale duplication events support a greater likelihood for novel functions (24).

Table 2.1: Acyltransferase homology blocks[a]

	Block I	Block II	Block III	Block IV	Accession[b]
GPAT	303[c]	348	382	417	
E. coli	VPC**HRS**HM**D**YLLL	**G**AF**FIR**R	Y**F**V**EGGR**SRT**G**R	ITLI**P**IYI	130326
H. influenza	VPC**HRS**HM**D**YLLL	**G**AF**FIR**R	Y**F**V**EGGR**SRT**G**R	ISIV**P**VYV	1172533
M. turberculosis	AFS**HRS**YL**D**GMLL	**G**AI**FIR**R	WSI**EGGR**TRT**G**K	VYLV**P**TSI	2791522
C. elegans	ICL**HRS**HL**D**ILSM	NTI**FIR**R	F**FLEGTR**SRF**G**K	ISII**P**VVF	1458332
M. musculus	LPV**HRS**HI**D**YLLL	**G**GF**FIR**R	I**FLEGTR**SRS**G**K	ILVI**P**VGI	2498786
R. norvegicus	LPV**HRS**HI**D**YLLL	**G**GF**FIR**R	I**FLEGTR**SRS**G**K	ILVI**P**VGI	2444459
GPAT consensus	φ--**HRS**-φ**D**φφ--	**G**–φ**FIR**R	φ**F**φ**EGTR**SR-**G**K	φφφφ**P**φφφ	

[a]Blocks of homology were identified on the basis of amino acid alignments using the CLUSTAWL algorithm. [b]Accession numbers are for the National Center for Biotechnology Information Protein Database. [c]Numbers indicate the amino acid residue number at the beginning of each block in *E. coli* GPAT.

GPAT isoform subcellular location, tissue distribution, nutritional regulation, and acyl-CoA preference

GPAT1

GPAT1 is the best-characterized GPAT isoform. GPAT1 is primarily localized to the outer mitochondrial membrane (**Fig 2.3**), possesses two transmembrane domains, and its active site faces the cytosol (25,26). Murine GPAT1 contains 828 aa, nearly

twice the size of GPAT3 and 4, and the extra C-terminal region of GPAT1 interacts with the active site region and is required for activity (27). The role of this C-terminal tail in cells or whole animals has not been further investigated.

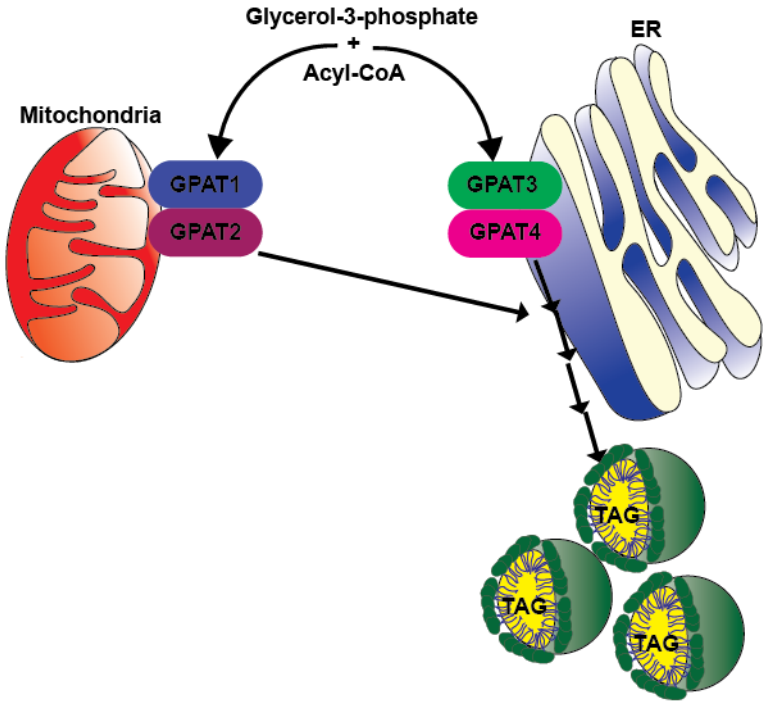

Figure 2.3: GPAT isozyme subcellular location. GPAT1 and GPAT2 are localized to the outer mitochondrial membrane whereas GPAT3 and GPAT4 are located on the endoplasmic reticulum.

In rodents, GPAT1 is most highly expressed in the liver, where it comprises between 20-50% of the total GPAT activity (5). In other tissues, GPAT1 is responsible for approximately 10% of the total GPAT activity (28). Following a 48 h fast, GPAT1 protein and activity in liver and adipose tissue are reduced 30-50% and when refed with a high sucrose diet for 24 h both protein amount and activity overshoot fed-state levels by 30-60% (29). Consistent with its regulation in response to nutrient status, AMP-activated kinase, active under conditions of low energy, was suggested to

phosphorylate GPAT1 and inhibit its activity (30). GPAT1 possesses a strong preference for saturated acyl-CoA and its activity is resistant to inhibition by sulfhydryl reagents (18,31). Based upon its high activity for saturated acyl-CoAs and the observation that the *sn*-1 position of most phospholipids contains saturated fatty acids, it is inferred that GPAT possesses an *sn*-1 preference for esterification of an acyl-CoA to the glycerol-3-phosphate backbone. It should also be noted that the acyl-CoA preference for GPAT has not been directly compared, but inferred based upon the high proportion of saturated fatty acids in the *sn*-1 position. Confirming a functional regulation of GPAT1 by sterol regulatory element binding protein 1c (SREBP1c), GPAT1 deficiency in *ob/ob* mice did not restore insulin sensitivity, but did prevent hepatic steatosis (32). Consistent with these findings, in HepG2 cells, SREBP1c dramatically increased GPAT1 promoter activity, suggesting that GPAT1 is a key element in the SREBP1c-mediated increase in lipogenesis (33).

GPAT2

GPAT2 is located on the outer mitochondrial membrane, possesses two transmembrane domains and its N and C-terminal regions face the cytosol (34). GPAT2 is most highly expressed in spermatic germ cells and GPAT2 overexpression in CHO-K1 cells increased the incorporation of [1-14C]arachidonate into TAG, suggesting a preference for 20:4-CoA as an acyl donor (9). Consistent with a role for GPAT2 in arachidonyl-CoA metabolism, GPAT2 overexpression increases GPAT and AGPAT activity 2-fold when arachidonyl-CoA is used as the acyl donor, suggesting that GPAT2 might be able to acylate both glycerol-3-phosphate and lysophosphatidic acid. In

contrast, when other saturated or unsaturated acyl donors are used, GPAT2 overexpression does not change GPAT activity (9). GPAT2 has been identified as a cancer testis gene that promotes growth in the breast cancer cell line, MDA-MB-231 (35). However, the mechanism whereby GPAT2 mediates tumorigenicity remains obscure.

GPAT3

GPAT3 is located on the endoplasmic reticulum and is highly expressed in white adipose tissue, comprising approximately 80% of the total GPAT activity in that tissue (11). GPAT3 is also highly expressed in small intestine, kidney, and heart, however, its contribution to total GPAT activity in these tissues has not been determined (10). Upon differentiation of 3T3L1 preadipocyte cells, GPAT3 mRNA is upregulated 70 to 100-fold, and insulin-dependent phosphorylation of GPAT3 increases its activity 1.5-fold (10,36). In 3T3L1 cells, shRNA-mediated knockdown of GPAT3 decreases GPAT activity and lipid accumulation, and reduces the expression of a number of adipogenic genes, suggesting a role for GPAT3 in adipogenesis (35). In contrast to these observations, GPAT3 deficiency in mice does not affect white adipose tissue development or TAG accumulation, suggesting that further research is necessary to understand its role in WAT (11).

GPAT4

GPAT3 shares an 86.6% identical amino acid sequence to the second microsomal GPAT isoform, GPAT4 (12). GPAT4 is located on the endoplasmic reticulum and the drosophila orthologue of GPAT4 is also found on the surface of

growing lipid droplets, suggesting that under specific conditions GPAT4 may move from the ER to the lipid droplet monolayer (37). GPAT4 is a major GPAT isoform in BAT and liver, comprising 65% and 45% of the total GPAT activity in each tissue, respectively (38). The activity of GPAT4 is highest with 16:0-CoA, followed by 18:0 and 18:2-CoA (12). In contrast to GPAT3 deficiency, GPAT4 deficiency does not change GPAT activity in white adipose tissue (12). Furthermore, shRNA-mediated knockdown of GPAT4 in 3T3L1 cells does not alter GPAT activity, lipid accumulation, or adipogenic gene expression during adipocyte differentiation (36), suggesting an alternate function for GPAT4 in white adipose tissue.

Consistent with a tissue-dependent function of each GPAT isoform, in Cos-7 cells, the overexpression of GPAT1 increases [1-^{14}C]oleate incorporation into DAG and TAG. In contrast, the overexpression of GPAT4 increases [1-^{14}C]oleate incorporation into DAG, but not TAG (38). Because livers of chow-fed *Gpat4*$^{-/-}$ mice contain 45% less TAG than livers of wild type mice, we assume that GPAT4 in vivo initiates TAG synthesis and that Cos-7 cells might lack the necessary interacting partners to enable the esterification of excess GPAT4-derived DAG. This observation suggests that each GPAT isoform may interact with specific downstream enzymes or enzyme complexes that contribute to their diverse functions. A summary of these characteristics can be found in **Table 2.2**.

Table 2.2: Summary of subcellular location, tissue expression patter, nutritional regulation, and acyl-CoA preference.

Isoform	Subcellular Location	Tissue Expression[a]	Nutritional Regulation	Acyl-CoA preference
GPAT1	OMM	Liver	mRNA, protein, activity decreased by fasting, increased following refeeding with high sucrose diet activity increased 10-fold with 3T3L1 cell differentiation SREBP1c increases mRNA AMPK phosphorylates and inhibits activity	Activity with 16:0-CoA 2 to 3-fold greater than with 18:0-CoA or 18:1 CoA
GPAT2	OMM	Testis	Unknown	No preference for 16:0-CoA over 18:1-CoA
GPAT3	ER	white adipose, small intestine	mRNA, protein, and activity dramatically increased with adipocyte differentiation insulin-dependent phosphorylation increases activity	Not tested
GPAT4	ER and LD	Liver, Brown adipose, small intestine	Insulin-dependent phosphorylation increases activity	When overexpressed in Cos-7 cells activity was highest with 18:2-CoA, followed by 16:0-CoA, 18:0-CoA, and 18:1-CoA

[a]indicates highest tissue expression in rodents. OMM, outer mitochondrial membrane; ER, endoplasmic reticulum; LD, lipid droplet.

Diverse phenotypes of GPAT-deficient mice

Consistent with the hypothesis that each GPAT isoform performs a distinct function in directing acyl-CoAs toward glycerolipid synthesis, mice with deleted GPATs express vastly different phenotypes. Mice lacking GPAT1 are resistant to diet-induced hepatic steatosis (but not weight gain) and insulin resistance, are protected from diethylnitrosamine-induced hepatocellular carcinoma, and have increased hepatic β-oxidation (5,6,8,39). In contrast, although GPAT4 comprises nearly 50% of total GPAT activity in liver and mice lacking GPAT4 have 45% less hepatic TAG than controls, hepatic β-oxidation in *Gpat4*$^{-/-}$ mice is unchanged. This may be partially explained by the fact that *Gpat4*$^{-/-}$ mice are resistant to diet and genetically induced obesity and their metabolic rate is 4-6% higher than controls (40). Thus, the reduction in hepatic TAG in *Gpat4*$^{-/-}$ mice is the result of an increase in whole-body energy metabolism.

Despite the loss of 80% of total GPAT activity in white adipose, the mass of adipose tissue in mice lacking GPAT3 was normal in chow-fed mice and, with high-fat feeding, grew similar to controls (11). Although GPAT activity in livers of *Gpat3*$^{-/-}$ mice was unchanged, the *N*-ethylmaleimide-sensitive GPAT activity was 30% lower than controls, suggesting compensation by mitochondrial GPAT1. When fed a high-fat diet, cholesterol homeostasis in *Gpat3*$^{-/-}$ mice was abnormal, however, the mechanism for this abnormality remains unclear (11).

Mice with a targeted deletion of GPAT4 are born a normal size, at weaning weigh 25% less and are 10% shorter, and as adults, are resistant to diet and genetic-

induced obesity and insulin resistance (14,15). In contrast to other GPAT-null mice, energy expenditure in chow-fed *Gpat4*$^{-/-}$ mice is 4-6% higher than controls. Consistent with an increase in global metabolic activity, *Gpat4*$^{-/-}$ male mice fed a chow diet accumulate less TAG in brown adipose, liver, and gonadal white adipose tissue than wild type mice. At 12 weeks of age, *Gpat4*$^{-/-}$ mice fed a chow diet lack subdermal adipose tissue and Vergnes et al hypothesized that the lack of subdermal adipose tissue in *Gpat4*$^{-/-}$ mice increases heat loss through the skin and, thus, increases metabolic rate. However, *Gpat4*$^{-/-}$ mice have normal cold tolerance, suggesting that even under extreme conditions, these mice are not losing excess heat. Therefore, because the precise mechanism whereby *Gpat4*$^{-/-}$ mice are resistant to obesity remains unclear, we proposed to determine why the lack of GPAT4 protects mice from diet-induced obesity. Based upon the expression of GPAT4 in the BAT, the known role of GPATs in lipid synthesis, and the known function of brown adipose tissue, we hypothesized that *lack of GPAT4 in BAT increases acyl-CoA availability for oxidation, activates PPARα and increases uncoupled mitochondrial oxidation* (**Fig 2.4**). Beyond this function for GPAT4, additional phenotypic characterization and direct comparisons of mice lacking GPAT isozymes are necessary to understand how each isoform contributes to glycerolipid biosynthesis in a physiological context.

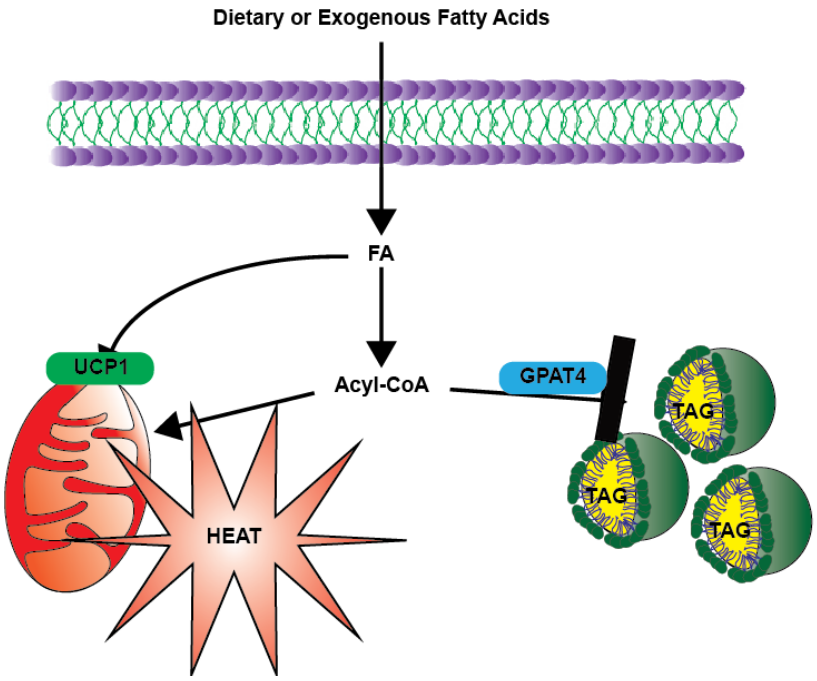

Figure 2.4: Hypothesis about the role of GPAT4 in BAT metabolism. We hypothesize that in the absence of GPAT4 in BAT, exogenous FA can be directly oxidized. Because FA and acyl-CoAs are not metabolized to TAG, they are available to be oxidized, activate UCP1, uncouple oxidation from ATP synthesis and generate heat.

Enzymes of the Kennedy Pathway are key regulators of energy metabolism

Several of the acyltransferase-null mouse models are protected from diet-induced obesity, suggesting that members of the acyltransferase family are key regulators of energy homeostasis (15,41-43). Unsurprisingly, the mechanism whereby lack of each acyltransferase confers resistance to obesity is related to the tissue expression and relative contribution to total enzyme activity in that tissue. For example, a role for MGAT2 in TAG absorption was highlighted by its high expression and activity within enterocytes (44,45). Absence of MGAT2 in mice results in delayed TAG absorption, uncoupled nutrient intake from insulin secretion, and increased total energy expenditure (42,46). Similar to the GPAT isoforms, DGAT1 and DGAT2 are synthesized from separate genes and have unique tissue expression patterns. The

absence of DGAT1 in mice reduces the rate of TAG absorption and protects mice from high fat diet-induced weight gain (43). DGAT2 deficiency in the skin increases skin permeability and hair loss after puberty (47). Together, these studies suggest a major role for acyltransferase enzymes in whole-body energy metabolism and highlight the importance of understanding the basic biological mechanisms linking triacylglycerol synthesis and metabolic efficiency.

GPAT-derived lipid intermediates and insulin resistance

The metabolic syndrome, a group of metabolic derangements including insulin resistance, obesity, hyperlipidemia, and cardiovascular disease, is strongly associated with increased TAG accumulation in adipose and non-adipose tissues (4). Classically, TAG synthesis has been thought to be a protective mechanism against the buildup of cytotoxic lipid metabolites. However, recent discoveries demonstrate that intermediates of TAG synthesis are critical metabolites for modulating intracellular signaling, most notably, the insulin-signaling pathway (48-50). Based upon these findings, the flux of lipids toward TAG can be considered an important source of signaling molecules that coordinates nutrient flux and intracellular signaling (**Table 2.3**). Two lipid intermediates implicated in the insulin-signaling pathway are DAG and PA. An abundance of evidence describes the role of these lipid intermediates in different reactions of the insulin-signaling pathway; DAG activates PKCε and PA dissociates the mTORC2 complex (51-55).

Mitochondrial GPAT1 has been implicated in the generation of PA and DAG. First, hepatic overexpression of GPAT1 in mice increased hepatic DAG content, increased the amount of PKCε in membranes, and impaired insulin-dependent phosphorylation of IRS1/2 (48). Inversely, GPAT1-deficient mice are protected from high-fat/high-safflower oil diet-induced hepatic steatosis and insulin resistance (6). Although PKC activity was not measured, these changes are associated with reduced hepatic DAG content and PKCε translocation to membranes. In primary hepatocytes, GPAT1 overexpression increased intracellular DAG content, but also intracellular PA content (52). In this model, the overexpression of GPAT1 led to increases in 16:0-containing DAG and PA species and was associated with the dissociation of the mTORC2 complex, but insulin-dependent phosphorylation of IRS1/2 was unchanged. Similar results were observed with overexpression of GPAT4, but not GPAT3 (14). Specifically di-16:0 PA disrupted the association of the mTORC2 complex, impairing phosphorylation of AKT at Ser473 and Thr308 (14). Furthermore, when *Gpat1*$^{-/-}$ and *Gpat4*$^{-/-}$ mice were fed the high-fat/high-safflower oil diet, they remained insulin sensitive and hepatic PA content was diminished relative to controls (14). Although hepatic DAG content in *Gpat1*$^{-/-}$ and *Gpat4*$^{-/-}$ mice was lower than controls, PKCε activity and phosphorylation of IRS1/2 was unchanged.

The discrepancies between these studies rest primarily with the methods for assessing PKCε activation. The translocation of PKCε from the cytosol to membranes is required for its activation, however, this is not sufficient for PKCε activation (56). In primary hepatocytes, increasing intracellular PA levels did increase the proportion of

PKCε located on the membrane, but PKCε activity remained unchanged. Based upon these results, the authors concluded that PA, but not DAG, was responsible for impairing the insulin-signaling pathway.

These results are not without caveats. First, primary hepatocytes are often cultured in media containing 25 mM glucose, thus increasing *de novo* fatty acid synthesis and the amount of 16:0-fatty acids available for use in glycerolipid synthesis. Because di-16:0 PA impairs insulin-signaling via dissociation of mTORC2, concluding that only PA, but not DAG, impairs insulin signaling excludes the possibility that the acyl chain composition of the lipid intermediate is important for its signaling properties. Consistent with the role of acyl chain composition in affecting the potency of lipid intermediates, in vitro activation of PKC isozymes varies in response to different DAG species (57). Notably, the high-fat/high-safflower oil diet contains a large proportion of 18:2 fatty acids and thus a smaller portion of 16:0 fatty acids would be available. Therefore, it is possible that DAG containing unsaturated FA are more potent activators of PKCε and that PA containing saturated FA are potent activators of mTORC2, suggesting that hepatic insulin signaling may be modulated by different lipid intermediates in an acyl chain composition-dependent manner.

Table 2.3: Summary of GPAT-derived signaling intermediates.

Isoform	Lipid Intermediate	Affected Pathway	Function
GPAT1	LPA	Mitochondrial fusion (mechanism unknown)	Impaired mitochondrial fusion
	PA, specifically di-16:0 PA	When increased in primary mouse hepatocytes, dissociates mTORC2/rictor association	Inhibits insulin signaling
	DAG	When increased in mouse liver activates PKCε and inhibits phosphorylation of IRS1/2	Inhibits insulin-signaling
GPAT2	Not investigated		
GPAT3	unclear	When activity is increased activates mTORC-dependent phosphorylation of p70S6K	Proposed to stimulate growth (unconfirmed)
GPAT4	PA, specifically di-16:0 PA	When increased in primary mouse hepatocytes, dissociates mTORC2/rictor association	Inhibits insulin signaling

Lipid droplet metabolism and GPAT

Lipid droplets containing TAG and cholesterol-esters stores can be found in virtually all tissues. A complete review of lipid droplet biogenesis has been published elsewhere (58,59). Under conditions of calorie surplus, tissues such as liver, brown adipose, and white adipose accumulate large lipid droplets. Lipid droplet proteomics show that all of the necessary TAG synthetic enzymes, including GPAT4, are present on the membrane of lipid droplets (37). Unlike that of the endoplasmic reticulum, the outer coat of lipid droplets is a phospholipid monolayer, requiring that each of the active proteins found on the LD surface possess a monolayer-integrating domain. Upon oleate loading, GPAT4 moves from the ER onto the outer layer of the growing lipid

droplet and this movement results in the accumulation of large lipid droplets (37). In the absence of GPAT4, lipid droplets are sparse. Interestingly, when mitochondrial GPAT1 is overexpressed in GPAT4-deficient *Drosophila* cells numerous small lipid droplets are present (37). These data suggest two key points regarding lipid droplet biogenesis. First, in non-adipocytes, lipid droplets do not grow by fusion of smaller droplets, but potentially by the synthesis of TAG on the LD surface. Second, LD size and number depends on which GPAT isoform initiates TAG synthesis and not just on the total GPAT activity in the tissue. Further studies are required to determine whether differences in LD number and size result in distinct metabolic consequences.

Therapeutic potential of pharmacological inhibition of GPAT

Based on the known role of GPAT and lipid metabolic enzymes in energy homeostasis and insulin resistance, a great deal of interest surrounds their potential as therapeutic targets for the treatment of obesity and fatty liver disease (60,61). However, attempts to treat metabolic disease by pharmacological inhibition of GPAT or other metabolic enzymes have had limited success. Partial efficacy in reducing TAG absorption has been achieved with Orlistat, through inhibiting the action of pancreatic lipase (62). The predominant side effect is an increase in fecal TAG excretion, making its long-term use unpleasant (62). Because Orlistat does not alter systemic energy metabolism, this treatment is ineffective at reducing weight in those individuals consuming high-carbohydrate diets.

Despite the lack of obvious success stories, some progress has been made with regard to the design and synthesis of chemical inhibitors of GPAT activity. The fundamental design of compounds is focused on structures that mimic the phosphate group of glycerol-3-phosphate and possess a long saturated chain similar to that of an acyl-CoA (63,64) (**Fig 2.5**). This work identified 2-(nonylsulfonamido)benzoic acid as possessing potent GPAT inhibitory activity. The structure-activity relationship, a description of the specific chemical properties required for inhibitory activity, reveals that medium to long-chain alkyl sulfonamide modifications are necessary for activity. All reported modifications or replacements of the benzoic acid ring decreased inhibitory activity. Based on their occlusion from the GPAT active site, a subsequent study excluded a class of compounds that substituted the benzoic acid ring for racemic cyclopentane and cyclohexane carboxylic acids (64). The compound with the most GPAT inhibitory activity demonstrates an IC_{50} = 24.7 μM, meaning that 50% of the in vitro GPAT activity was inhibited by a compound concentration of 24.7 μM.

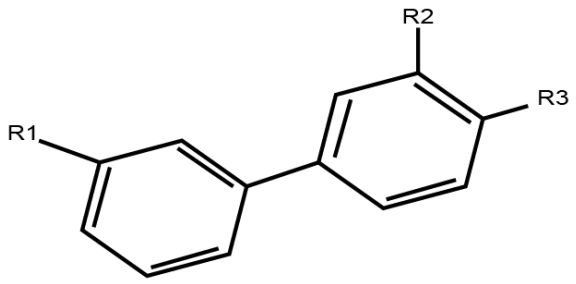

Figure 2.5: Class of compounds possessing GPAT inhibitory activity. Compounds must contain at least 1 benzoic acid ring, and substitutions at R1 and R2 must be polar. Substitutions at R3 are required to possess a sulfonamide group with an acyl chain that can vary in length. These compounds are designed to mimic the phosphate group of glycerol-3-phosphate and the acyl chain of an acyl-CoA.

As a proof of concept, this compound (renamed FSG67) was used in cellular and mouse models (65). When differentiated 3T3L1 adipocytes were treated with FSG67,

TAG accumulation was inhibited in a dose-dependent manner, and at concentrations as high as 150 μM, no toxicity was observed. Intraperitoneal injection of lean or diet-induced obese mice with 5 or 20 mg/kg FSG67, before the onset of the dark cycle, resulted in a ~4% weight loss. Because this weight loss was paired with reduced intake, the authors concluded that FSG67 possesses potent appetite-suppressing activity. Although many drugs possess appetite-suppressing effects, chronic dosing of 5 mg/kg FSG67 did not impair conditioned taste aversion while still resulting in weight loss, suggesting that the decreased food intake was not due to food avoidance. Metabolic analysis of FSG67-treated mice revealed reversible weight loss in diet-induced obese mice after 8 days, resulting primarily from reduced food intake. Daily treatment of DIO mice for 18 days improved glucose tolerance and insulin sensitivity. Suggesting that FSG67 regulated central satiety, intracerebroventricular administration produced similar effects on weight loss and food intake.

The results from these studies provide some suggestion that pharmacological inhibition of GPAT activity is a viable strategy for the treatment of obesity. However, this approach may be problematic. FSG67-dependent hypophagia is transient, suggesting that the long-term, weight loss benefits would be limited. Second, the GPAT inhibitory activity of FSG67 exhibited no GPAT isoform selectivity. Based on the diverse functions of the different GPAT isoforms, long-term inhibition of all GPAT activity is likely to produce serious side effects. Although existing GPAT-null mice are viable, these models are only evaluating the absence of a single GPAT isoform, and it is unclear whether the loss of multiple GPAT isoforms simultaneously would be compatible with

life. Clearly, improving our understanding of the distinct roles of each GPAT isoform will provide valuable information in the search for improved therapies for obesity.

Lipodystrophies and Glycerolipid Signals

Lipodystrophies are a cluster of disorders characterized by impaired adipose tissue development or progressive loss of adipose tissue. Lipodystrophies are divided into three major categories: congenital generalized (CGL), familial partial (FPL), and acquired (66). Acquired lipodystrophies are most common in individuals undergoing anti-retroviral therapy, affecting nearly 100,000 patients in the US (66,67). Loss of adipose tissue in patients with acquired lipodystrophies is highly variable. The inherited lipodystrophies, CGL and FPL, are rare genetic disorders characterized by selective and variable lack of adipose tissue (68). Often diagnosed in the neonatal period, children with CGL have accelerated growth rates and uncontrolled appetites (68). The lack of functional adipose tissue for storage of TAG, results in ectopic TAG accumulation in the liver and, if untreated, can lead to cirrhosis (68). Some patients present with enlarged hearts and mild mental retardation. Although several loci remain unidentified, recent advances have led to the identification of eight genetic loci linked to CGL (68). Patients with type 2 CGL present with the most severe symptoms, most likely due to the absence of both metabolic and structural adipose tissue (69). Although the underlying mechanisms in the development of lipodystrophies remain obscure, recent studies have revealed a link between CGL and glycerolipid synthesis (70).

Type 2 CGL is caused by loss-of-function mutations in Berardinelli-Seip Congenital Lipodystrophy 2 (*BSCL2*), the gene encoding for the protein Seipin. Because Seipin does not posses any known functional domains, it is unlikely that Seipin acts as an enzyme in TAG synthesis. Although its function has yet to be fully described, initial reports have identified a role for Seipin in lipid droplet biogenesis (71). Seipin is an endoplasmic reticulum membrane protein, and its mRNA expression is highly upregulated with adipocyte differentiation (72); the loss of Seipin is associated with increased intracellular PA levels (73,74). Because of the known role for PA in intracellular signaling, it has been suggested that the increased PA acts as negative regulator of adipogenesis by inhibiting the master regulator of adipocyte differentiation, peroxisome-proliferator activated receptor isoform γ (PPARγ) (75). PPARγ is a nuclear receptor that, in tandem with another transcription factor C/EBPβ, plays a vital role in the differentiation of preadipocytes to mature adipocytes (76). During this transition, PPARγ upregulates a host of genes involved with lipid uptake and storage. Unsurprisingly, one of the 5 types of familial partial lipodystrophy is caused by PPARγ deficiency (66). PPARγ activity can by modified by a number of ligands including the thiazolidinedione class of antidiabetic drugs and naturally occurring lipids (76). Some of these lipid species are intermediates in glycerolipid synthesis. In Chinese hamster ovary cells, the overexpression of GPAT1 increased intracellular LPA levels and stimulated PPARγ activation (77). Conversely, overexpression of AGPAT2 increased intracellular PA levels and was a potent inhibitor of PPARγ activation (77). Thus, the increased intracellular PA in CGL tissues, the potential for PA to act as an antagonist of PPARγ, and the role for GPAT in modulating intracellular PA levels strongly suggests a

role for GPAT in CGL. Our current hypothesis is that during differentiation, Seipin regulates GPAT activity and controls intracellular PA levels (**Fig 2.6**).

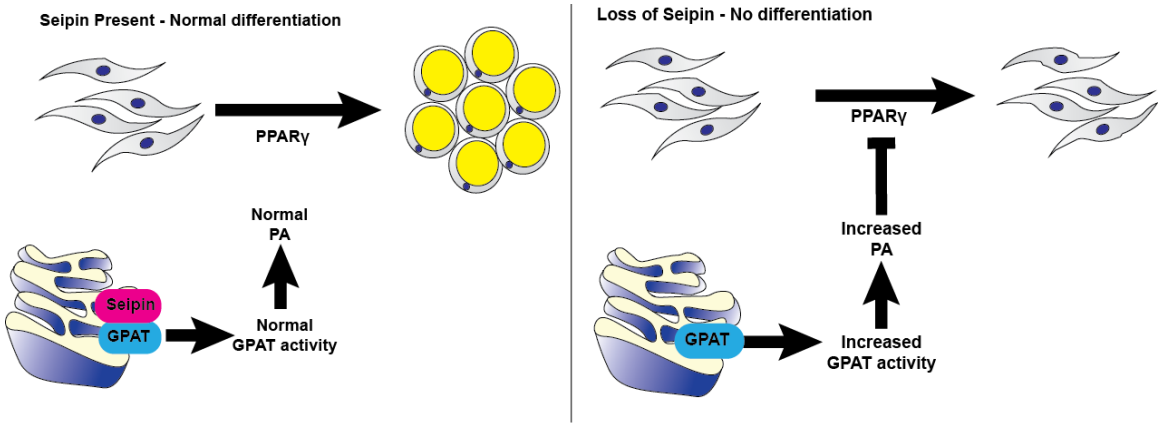

Figure 2.6: Hypothesis for relationship between Seipin, GPAT, and adipogenesis. When Seipin is present, GPAT activity and intracellular PA levels are normal, and PPARγ can be activated to initiate adipogenesis. When Seipin is absent, GPAT activity and PA levels are increased, thereby inhibiting PPARγ activity and adipocyte differentiation. ER, endoplasmic reticulum; PA, phosphatidic acid.

CHAPTER III: GLYCEROL-3-PHOSPHATE ACYLTRANSFERASE (GPAT)-1, BUT NOT GPAT4, INCORPORATES NEWLY SYNTHESIZED FATTY ACIDS INTO TRIACYLGLYCEROL AND DIMINISHES FATTY ACID OXIDATION[1]

Capsule

Background: The independent functions of the glycerol-3-phosphate acyltransferase (GPAT) isoforms are unknown.

Results: Compared to *Gpat4*$^{-/-}$, *Gpat1*$^{-/-}$ hepatocytes oxidized more fatty acids (FA) and were unable to incorporate de novo synthesized FA into triacylglycerol.

Conclusion: GPAT1, but not GPAT4, metabolizes FA synthesized de novo from [^{14}C]acetate and diverts FA away from mitochondrial oxidation.

Significance: GPAT1 and GPAT4 use different cellular pools of FA.

[1] This chapter previously appeared in an article in the Journal of Biological Chemistry. The original

Summary

Four glycerol-3-phosphate acyltransferase (GPAT) isoforms, each encoded by a separate gene, catalyze the initial step in glycerolipid synthesis; in liver, the major isoforms are GPAT1 and GPAT4. To determine whether each of these hepatic isoforms performs a unique function in the metabolism of fatty acid, we measured the incorporation of *de novo* synthesized fatty acid or exogenous fatty acid into complex lipids in primary mouse hepatocytes from control, *Gpat1*$^{-/-}$ and *Gpat4*$^{-/-}$ mice. Although hepatocytes from each genotype incorporated a similar amount of exogenous fatty acid into TAG, only control and *Gpat4*$^{-/-}$ hepatocytes were able to incorporate *de novo* synthesized fatty acid into TAG. Compared to controls, *Gpat1*$^{-/-}$ hepatocytes oxidized twice as much exogenous fatty acid. To confirm these findings and to assess hepatic β-oxidation metabolites, we measured acylcarnitines in liver from mice after a 24 h fast and after a 24 h fast followed by 48 h of refeeding with a high sucrose diet to promote lipogenesis. Confirming the *in vitro* findings, the hepatic content of long-chain acylcarnitine in fasted *Gpat1*$^{-/-}$ mice was 3-fold higher than in controls. Compared to control and *Gpat4*$^{-/-}$ mice, after the fasting-refeeding protocol, *Gpat1*$^{-/-}$ hepatic TAG was depleted and long-chain acylcarnitine content was 3.5-fold higher. Taken together, these data demonstrate that GPAT1, but not GPAT4, is required to incorporate *de novo* synthesized fatty acids into TAG and to divert them away from oxidation.

Introduction

Glycerol-3-phosphate acyltransferase (GPAT; EC 2.3.1.15) initiates the pathway of TAG synthesis by esterifying a long-chain fatty acyl-CoA to a glycerol-3-phosphate backbone at the *sn*-1 position to form *sn*-1-acylglycerol-3-phosphate (lysophosphatidic acid) (28). A second esterification at the *sn*-2 position, is catalyzed by acylglycerol-3-phosphate acyltransferase. The phosphate is then hydrolyzed by phosphatidic acid phosphohydrolase (lipin), and then a final acylation is catalyzed by diacylglycerol acyltransferase to form TAG. In addition to their roles in TAG synthesis, the phosphatidic acid and diacylglycerol intermediates in this pathway are precursors for all the glycerophospholipids, and they initiate signaling pathways.

The pathway of TAG biosynthesis is remarkable for the number of isoenzymes that catalyze each step. For example, four independent GPAT isoforms, each encoded by a separate gene, catalyze the formation of lysophosphatidic acid, but it is unclear why GPAT enzyme redundancy is required. Studies of mice with deleted GPATs show that the isoforms present in liver include primarily GPAT1 (78) and GPAT4 (12,22), with lower expression of GPAT2 (79) and GPAT3 (10). Each of the GPAT isoforms is an intrinsic membrane protein whose active site faces the cytosol (19). GPAT1, located on the outer mitochondrial membrane and at contact sites with the endoplasmic reticulum (80), has a strong preference for saturated fatty acids (28). GPAT1 comprises 30-50% of total activity in liver (28), and *Gpat1* mRNA expression is highly responsive to SREBP1c and is upregulated when dietary carbohydrate intake and circulating insulin concentrations are high (81). Absent GPAT1 protects against the development of

hepatic steatosis caused by a high fat diet (5) or by the upregulation of SREBP1c in *ob/ob* mice (32). Conversely, GPAT1 overexpression causes hepatic steatosis (48) and insulin resistance (39). GPAT4, which is located on the endoplasmic reticulum and on lipid droplets (37), contributes 40-50% of total hepatic GPAT activity (12). Like GPAT1, GPAT4 also appears to be important for hepatic TAG synthesis, because the TAG content in *Gpat4*$^{-/-}$ liver is 42% lower than in control mice (12).

Hepatic triacylglycerol synthesis is enhanced by the increased availability of long-chain fatty acids synthesized within hepatocytes from dietary glucose, or from fatty acid that enters hepatocytes exogenously from dietary chylomicron remnants or as free fatty acids lipolyzed from adipose tissue. Because SREBP1c concomitantly upregulates both GPAT1 and the enzymes that catalyze the *de novo* synthesis of fatty acids, including acetyl-CoA carboxylase and fatty acid synthase (82), we hypothesized that the function of GPAT1 and *de novo* lipogenesis might be intrinsically linked. To test this hypothesis, we compared the ability of GPAT1 and GPAT4 to use exogenous versus *de novo* synthesized fatty acids in control and knockout mice and in their hepatocytes.

Experimental Procedures

Materials

Type I collagenase was from Worthington Biochemical Corporation. [1-^{14}C]acetic acid and [1-^{14}C]palmitic acid were purchased from PerkinElmer Life Sciences. Silica G gel plates were from Whatman. Tissue culture plates were from BD Biosciences, and media were obtained from Invitrogen. Sigma was the source of 4-methylene-2-octyl-5-oxotetrahydrofuran-3-carboxylic acid (C75) and all other chemicals, unless otherwise indicated.

Animal care and hepatocyte isolation

Animal protocols were approved by the University of North Carolina at Chapel Hill Institutional Animal Care and Use Committee. Mice were housed in a pathogen-free barrier facility on a 12-h light/dark cycle with free access to water and food (Prolab 5P76 Isopro 3000; 5.4% fat by weight). *Gpat1*$^{-/-}$ (5) and *Gpat4*$^{-/-}$ (12,13) mice had been backcrossed at least eight times onto a C57BL6/J background. At 8 weeks of age, littermate controls, and *Gpat1*$^{-/-}$, and *Gpat4*$^{-/-}$ mice were either fasted for 24 h or fasted for 24 h and then refed a high sucrose diet for 48 h before sacrifice. The high sucrose diet was modified from Research Diets D12450B **(**10% kcal fat, 20% kcal protein and 70% kcal carbohydrate (525 g/kg sucrose, 175 g/kg corn starch)).

To isolate hepatocytes, after mice were anesthetized with 250 mg/kg Avertin, a 22G catheter was inserted into the vena cava, and the liver was perfused with wash buffer (10 mM Hepes, 132 mM NaCl, 6.7 mM KCl, 20 mM glucose, 0.5 M adenosine,

100 mM EGTA, 140 nM insulin, pH7.4), and then with digestion buffer (100 mM HEPES, 57 mM NaCl, 6.7 mM KCl, 5 mM $CaCl_2$, 20 mM glucose, 0.45 mg/ml type 1 collagenase, pH 7.4). The digested liver was removed and placed in a 100 mm dish on ice with Hanks/BSA buffer (10 mM HEPES, 137 mM NaCl, 5.4 mM KCl, 1.26 mM $CaCl_2$, 0.8 mM $MgSO_4$, 4.2 mM $NaHCO_3$, 0.34 mM Na_2HPO_4, 0.44 mM KH_2PO_4, 5 mM glucose, pH7.4). The hepatocytes were dissociated and filtered through a cell strainer, centrifuged at 4°C at 50 × g for 3 min, then washed once in Williams' medium E. The cells were re-suspended in Williams' Medium E:Percoll (16 ml:14 ml), centrifuged at 4°C at 400 × g for 8 min, and washed with Williams' medium E. Cells were plated onto 60 mm collagen-coated dishes and incubated for 90 min in Williams' medium E + 10% FBS. After the cells attached, the medium was changed to Williams' medium E, 100 U penicillin/streptomycin, 50 nM insulin, 0.1 μM dexamethasone, and 0.1% BSA.

GPAT Activity

Hepatocytes were cultured overnight in 60 mm plates, then scraped and homogenized in cold Medium I (250 mM sucrose, 10 mM Tris, pH 7.4, 1 mM EDTA, 1 mM dithiothreitol) with 10 up-and-down strokes with a Teflon-glass motor-driven homogenizer. Liver was minced, then homogenized similarly. Total membranes were isolated by centrifuging the homogenate at 100,000 x g for 1 h. GPAT specific activity was assayed for 10 min at room temperature in a 200 μl reaction mixture containing 75 mM Tris-HCl, pH 7.5, 4 mM $MgCl_2$, 1 mg/ml BSA (essentially fatty acid–free), 1 mM dithiothreitol, 8 mM NaF, 800 μM [^{3}H]glycerol 3-phosphate, and 80 μM palmitoyl-CoA (80). The reaction was initiated by adding 10-30 μg of membrane protein after

incubating the membrane protein on ice for 15 min in the presence or absence of 2 mM *N*-ethylmaleimide (NEM), which inactivates GPAT isoforms 2, 3, and 4. The reaction products were extracted into $CHCl_3$, dried under N_2, resuspended in 4 mLs Cytoscint and counted on scintillation counter. NEM-resistant activity (GPAT1) was calculated by subtracting NEM-sensitive activity from total activity.

RNA extraction and RT-PCR

Total RNA was extracted from overnight cultures of hepatocytes with TRIzol (Invitrogen). cDNA synthesis and real time RT-PCR were performed as described (83). Primer sequences for each GPAT isoform and data normalization used were described (52,83).

Labeling, Oxidation, and Lipid Extraction

Sixteen to 20 h after plating, hepatocytes were labeled with 0.5 ml of labeling buffer (Krebs Ringer buffer, 10 mM HEPES, 5.5 mM glucose, 0.25% fatty acid-free bovine serum albumin (BSA), and 1 mM carnitine) containing 500 μM [1-^{14}C]acetic acid or [1-^{14}C]palmitic acid for 2 h. Media were removed, and CO_2 was liberated by adding 100 μl 70% perchloric acid, and trapped in 1M NaOH. An aliquot of the NaOH was counted to measure radiolabeled CO_2. To quantify intracellular oxidation metabolites, fresh Krebs Ringer buffer and 100 μL 70% perchloric acid were added to each plate and acidified supernatants were collected. The acidified media and cell supernatants were incubated overnight with BSA and then centrifuged at 14,000 x g for 20 min. Aliquots of the supernatant were counted to measure radiolabeled acid soluble metabolites (ASM),

a measure of incomplete fatty acid oxidation. Cells were washed with 1% BSA and then with phosphate buffered saline before lipids were extracted (84). Lipid extracts and standards were separated by thin layer chromatography on Partisil LK5D Silica gel plates in a two-phase system: chloroform: methanol: ammonium hydroxide (65:25:4, v/v/v) run to 50% of the plate, then dried and followed by heptane: isopropyl ether: acetic acid (60:40:4, v/v/v) run to the top of the plate. Radiolabeled lipids were quantified with a Bioscan AR-2000 Imaging Scanner. Lipid standards were visualized by iodine staining.

Blood Chemistries and Lipids

Before blood collection, mice were either fasted for 24 h or fasted 24 h and then fed a high sucrose diet for 48 h. Plasma TAG (Stanbio, Boerne, TX), free fatty acid (Wako Diagnostics, Richmond, VA), glucose (Glucose CII, Wako Diagnostics), and b-hydroxybutyrate (Wako Diagnostics) were determined by enzymatic colorimetric methods.

Lipid Extraction and TAG Measurement in Liver

Liver lipids were extracted (39), dried under N_2 gas, resuspended in 200 µL tert-butanol:methanol:TritonX-100 (3:1:1, v/v), and analyzed colorimetrically as described above.

Liver Acylcarnitine Measurement

Livers were snap-frozen in liquid nitrogen, pulverized, and weighed. The pulverized liver (50-100 mg) was homogenized in acetonitrile:water:formic acid (50:49.7:0.3; v/v) at a final concentration of 50 mg/ml. Acyl-carnitines, were analyzed by flow injection tandem mass spectrometry (85). Samples were stored at -80 ^{o}C before analysis.

Statistics

Data represent means ± SEM of at least three independent experiments performed in triplicate unless indicated otherwise. In vitro models were analyzed by 1-way ANOVA comparing each genotype versus controls, and post-hoc comparisons of diet conditions within each genotype. Data were considered significant at $P<0.05$.

Results

Isolated and cultured primary hepatocytes retained GPAT specific activity.

In order to compare the contributions of GPAT1 and GPAT4 to the total amount of GPAT activity, we isolated and cultured primary hepatocytes from control, *Gpat1*$^{-/-}$ and *Gpat4*$^{-/-}$ mice and measured GPAT specific activity in the presence and absence of NEM, which inhibits GPAT2, 3, and 4 (**Fig 3.1A**). Compared to wild type hepatocytes, total GPAT specific activity in *Gpat1*$^{-/-}$ hepatocytes was 35% lower and minimal residual NEM-resistant GPAT activity remained, whereas NEM-sensitive GPAT activity was unchanged. Total GPAT specific activity in *Gpat4*$^{-/-}$ hepatocytes was 42% lower than in control hepatocytes; NEM-resistant GPAT specific activity was unchanged, but NEM-sensitive GPAT activity was 60% lower. The residual NEM-sensitive GPAT activity is likely due to GPAT2 and 3. These results show that isolated and cultured primary hepatocytes retained GPAT activity and that the specific activity was similar in *Gpat1*$^{-/-}$ and *Gpat4*$^{-/-}$ hepatocytes.

To determine whether other GPAT isoforms were affected by deletion of either GPAT1 or GPAT4, we measured mRNA expression of each GPAT isoform (**Fig 3.1B**). In *Gpat1*$^{-/-}$ hepatocytes GPAT3 mRNA abundance was 2-fold higher than in wild type hepatocytes, but NEM-sensitive GPAT activity did not change, indicating a lack of compensation. In the absence of GPAT4, the mRNA expression of GPAT2 and 3 increased 2.5- and 3.5-fold, respectively. GPAT2 activity is extremely low in liver (79), and even when the amount of GPAT2 mRNA doubles, probably does not contribute substantially to total NEM-sensitive GPAT activity. However, we cannot differentiate

between GPAT3 and GPAT4 protein or activity, so the 42% lower NEM-sensitive GPAT activity (Fig. 1B) may reflect partial compensation by GPAT3.

The incorporation of de novo synthesized fatty acid into TAG required GPAT1

Because GPAT1 is upregulated by SREBP1c, we hypothesized that it might be functionally and specifically linked to *de novo* lipogenesis, such that newly synthesized fatty acids would be incorporated into TAG. Using [1-^{14}C]acetate, we measured the ability of control, *Gpat1*$^{-/-}$ and *Gpat4*$^{-/-}$ hepatocytes to incorporate *de novo* synthesized fatty acid into TAG and PL. The incorporation of acetate into TAG and PL was equal in hepatocytes from wild type and *Gpat4*$^{-/-}$ mice, however in *Gpat1*$^{-/-}$ hepatocytes, the incorporation of [^{14}C]acetate into PL was 78% lower than in controls, and the incorporation into TAG was virtually absent (**Fig 3.2A,B**). When wild type and *Gpat4*$^{-/-}$ hepatocytes were cultured in the presence of the fatty acid synthase inhibitor C75, [^{14}C]acetate incorporation into TAG was inhibited 80-85% (**Fig 3.2A**). However, in *Gpat1*$^{-/-}$ hepatocytes, C75 had no additional effect, indicating that the absence of GPAT1 in hepatocytes had abolished the incorporation of the *de novo* synthesized fatty acid. In wild type and *Gpat4*$^{-/-}$ hepatocytes, C75 decreased acetate incorporation into PL by 60%, but only by 27% in *Gpat1*$^{-/-}$ hepatocytes (**Fig 3.2B**). In each group of hepatocytes, the addition of C75 decreased the incorporation of acetate into free fatty acids by more than 72% (data not shown). These results show that GPAT1, but not GPAT4, is required to incorporate *de novo* synthesized FA into complex lipids.

Both GPAT1 and GPAT4 can incorporate exogenous fatty acids into TAG and phospholipid

In addition to *de novo* synthesis, liver fatty acids are also derived from exogenous sources. To distinguish between the functions of GPAT1 and GPAT4 in the use of exogenous fatty acids, we measured the incorporation of [1-^{14}C]palmitate into glycerolipids in primary hepatocytes. In contrast to fatty acids derived from *de novo* synthesis, the incorporation of [1-^{14}C]palmitate into TAG and PL was not altered by the absence of either GPAT1 or GPAT4 (**Fig 3.3A,B**), indicating that neither isoform was essential for use of exogenous fatty acid. Thus, in both *Gpat4*$^{-/-}$ or *Gpat1*$^{-/-}$ hepatocytes, the remaining GPAT isoforms can fully incorporate exogenous fatty acid into glycerolipids.

In hepatocytes, the absence of GPAT1, but not GPAT4, increased fatty acid oxidation

Previous studies have strongly suggested that GPAT1 competes with CPT1 for acyl-CoAs at the outer mitochondrial membrane (39). To confirm this competition for acyl-CoAs and to determine whether GPAT4 located on the endoplasmic reticulum competes similarly, we measured the incorporation of [1-^{14}C]palmitate into ASM, a measure of incomplete fatty acid oxidation. *Gpat1*$^{-/-}$ hepatocytes oxidized [^{14}C]palmitate at a rate 200% higher than control hepatocytes, but the incorporation of [^{14}C]palmitate into ASM by *Gpat4*$^{-/-}$ hepatocytes was unchanged (**Fig 3.3C**). Of the total ASM extracted from the media and cells, intracellular ASM comprises only 5% of the total ASM **(see inset Fig 3.3C**); thus, media ASM reflects 95% of the total ASM produced.

These data show that only GPAT1 competes with CPT1 for acyl-CoAs, thereby diminishing the flux of fatty acid into the mitochondria for oxidation.

Hepatic GPAT1 diminished fatty acid transport into mitochondria in vivo.

To confirm the disparate effects of each GPAT isoform on the β-oxidation of exogenous versus *de novo* synthesized fatty acid *in vivo,* we measured hepatic acylcarnitine content in wild type, *Gpat1*$^{-/-}$ and *Gpat4*$^{-/-}$ mice after food was removed for 24 h. Because fasting increases the flux of adipose-derived fatty acids into the liver, more fatty acids are transported to the mitochondria via CPT1, thereby elevating the content of hepatic long-chain acylcarnitines. These metabolites are subsequently reconverted to acyl-CoAs in the mitochondrial matrix, where they enter the β-oxidation pathway. In fasting mice of each genotype, the content of free carnitine (C0), acetylcarnitine (C2), short-chain (C3-C6), and medium-chain (C8-C12) acylcarnitine species was similar (**Fig 3.4A,C**). Consistent with the hypothesized ability of GPAT1 to compete with CPT1 for acyl-CoAs, total long-chain (C14-C22) acylcarnitine content in fasted *Gpat1*$^{-/-}$ liver was 3-fold higher than in control liver (**Fig 3.4C).** The most abundant long-chain acylcarnitine species, 14:0, 16:1, 16:0, 18:2, 18:1 and 18:0, were 2- to 6-fold higher than in control liver (**Fig 3.4E)**. In contrast, and consistent with the *in vitro* data, the acylcarnitine content in livers of fasted *Gpat4*$^{-/-}$ mice was similar to that of control mice.

Because GPAT1 was essential for the incorporation of *de novo* synthesized fatty acids into complex lipids *in vitro,* we predicted that the absence of hepatic GPAT1 *in*

vivo would also increase the transport of *de novo* synthesized fatty acids into mitochondria. To test this hypothesis, we fasted mice for 24 h, then refed with a high sucrose diet for 48 h to stimulate *de novo* lipogenesis. The total long-chain (C14-C22) acylcarnitine content of *Gpat1*$^{-/-}$ liver remained 3.5-fold higher than that of controls, and the most abundant long-chain acylcarnitine species, 14:0, 16:1, 16:0, 18:2, 18:1 and 18:0, ranged from 2- to 5-fold higher (**Fig 3.4D,F**). In contrast, no differences were observed in the hepatic acylcarnitine content of *Gpat4*$^{-/-}$ mice that had been fasted and then refed (**Fig 3.4B,D,F**). Thus, GPAT1, but not GPAT4, was required *in vivo* to diminish CPT1-mediated transport of both *de novo* synthesized and exogenous fatty acid.

Hepatic GPAT1 was essential for the incorporation of de novo synthesized fatty acid into TAG.

Because the absence of GPAT1 increased hepatic β-oxidation of *de novo* synthesized fatty acids *in vivo,* we predicted that the liver TAG content would be low. After a 24 h fast, hepatic TAG content in control, *Gpat4*$^{-/-}$ and *Gpat1*$^{-/-}$ liver was similar. After refeeding a high sucrose diet to enhance *de novo* lipogenesis, the TAG content in control and *Gpat4*$^{-/-}$ liver increased 2- to 2.5-fold (**Fig 3.5A**), however, the hepatic TAG content of *Gpat1*$^{-/-}$ liver did not increase. These data support the conclusion that GPAT1 is essential for the incorporation of *de novo* synthesized fatty acid into TAG and for diverting those fatty acids away from mitochondrial oxidation.

The absence of GPAT1, but not GPAT4, increased ketogenesis during fasting.

When the concentration of plasma glucose decreases during an extended fast, adipocyte-derived fatty acids flood into the liver, their oxidation rate increases, and ketone bodies are synthesized and secreted into the blood. The accumulation of long-chain acylcarnitines in the liver and an elevated plasma concentration of ketone bodies suggests an increased rate of hepatic fatty acid oxidation. Because, GPAT1 diminishes the oxidation of exogenous fatty acid *in vitro* and the absence of GPAT1 in liver results in the accumulation acylcarnitines, we predicted that fasting would result in a higher rate of hepatic β-oxidation in *Gpat1*$^{-/-}$ mice than in controls. To confirm this hypothesis we measured plasma ketone bodies in control, *Gpat1*$^{-/-}$ and *Gpat4*$^{-/-}$ mice. After a 24 h fast, the concentrations of plasma glucose and TAG in control and *Gpat1*$^{-/-}$ mice were similar (**Fig 3.5B,C**), but plasma fatty acid concentration in *Gpat1*$^{-/-}$ mice was elevated 1.5-fold compared to controls (**Fig 3.5D**). Consistent with elevated fatty acid oxidation in *Gpat1*$^{-/-}$ mice, plasma β-hydroxybutyrate concentration was 2-fold higher than controls (**Fig 3.5E**).

Ketogenesis remained elevated in Gpat1$^{-/-}$ *mice during refeeding.*

After a 24 h fast, refeeding with high sucrose drives hepatic *de novo* lipogenesis, promotes TAG storage, and blocks fatty acid oxidation (86). Because our data suggested that GPAT1 esterifies *de novo* synthesized fatty acids, we asked whether the rate of hepatic fatty acid oxidation would remain elevated during short-term high sucrose refeeding. Consistent with a higher rate of hepatic fatty acid oxidation in the absence of GPAT1, the plasma β-hydroxybutyrate concentration in *Gpat1*$^{-/-}$ mice was 3-

fold higher than in control or *Gpat4*$^{-/-}$ mice (**Fig 3.5D**). Consistent with diminished hepatic TAG synthesis in both *Gpat1* and *Gpat4* null mice, compared to controls, the plasma TAG concentration was 48% lower in *Gpat1*$^{-/-}$ mice and 25% lower in *Gpat4*$^{-/-}$ mice (**Fig 3.5C**). Plasma glucose and fatty acid concentrations in each genotype were similar (**Fig 3.5B,E**).

Discussion

With the discovery of 4 independent GPAT isoforms that differ in tissue distribution, subcellular location, acyl-CoA preference, and transcriptional regulation, questions have arisen as to the specific function of each isoform (28). *Gpat2* mRNA is most strongly expressed in testes and probably plays a minor role in liver, but the mRNA expression and activities in liver of the remaining GPAT isoforms are high (10,28,79,87). Although studies suggest that GPAT3 is regulated by PPARγ and PPARδ in keratinocytes (88) and by insulin-mediated phosphorylation in 3T3-L1 adipocytes (36), the regulation and specific contributions of hepatic GPAT3 to glycerolipid synthesis are unknown. The availability of *Gpat1*- and *Gpat4*- knockout mice, however, has allowed us to directly compare them and to delineate the specific roles of each isoform.

The function of GPAT1 in the esterification of fatty acids has been best studied. GPAT1 esterification rates for 16:0-CoA are 3- to 10-times higher than those observed with 18:0-, 18:1-, 18:2n6-, and 18:3n3-CoAs (31,89-91). Examination of the glycerolipid species in *Gpat1*$^{-/-}$ liver have confirmed the preference of GPAT1 for 16:0-CoA, because the absence of GPAT1 results in decreases in the amounts of 16:0 esterified to phosphatidylcholine and phosphatidylethanolamine in membranes from total liver (5) and from liver mitochondria (7). The 16:0 deficiencies at the *sn*-1 position of phosphatidylcholine and phosphatidylethanolamine are compensated for by increases in the content of 18:1 at the *sn*-1 position and of 20:4n6 at the *sn*-2 position.

A second function of GPAT1 is related to *de novo* lipogenesis. This role is implied by the fact that GPAT1's specific activity is low in liver during fasting, in part because of inhibition by AMP-activated kinase (30), and is upregulated transcriptionally when lipogenesis from carbohydrate precursors is enhanced. Similar to acyl-CoA carboxylase and fatty acid synthase, *Gpat1* mRNA, protein, and specific activity increase in response to SREBP1c upregulation, which, in turn, is stimulated by insulin and depressed via LXR by polyunsaturated fatty acids (81). Thus, GPAT1 is markedly elevated in *ob/ob* mice, and a deficiency in *ob/ob* mice of either *Gpat1* itself (32) or of SREBP1c (82) protects against the development of a fatty liver. In addition to promoting the synthesis of TAG, indirect evidence suggests that GPAT1 diverts acyl-CoAs away from CPT1 and β-oxidation, because long-chain acylcarnitines and β-hydroxybutyrate increase in *Gpat1*$^{-/-}$ mice fed an obesigenic diet that is high in sucrose and palm oil (39). Thus, under conditions when the synthesis of fatty acid is elevated, the presence of GPAT1 would ensure that the resulting fatty acids are esterified rather than oxidized. Our current data directly support this idea.

In isolated hepatocytes, incubation with [^{14}C]acetate showed that only the deficiency of GPAT1 blocked the incorporation of *de novo* synthesized fatty acids into glycerolipids. The incorporation was equivalent in control and *Gpat4*$^{-/-}$ hepatocytes and was diminished equally by the fatty acid synthase inhibitor C75. These data suggest that fatty acids synthesized *de novo* from glucose require GPAT1 in order to be incorporated into TAG. Perhaps because of GPAT1's preference for 16:0-CoA, the predominant species synthesized *de novo* by fatty acid synthase, GPAT1 was also

responsible for most of the acetate-derived fatty acid that was incorporated into PL. Inhibition of fatty acid synthesis by C75 had a weaker effect on PL synthesis than it did on TAG synthesis, suggesting that *de novo* synthesized fatty acids may be preferentially directed to TAG storage, consistent with the fact that lipogenesis is upregulated when high carbohydrate intake and insulin concentrations activate SREBP1c. The final step in the synthesis of TAG is catalyzed by DGAT1 and DGAT2. Stable isotope studies show that only DGAT2 incorporates fatty acids synthesized de novo (92).

Because *Gpat1*$^{-/-}$ hepatocytes failed to incorporate label from [^{14}C]acetate into TAG, we concluded that GPAT1 is required for the synthesis of TAG from *de novo* lipogenesis. Confirming this interpretation, after the fast-refeeding protocol to promote hepatic *de novo* lipogenesis, *Gpat1*$^{-/-}$ liver contained 53% less TAG than did controls. Compared to fasted mice, the hepatic TAG content in both refed-control and refed-*Gpat4*$^{-/-}$ mice increased 2- and 3-fold, respectively, but liver TAG content in refed-*Gpat1*$^{-/-}$ mice did not change, indicating that *Gpat1*$^{-/-}$ failed to incorporate *de novo*-derived fatty acid into hepatic TAG. A direct comparison of hepatic β-oxidation revealed that compared to controls, long-chain acylcarnitines and β-hydroxybutyrate in *Gpat1*$^{-/-}$ mice were 3.5- and 2-fold higher, respectively. Thus, when hepatic GPAT1 was absent, the *de novo* synthesized fatty acids were oxidized rather than incorporated into TAG. These data are consistent with our *in vitro* findings and confirm that GPAT1 is required to incorporate *de novo* synthesized fatty acids into TAG and diminish fatty acid oxidation.

In humans, VLDL secretion is stimulated by dietary sugars, and after a high carbohydrate load, *de novo* synthesized fatty acids comprise roughly 37% of plasma VLDL-TAG (93,94). Consistent with a role for GPAT1 in incorporating *de novo* synthesized fatty acids into VLDL, *Gpat1*$^{-/-}$ mice fed a diet containing 60% of calories from sucrose were protected from hypertriglyceridemia and showed diminished VLDL secretion rates (95). After the fasting-refeeding protocol, plasma TAG concentrations in *Gpat1*$^{-/-}$ mice did not change, suggesting that GPAT1 is essential for the postprandial lipemia that is stimulated by carbohydrate feeding. In contrast, plasma TAG in refed control and *Gpat4*$^{-/-}$ mice increased 2 and 3.5-fold, respectively, consistent with the continued presence and function of GPAT1 in using *de novo* synthesized TAG in VLDL.

The absence of either GPAT1 or GPAT4 did not block the incorporation of exogenous fatty acid into TAG or PL. Normal incorporation seems surprising because TAG content in both *Gpat1*$^{-/-}$ and *Gpat4*$^{-/-}$ liver is 40-50% lower than controls (5,15). However, our hepatocytes studies measured TAG synthesis from [^{14}C]palmitate in the absence of insulin. Normally after a 24 h fast, when insulin levels are low, fatty acids released from adipocytes constitute the majority of the fatty acid entering the liver to be stored or incorporated into VLDL-TAG, a process that is not sensitive to plasma insulin levels (93). Under these conditions, fatty acids entering the liver might be preferentially oxidized for energy, and the remaining low GPAT activity would suffice for a minimal demand for TAG synthesis for storage or for VLDL secretion. Consistent with this idea and with our *in vitro* results, liver TAG content was similar in fasting control, *Gpat1*$^{-/-}$ and *Gpat4*$^{-/-}$ mice. After feeding in humans, concomitant with a rise in plasma insulin, both

dietary fatty acids and those derived from *de novo* synthesis are incorporated into TAG (93). Because the TAG content in *Gpat1*$^{-/-}$ liver was lower than in controls after high sucrose refeeding, it is likely that insulin-induced SREBP1c activity drove fatty acid flux toward TAG storage; however, in the absence of GPAT1, the remaining GPAT activity was unable to meet the demand for higher TAG synthesis.

Because *Gpat1*$^{-/-}$ mice fed low or high fat diets for 4 months had a higher content of plasma and liver acylcarnitines and higher concentrations of plasma β-hydroxybutyrate, we had speculated that GPAT1 might normally divert fatty acids away from CPT1 and β-oxidation (39). The present results directly support this hypothesis by showing that, compared to controls, *Gpat1*$^{-/-}$ hepatocytes produced twice as much ASM from [^{14}C]palmitate and that plasma β-hydroxybutyrate and hepatic acylcarnitines were markedly elevated in *Gpat1*$^{-/-}$ mice under both fasted and refed conditions. In contrast, ASM production was similar in *Gpat4*$^{-/-}$ and control hepatocytes under both conditions, indicating that lack of GPAT4 did not increase the use of excess acyl-CoAs for β-oxidation.

In order to directly compare β-oxidation metabolites from the two *Gpat* null genotypes, we investigated acylcarnitines. After a 24 h fast, the hepatic content of long-chain acylcarnitines was equivalent in control and *Gpat4*$^{-/-}$ mice. Confirming the hypothesis that GPAT1 competes with CPT1 for acyl-CoAs and diverts them away from mitochondria, the content of long-chain acylcarnitines in *Gpat1*$^{-/-}$ livers was 3-fold higher than controls. Thus, despite the observation that exogenous fatty acid incorporation into

TAG was unaffected by a deficiency of either GPAT1 or GPAT4, these results further support GPAT1's unique function of diverting fatty acids away from β-oxidation.

These studies clearly differentiate the roles of the major hepatic isoforms, GPAT1 and GPAT4. GPAT1, but not GPAT4, reciprocally regulates hepatic *de novo* glycerolipid synthesis and fatty acid oxidation. In this role, the absence of GPAT1 protects mice from high fat diet- and genetic- induced hepatic steatosis and hepatic insulin resistance (32). Conversely, the increased expression of GPAT1 may contribute to insulin resistance, both by diverting fatty acids away from oxidation and towards glycerolipid synthesis and by increasing lipid intermediates like diacylglycerol and phosphatidic acid which impair hepatic insulin signaling (48,52).

Additional Contributions

This work was supported by National Institutes of Health grants DK56598 (RAC), DK089312 (DMM), DK083157 (AAW), and T32HD057824 (DEC).

Figures

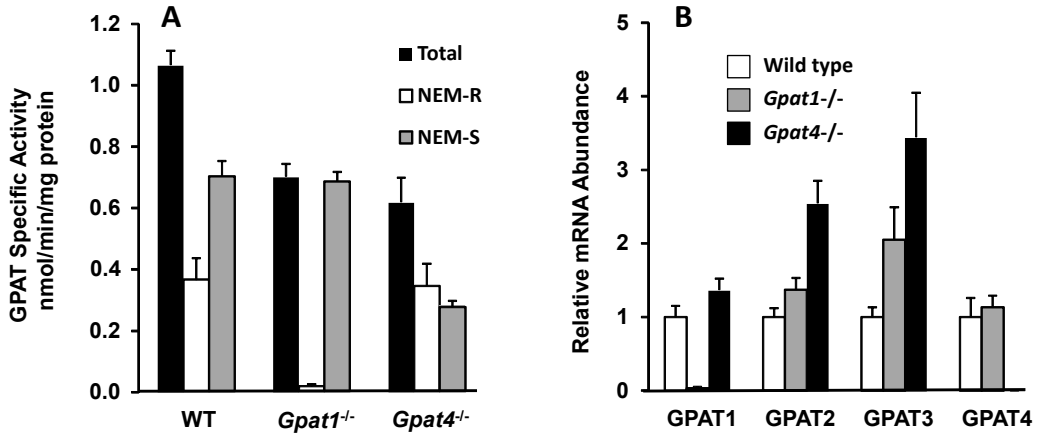

Figure 3.1: GPAT specific activity and mRNA expression in primary hepatocytes from wild type, *Gpat1*$^{-/-}$ and *Gpat4*$^{-/-}$ mice. A) GPAT specific activity was measured in total particulate preparations of primary hepatocytes cultured for 16 h; triplicates from two independent experiments. Total, *N*-Ethylmaleimide-resistant (NEM-R) and sensitive (NEM-S) GPAT specific activities are shown. B) mRNA expression of each GPAT isoform was measured by RT-PCR. Total RNA was obtained from primary hepatocytes in triplicate from two experiments. Data are presented as means ± SE.

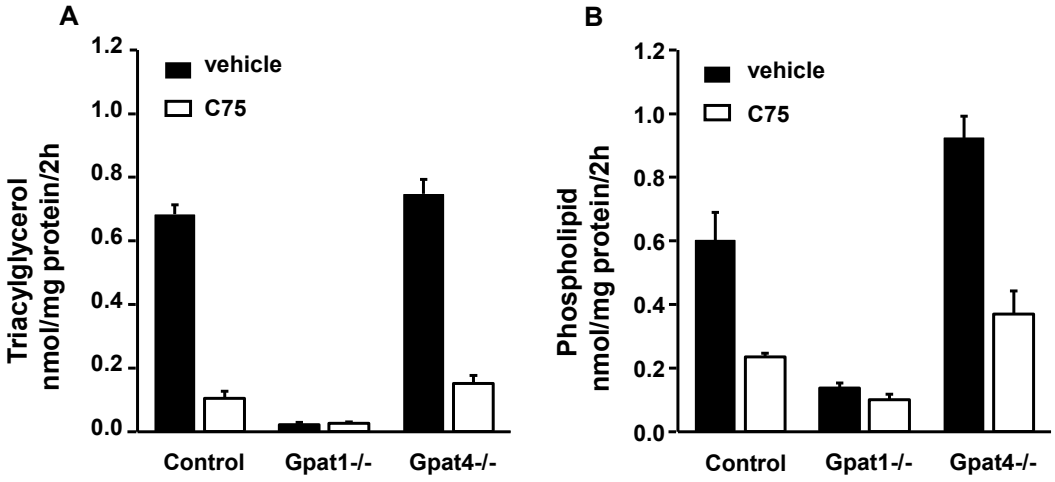

Figure 3.2: *Gpat1*$^{-/-}$ hepatocytes incorporated less [^{14}C]acetate into glycerolipids. Hepatocytes were labeled with 500 μM [1-^{14}C]acetate in the presence or absence of 20 μg/ml C75 for 2 h. [1-^{14}C]acetate incorporation into A) triacylglycerol or B) phospholipids in control, *Gpat1*$^{-/-}$, or *Gpat4*$^{-/-}$ hepatocytes. Data show means ± SE of two experiments performed in triplicate.

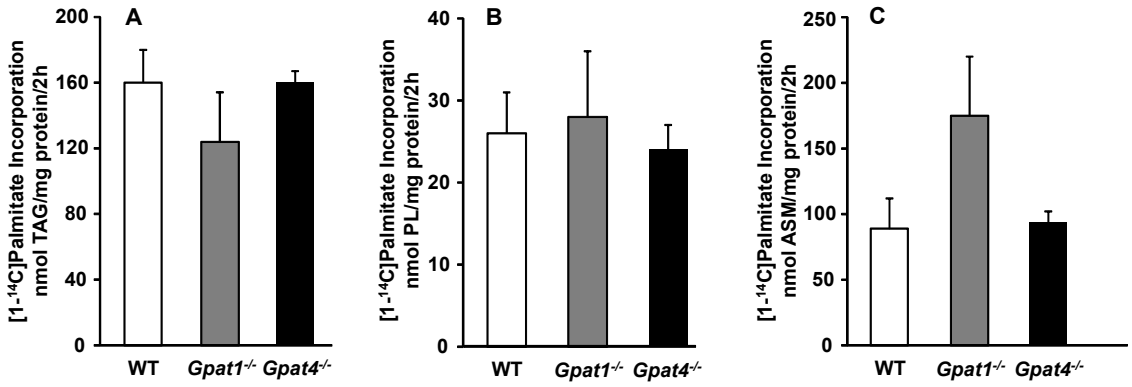

Figure 3.3: GPAT1 was not required for the incorporation of exogenous fatty acid, however β-oxidation was higher in *Gpat1*$^{-/-}$ hepatocytes. Hepatocytes from wild type, *Gpat1*$^{-/-}$ (*G1*$^{-/-}$) or *Gpat4*$^{-/-}$ (*G4*$^{-/-}$) mice were labeled with 500 μM [1-^{14}C]palmitic acid for 2 h. [1-^{14}C]palmitic acid incorporation into A) triacylglycerol, B) phospholipids and C) ASM. Data show means ± SE of two experiments performed in triplicate. D) Comparison of cell media and intracellular (IntraC) ASM. Data show means of one experiment performed in quadruplicate.

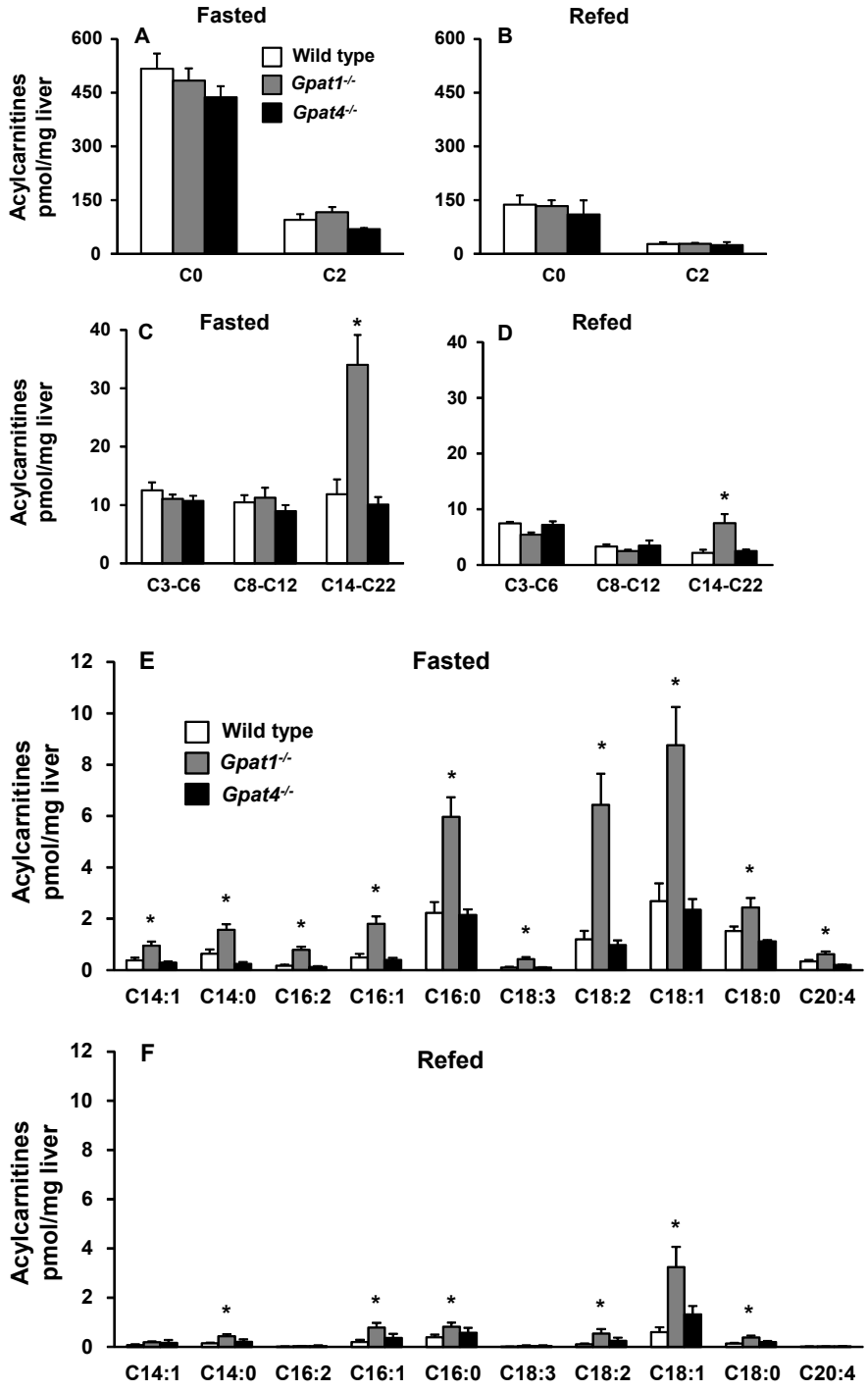

Figure 3.4: Long-chain acylcarnitine content was higher in *Gpat1*$^{-/-}$ liver than controls after a 24 h fast and after 48 h of refeeding. Wild type, *Gpat1*$^{-/-}$, and *Gpat4*$^{-/-}$ mice were fasted for 24 h or fasted for 24 h and then refed with a high sucrose diet for 48 h. Hepatic content of free carnitine (C0), acetylcarnitine (C2) (A and B). Short, medium and long-chain acylcarnitine content of mouse liver (C and D). Major hepatic long-chain acylcarnitine species from mice (E and F). Data are shown as means ± SE. Significant differences are indicated by (*) for genotype and (#) for diet challenge. (*P* <.05, ANOVA) (n=6 diet, genotype).

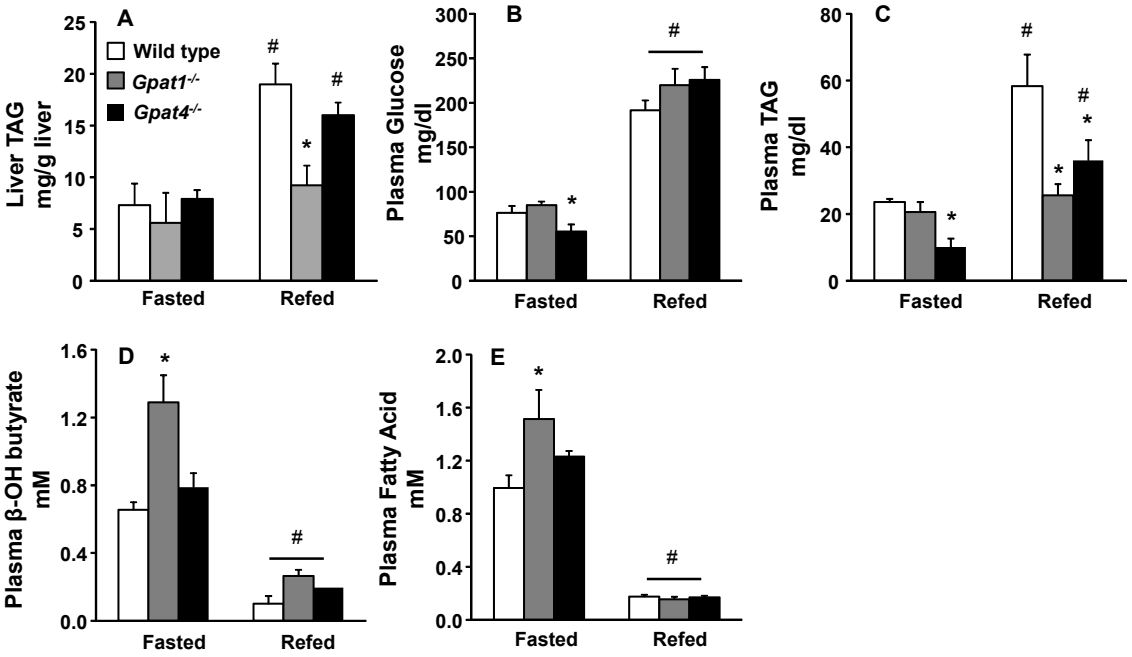

Figure 3.5: Liver and plasma metabolites. Liver TAG content of wild type, *Gpat1*$^{-/-}$, and *Gpat4*$^{-/-}$ mice fasted for 24 h or fasted for 24 h then refed with a high sucrose diet for 48 h. Plasma B) β hydroxybutyrate, C) fatty acid, D) glucose, and E) TAG. Data are shown as means ± SE. Significant differences are indicated by (*) for genotype and (#) for diet challenge. (P <.05, ANOVA) (n=6 diet, genotype).

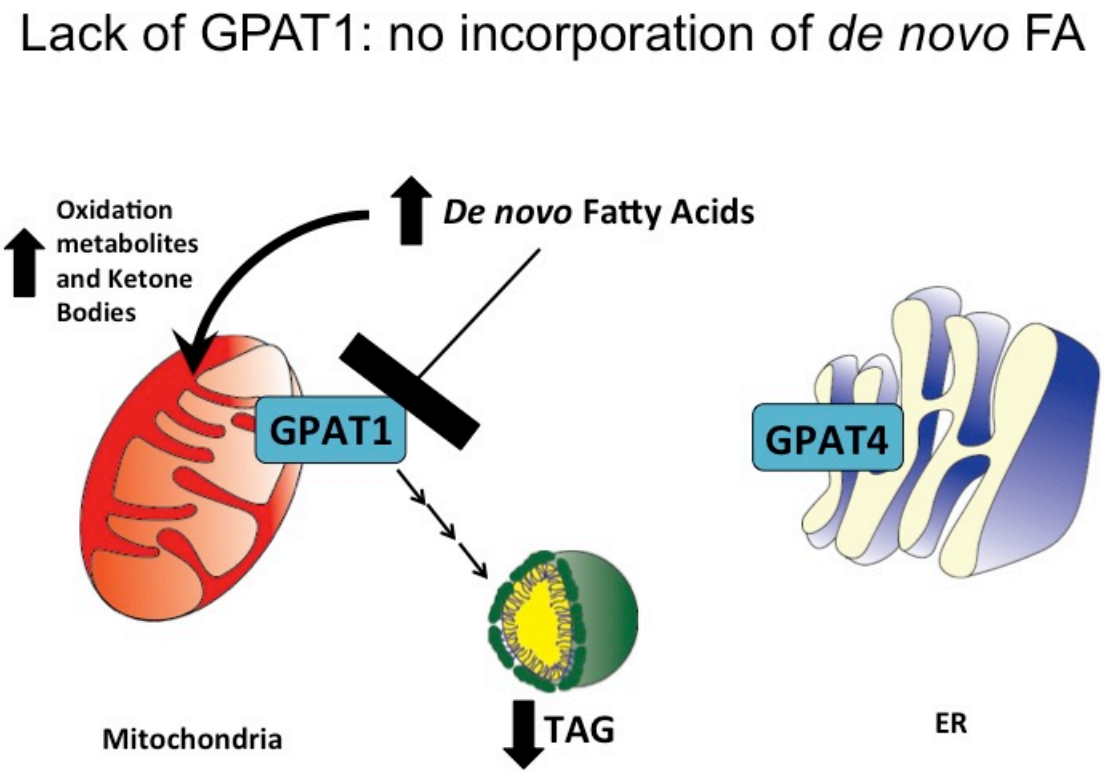

Figure 3.6: GPAT1, but not GPAT4, is required for the incorporation of *de novo* synthesized fatty acids into triacylglycerol and to divert fatty acids away from β-oxidation.

Chapter IV: GLYCEROL-3-PHOSPHATE ACYLTRANSFERASE ISOFORM-4 (GPAT4) LIMITS OXIDATION OF EXOGENOUS FATTY ACIDS IN BROWN ADIPOCYTES[2]

Capsule

Background: GPAT4 is a major GPAT isoform in brown adipose tissue.

Results: Compared to control cells, brown adipocytes lacking GPAT4 oxidize 40% more exogenous fatty acids.

Conclusion: GPAT4 in BAT is required to limit oxidation of exogenous fatty acid.

Significance: The function of each GPAT isoform is tissue-specific and evolved to perform a unique function within a physiological context.

[2] This manuscript has been accepted for publication in the Journal of Biological Chemistry. The citation currently appears as Cooper DE, Grevengoed TJ, Klett EL, and Coleman RA. *J Biol Chem.* Accepted with revision. March 18, 2015.

Summary

Glycerol-3-phosphate acyltransferase-4 (GPAT4) null pups grew poorly during the suckling period and, as adults, were protected from high fat diet-induced obesity. To determine why *Gpat4*$^{-/-}$ mice failed to gain weight during these two periods of high-fat feeding, we examined energy metabolism. Compared to controls, the metabolic rate of *Gpat4*$^{-/-}$ mice fed a 45% fat diet was 12% higher. Core body temperature was 1°C higher after high-fat feeding. Food intake, fat absorption, and activity were similar in both genotypes. Impaired weight gain in *Gpat4*$^{-/-}$ mice did not result from increased heat loss, because both cold tolerance and response to a β3-adrenergic agonist were similar in both genotypes. Because GPAT4 comprises 65% of the total GPAT activity in brown adipose tissue (BAT), we characterized BAT function. A 45% fat diet increased the *Gpat4*$^{-/-}$ BAT expression of PPARα target genes, *Cpt1α, Pgc1α*, and *Ucp1*, and BAT mitochondria oxidized oleate and pyruvate at higher rates than controls, suggesting that fatty acid signaling and flux through the TCA cycle were enhanced. To assess the role of GPAT4 directly, neonatal BAT preadipocytes were differentiated to adipocytes. Compared to controls, *Gpat4*$^{-/-}$ brown adipocytes incorporated 33% less fatty acid into triacylglycerol and 46% more into the pathway of β-oxidation. The increased oxidation rate was due solely to an increase in the oxidation of exogenous fatty acids. These data suggest that in the absence of cold exposure, GPAT4 limits excessive fatty acid oxidation and the detrimental induction of a hypermetabolic state.

Introduction

Glycerol-3-phosphate acyltransferase (GPAT; EC 2.3.1.15) catalyzes the esterification of long-chain acyl-CoAs at the *sn*-1 position of glycerol-3-P and is the initial and rate limiting step for the synthesis of triacylglycerol (TAG) and all the glycerophospholipids. Four mammalian GPAT isoforms, each the product of a separate gene, have been identified, and the phenotypes differ in mice deficient in GPAT1, -3, and -4. Lack of GPAT1 results in lower hepatic TAG content with less palmitate in the *sn*-1 position of phosphatidylcholine and phosphatidylethanolamine, resistance to high fat diet (HFD)–induced insulin resistance (5,6), increased hepatic fatty acid oxidation (6), and resistance to diethylnitrosamine-induced hepatocellular carcinoma (8). GPAT3 contributes nearly 80% of total GPAT activity in white adipose tissue, but GPAT3 deficient mice are not lipodystrophic and gain weight normally when fed a high fat diet (10,11). A mouse deficient in GPAT2 has not been reported, and recent data suggest that GPAT2 may esterify both glycerol-3-P and lysoglycerol-3-P in testis (9). Many of the phenotypic differences in GPAT-null animals are likely due to variation in nutritional regulation and tissue-dependent expression of each GPAT isoform.

Previously called acylglycerol-3-phosphate acyltransferase isoform 6 (AGPAT6) because of its similarity to AGPAT1 and -2, GPAT4 has 66 % amino acid identity to GPAT3 and does not possess AGPAT activity (15). GPAT4 is a major GPAT isoform in liver (12) and is highly expressed in the mammary gland where it is required for development and for the deposition of diacylglycerol and TAG in milk (13). In *Gpat4*$^{-/-}$ liver, compared to controls, total GPAT specific activity and TAG content are 45% lower

(14,15). Mice deficient in GPAT4 are protected from diet and genetically induced obesity, and, compared to controls, their metabolic rate was reported to be 5% higher (5). This metabolic phenotype had been attributed to the absence of a subdermal adipose layer at 12 weeks of age (15). However, it is unclear whether the lack of subdermal adipose in *Gpat4*$^{-/-}$ mice is the cause of or an adaptation to the higher metabolic rate.

In order to determine whether *Gpat4*$^{-/-}$ mice are resistant to adipose tissue accumulation because of a broader influence on energy metabolism and to investigate the mechanism whereby GPAT4-deficient mice are protected from obesity, we characterized the growth and weight gain of littermate control and *Gpat4*$^{-/-}$ mice from birth to 8 weeks of age. Additionally, we evaluated the metabolic changes in female mice after a 4 week 45% fat diet challenge. These studies enabled us to evaluate metabolic changes associated with a shift in dietary substrate before the onset of obesity, and indicated that the mice were hypermetabolic and had excess FA use in brown adipose tissue. Although GPAT4 comprises 65% of the total GPAT activity in BAT, its role in this tissue had not been investigated (12). Our studies provide evidence that the lack of GPAT4 protects mice from obesity because GPAT4 normally limits the oxidation of exogenously provided FA by brown adipocytes.

Results

When dietary fat was the major macronutrient, the growth and weight gain in Gpat4$^{-/-}$ mice were impaired

Gpat4$^{-/-}$ mice were a normal size at birth, but in contrast to the phenotype of mouse pups lacking GPAT1 (5) or GPAT3 (4), at weaning they were smaller than their littermates; by postnatal day 21, *Gpat4$^{-/-}$* weanling mice had gained 25% less weight than controls and were 10% shorter (**Fig 4.1A,B**). Between the second and the fifth week of life, the growth rate of the *Gpat4$^{-/-}$* mice was slower than that of their littermates, but by six weeks of age the growth rates were similar (**Fig 4.1C**). Adult female mice lacking GPAT4 are protected from diet-induced obesity (15), and we wondered whether the growth lag during the suckling period was due to the composition of mouse milk, in which TAG comprises 40 to 55% of total caloric energy (96). To characterize an energy defect specifically associated with high dietary fat, control and *Gpat4$^{-/-}$* mice were fed either a 10% fat (LFD) or 45% fat diet (HFD) for 8 weeks. Weight gain was similar in genotypes fed the LFD. When fed the HFD, control mice became obese and accumulated 3-fold more inguinal adipose tissue (**Fig 4.1D,E**). In contrast, *Gpat4$^{-/-}$* male mice remained lean, and inguinal adipose mass was similar regardless of diet. The lack of adipose tissue accumulation in *Gpat4$^{-/-}$* mice was not due to a defect in TAG synthesis, because GPAT specific activity in inguinal adipose was identical in both genotypes (**Fig 4.1F**). Representative photos illustrate the differences in body size at birth, p17, p28, and 8 weeks of age, and after 8 weeks of consuming the HFD (**Fig 4.1G**). These data suggest that mice lacking GPAT4 grow poorly when fat is the

predominant macronutrient in the diet, both during the suckling period and with high-fat feeding.

GPAT4-deficient mice were hyper-metabolic with high-fat feeding

Our data showing that both suckling *Gpat4*$^{-/-}$ pups and adults fed a high fat diet are consistent with a previous report that the metabolic rate of adult female *Gpat4*$^{-/-}$ mice is 5% higher than controls (15). In order to determine whether the metabolic rate was higher during high-fat feeding, 8 week old control and *Gpat4*$^{-/-}$ mice were fed a 45% HFD for 4 weeks. This short-term HFD allowed us to evaluate the metabolic effects of dietary fat content without the confounding variable of obesity. The metabolic rate of *Gpat4*$^{-/-}$ mice fed the HFD was 12% higher than that of controls, with the major difference occurring primarily during the light cycle (**Fig 4.2A**). Food consumption and physical activity were similar between genotypes (**Fig 4.2B,C**). These findings suggest that the metabolic rate was accelerated in fat-fed *Gpat4*$^{-/-}$ mice.

In the absence of GPAT4, the absorption of dietary TAG was not impaired

It has been estimated that monoacylglycerol acyltransferase in intestinal epithelial cells is responsible for 75% of dietary TAG absorption (42). Although GPAT activity is responsible for the remaining 25%, it is not able to rescue the deficit in fat absorption when monoacylglycerol acyltransferase-2 is absent (42). To determine the importance of intestinal GPAT4 and whether its loss might play a role in the lack of weight gain of high fat-fed *Gpat4*$^{-/-}$ mice, GPAT activity was measured in intestinal mucosa from duodenum, upper and lower jejunum, and ileum. Compared to control

duodenum and upper jejunum, total GPAT specific activities of *Gpat4*$^{-/-}$ mice were 90% and 40% lower, respectively (**Fig 4.2D**). In the lower jejunum, total GPAT specific activity was similar in both genotypes, but in the ileum, the total GPAT specific activity of *Gpat4*$^{-/-}$ mice was 42% higher than that of controls, suggesting over-compensation by another GPAT isoform. Because duodenal GPAT activity in *Gpat4*$^{-/-}$ mice was 90% lower than controls, we wondered whether malabsorption of dietary fat might have reduced weight gain in these mice. However, during the 6 h after an oral fat tolerance test, the amount of TAG accumulation in plasma did not differ between genotypes, showing that the immediate absorption of dietary TAG in *Gpat4*$^{-/-}$ mice was not delayed (**Fig 4.2E**). To assess the impact of GPAT4-deficiency on fat absorption over a longer period of time, mice were housed individually and fed a 60% fat diet for one week. The amount of fecal TAG was similarly low in both genotypes, consistent with normal TAG absorption (**Fig 4.2F**), and lipid staining in the intestinal mucosa was also similar in both genotypes, showing that dietary TAG had not accumulated without being absorbed (**Fig 4.2G**). Taken together, these data confirm that, despite severely depleted GPAT activity in the upper intestine of *Gpat4*$^{-/-}$ mice, TAG absorption remained normal. It appears then, either that the activity of intestinal monoacylglycerol acyltransferase is sufficient for normal fat absorption or, less likely, that the upregulated GPAT activity in the ileum is sufficient to compensate for deficient absorption by the proximal intestine (42).

The increased metabolic rate of Gpat4$^{-/-}$ mice did not occur to maintain body temperature

Consistent with an increase in metabolic rate that is unrelated to increased heat loss, the daytime temperature of *Gpat4*$^{-/-}$ female mice fed a HFD was 1°C higher than controls (**Fig 4.3A**). To determine whether the previously reported lack of subdermal adipose tissue in *Gpat4*$^{-/-}$ mice (5) eliminates a necessary insulating layer, 12 week old control and *Gpat4*$^{-/-}$ mice were challenged with a cold tolerance test. Body temperatures during the challenge were similar between genotypes, suggesting that the insulating subcutaneous fat layer in *Gpat4*$^{-/-}$ mice was sufficient to prevent excessive heat loss (**Fig 4.3B**). In addition, GPAT4 contributes minimally to total GPAT activity in white adipose tissue (**Fig 4.1F**) **(**1). Maintenance of body temperature during cold exposure relies on an animal's ability to minimize heat loss and generate sufficient heat by shivering and BAT-mediated thermogenesis (97). Because BAT is modifiable in rodents, extended periods of exposure to temperatures below thermoneutrality (~30^{o}C) increases the thermogenic capacity of BAT. In order to test thermogenic capacity, we measured the oxygen consumption rate after intraperitoneal injection of the β3-adrenergic agonist, CL316243. If the lack of subdermal adipose tissue were causing excessive heat loss, *Gpat4*$^{-/-}$ mice would increase oxygen consumption more than controls. During the first hour after treatment with CL316243, the VO_2 of both genotypes increased 15-20%, and during the second hour the VO_2 remained 13-16% above baseline (**Fig 4.3C**). The response to CL316243-stimulated VO_2 is consistent with adequate heat retention by *Gpat4*$^{-/-}$ mice. Similarly, the uptake of 2-deoxy[1-^{14}C]glucose into BAT was similar in *Gpat4*$^{-/-}$ mice and controls (**Fig 4.3D**). Because

glucose uptake into BAT depends on the tissue's thermogenic activation (98), the finding that glucose uptake was similar suggests an equivalent degree of thermogenesis at RT in both genotypes. These responses strongly suggest that the hypermetabolic state of the *Gpat4*$^{-/-}$ mouse is not a response to maintain body temperature.

Despite normal FA uptake, Gpat4$^{-/-}$ *BAT contained less TAG than controls.*

Total and NEM-sensitive GPAT activity in *Gpat4*$^{-/-}$ BAT was 65% lower than controls, indicating that GPAT4 is the major GPAT activity in BAT (**Fig 4.4A**). *Gpat4*$^{-/-}$ BAT from mice fed the LFD contained 17% less TAG than controls (**Fig 4.4B**), and BAT from mice fed the HFD contained 25% less TAG than controls. To determine whether FA uptake was reduced in BAT, we measured the uptake of the non-metabolizable 2-Br-[1-^{14}C]palmitate. The uptake of 2-Br-[1-^{14}C]palmitate into BAT was similar in control and *Gpat4*$^{-/-}$ mice (**Fig 4.4C**), indicating that the lack of BAT TAG accumulation in GPAT4-deficient mice did not result from reduced FA uptake.

Thermogenic gene expression increased in BAT from Gpat4$^{-/-}$ *mice fed a HFD*

Fatty acids and acyl-CoAs are endogenous ligands for nuclear transcription factors, including peroxisome proliferator-activated receptors (PPARs) that, when activated, alter cellular energy metabolism (97). Because *Gpat4*$^{-/-}$ BAT contained lower TAG stores but had normal FA uptake, we hypothesized that intracellular FA or acyl-CoAs might influence the expression of PPAR target genes. The expression of the PPARα target genes, *Cpt1α, Pgc1α, Cte1*, and *Ucp1* was similar in control and *Gpat4*$^{-/-}$ mice fed a LFD (**Fig 4.4D**), but when *Gpat4*$^{-/-}$ mice were fed a HFD, *Cpt1α*, *Pgc1α*,

Cte1, and *Ucp1* expression in BAT was 8, 12, 1.7, and 2.5-fold higher, respectively, than in controls (**Fig 4.4D**). These diet-induced changes in gene expression suggest that the lack of GPAT4 might increase intracellular levels of FA or acyl-CoAs in BAT that might then signal to increase PPARα-mediated thermogenesis.

In order to determine whether lack of GPAT4 increased the expression of PPARα target genes in other tissues, heart mRNAs were examined. Despite the fact that in *Gpat4*$^{-/-}$ hearts, total and NEM-sensitive GPAT activities were 25% and 33% lower than in controls, respectively (**Fig 4.4F**), the expression of these PPARα target genes was unaffected in mice fed either diet (**Fig 4.4G**), suggesting that there might be a threshold for GPAT4 activity whereby activity below this level results in upregulation of PPARα target genes.

Mitochondria from Gpat4$^{-/-}$ *BAT oxidized more fatty acid and glucose than controls*

To determine whether the diet-induced increases in PPARα target gene expression led to increased mitochondrial oxidation, we measured oleate and pyruvate oxidation in BAT mitochondria. Mitochondria from control and *Gpat4*$^{-/-}$ mice fed a HFD were incubated with 200 μM [1-^{14}C]oleate and after 30 min [^{14}C]ASM and [$^{14}CO_2$] were measured. Compared to controls, isolated mitochondria from *Gpat4*$^{-/-}$ BAT oxidized 17% and 200% more oleate to ASM and CO_2, respectively (**Fig 4.4H**). Because the amount of [^{14}C]CO_2 was dramatically increased, these data suggested higher TCA cycle flux. To test TCA cycle flux directly, we measured the oxidation of [2-^{14}C]pyruvate. Note that use of [2-^{14}C]pyruvate (rather than [1-^{14}C]), permits the measurement of CO_2

release after a complete cycle through the TCA cycle. When isolated mitochondria were incubated with 200 μM [2-^{14}C]pyruvate, compared to controls, pyruvate oxidation to CO_2 in *Gpat4*$^{-/-}$ BAT was 150% higher (**Fig 4.4I**). Thus, when GPAT4 was absent, TCA cycle flux in BAT mitochondria was enhanced.

Adipogenesis was normal in primary brown adipocytes from Gpat4$^{-/-}$ mice

Because *in vivo* BAT metabolism is altered by the thermal prehistory of the animal (97), the role of GPAT4 in brown adipose was determined in mature brown adipocytes that had been differentiated from primary *Gpat4*$^{-/-}$ pre-adipocytes. Compared to controls, total GPAT specific activity in primary adipocytes lacking GPAT4 was 50% lower (**Fig 4.5A**). To confirm that differentiation was normal, pre-adipocytes from control and *Gpat4*$^{-/-}$ neonates were cultured in differentiation media for 0 (preadipocytes) or 7 (adipocytes) days and TAG accumulation and UCP1 expression were determined. In both control and *Gpat4*$^{-/-}$ preadipocytes at day 0, TAG content and UCP1 expression were undetectable (data not shown). Compared to controls, TAG content in differentiated brown adipocytes lacking GPAT4 was 20% lower (**Fig 4.5B**), and compared to day 0, the amount of UCP1 protein after 7 days of differentiation was markedly higher, but did not differ between genotypes (**Fig 4.5C**). Thus, although GPAT4 is the major GPAT isoform in brown adipocytes, it is not required for normal brown adipocyte differentiation.

GPAT4-deficient brown adipocytes oxidized more exogenous fatty acid than controls

Because GPAT initiates the esterification pathway of complex lipid synthesis, we

hypothesized that GPAT4-deficient brown adipocytes would esterify less acyl-CoA, thereby allowing more acyl-CoAs to be oxidized. To test this hypothesis, control and *Gpat4*$^{-/-}$ cells were incubated for 3 h with [1-^{14}C]oleate. Brown adipocytes lacking GPAT4 incorporated oleate into TAG at a 33% lower rate than controls, and oxidized oleate at a 40% higher rate (**Fig 4.5D,E**). The incorporation of [1-^{14}C]oleate into diacylglycerol and phospholipids was similar in cells from each genotype. These results suggest that when high amounts of FA enter BAT, GPAT4 would normally divert the FA away from β-oxidation and toward esterification into TAG.

Adding exogenous oleate to the culture media of brown adipocytes stimulates thermogenesis and FA oxidation (12). To distinguish between the oxidation of endogenous and exogenous FA pools, a pulse-chase experiment was performed. Differentiated primary brown adipocytes from control and *Gpat4*$^{-/-}$ neonates were labeled with [9,10-^{3}H]oleate for 1.5 h and the specific activity of the stored TAG was calculated. To measure total oxidation, fresh media containing [9,10-^{3}H]oleate was replaced for an additional 1.5 h. To measure endogenous oxidation, labeled cells were switched to media containing unlabeled oleate and exogenous oxidation was calculated by subtracting endogenous oxidation from total oxidation. Total oleate oxidation in *Gpat4*$^{-/-}$ brown adipocytes was 33% higher than controls (**Fig 4.5F**). In both control and *Gpat4*$^{-/-}$ cells, more than 90% of the total oleate oxidized originated exogenously and, compared to controls, *Gpat4*$^{-/-}$ brown adipocytes oxidized exogenous oleate at a rate that was 45% higher (**Fig 4.5F**). The remaining 10% of oxidized oleate originated from endogenous TAG stores and was oxidized at a similar rate by both genotypes. These

results indicate that when brown adipocytes are exposed to a high oleate concentration, they primarily oxidize the exogenous oleate. Because more oleate was oxidized by *Gpat4*$^{-/-}$ cells, it appears that the role of GPAT4 in BAT is to promote oleate storage as TAG and to diminish the availability of exogenous oleate for β-oxidation.

Discussion

The initial report describing *Gpat4*$^{-/-}$ mice suggested that they were protected from diet and genetically-induced obesity, and that their higher metabolic rate at 2 months resulted from an inadequate insulating subdermal adipose tissue layer (5). The higher metabolic rate of *Gpat4*$^{-/-}$ mice was attributed to increased adaptive thermogenesis in BAT. Because subdermal adipose tissue is minimally present until 2 months of age (5), any absence of subdermal adipose in *Gpat4*$^{-/-}$ mice would not explain impaired growth during the suckling period. Our findings suggest a different interpretation: that the increased metabolic rate resulted from the uncontrolled oxidation of excess exogenous FA by brown adipocytes. Supporting this interpretation are data showing that *Gpat4*$^{-/-}$ female mice fed a HFD for 4 weeks had a metabolic rate that was 12% higher and core body temperature 1^{o}C higher than controls. The higher metabolic rate and body temperature that occurs in *Gpat4*$^{-/-}$ mice is inconsistent with adaptive thermogenesis, which is designed to maintain normal body temperature. In addition, mice lacking GPAT4 displayed normal cold tolerance, and they reacted normally to the β3-adrenergic agonist CL316243. Taken together, these data indicate that the hypermetabolic state of *Gpat4*$^{-/-}$ mice is not a response to chronic heat loss.

BAT thermogenesis is activated by cold exposure, β-adrenergic stimulation, and FA in a UCP1-dependent manner (99,100). UCP1 is a gated pore that, when activated, permits the transport of protons across the inner mitochondrial membrane, thereby uncoupling the electron transport from ATP production (101). Active BAT replenishes its intracellular lipid stores via uptake of FA from plasma (102,103). Our data suggest

that GPAT4 is not only responsible for maintaining BAT TAG stores, but also for regulating the use of FAs by BAT.

In addition to their metabolic roles in energy metabolism, FAs and acyl-CoAs derived from exogenous FAs or from the lipolysis of endogenous pools of TAG, act as ligands for the PPAR family of nuclear transcription factors, which have broad effects on cellular energy metabolism (104). In HFD-fed *Gpat4*$^{-/-}$ mice, the increased mRNA abundance in BAT of the PPARα target genes, *Cpt1α*, *Pgc1α*, *Cte1*, and *Ucp1*, and the increased rate of oleate oxidation suggests an exogenous source of PPAR ligands. Lack of GPAT4, an enzyme present on the endoplasmic reticulum that is responsible for 65% of the initial esterification of glycerol-3-P in BAT, might be expected to markedly diminish the rate of glycerolipid synthesis and allow more acyl-CoAs to enter the mitochondrial matrix for β-oxidation. Additionally, because exogenous FAs entering brown adipocytes are effective PPARα ligands (105), the diminished capacity for FA esterification would allow FAs to be diverted to signaling pathways. This interpretation is supported by data showing that GPAT4$^{-/-}$ primary brown adipocytes oxidized exogenous, but not endogenous, oleate at a higher rate than controls; thus, the lipid signals in *Gpat4*$^{-/-}$ BAT were probably either exogenous FAs or metabolites derived from FA oxidation.

When the thermogenic effects of norepinephrine are blocked by the β-adrenergic receptor antagonist, propranolol, thermogenesis in brown fat cells can be stimulated by exogenous oleate (99), suggesting that exogenous FA can be oxidized independent of

lipolytic stimuli. Consistent with these observations, when primary brown adipocytes were incubated with [^{3}H]oleate, approximately 90% of the oxidized FA originated exogenously. TAG turnover in working hearts is similar (106); the entry of high amounts of exogenous FA diminishes use of stored TAG for energy. Because the lack of GPAT4 in brown adipocytes resulted in a 45% higher rate of exogenous FA oxidation than in control cells, GPAT4 appears to limit FA availability for FA-induced thermogenesis. Importantly, in GPAT4-deficient primary hepatocytes, oxidation of exogenously derived FA is normal (107), suggesting that the mechanism whereby GPAT4 limits exogenous FA oxidation is specific to BAT and likely involves the FA-activated protein, UCP1.

In brown adipocytes, maximal thermogenesis can be stimulated independently by oleate and by norepinephrine, but co-treatment is not synergistic (99), suggesting that FA-induced thermogenesis and cold-activated thermogenesis occurs through the same mechanism. Although limiting cold-activated thermogenesis would be counterproductive, preventing the occurrence of thermogenesis induced by the presence of excess exogenous FAs would ensure optimal metabolic efficiency. The abnormal thermogenesis that occurred with high fat feeding resulted in poor growth during the suckling period and a hypermetabolic phenotype in adults. These consequences suggest that in BAT GPAT4 normally limits the oxidation of exogenous FAs, particularly when increased thermogenesis would be inappropriate. Most studies find that high fat feeding increases *Ucp1* mRNA and protein content, although the magnitude of the increases are variable and do not correlate with either the percent of dietary fat or the duration of the fat feeding (108). The idea that excess calories might

provoke an increase in BAT-mediated energy wasting has seemed unlikely in an evolutionary sense, and the variability of the effect does not support it as a major feature of fat feeding. However, the findings that *Gpat4*$^{-/-}$ pups consuming high fat milk grow poorly and that adult *Gpat4*$^{-/-}$ mice fed a HFD are hypermetabolic strongly suggest that, in the absence of cold exposure, GPAT4 is required to limit excessive oxidation of exogenous FAs. When this limitation is absent, FA-induced thermogenesis induces a hypermetabolic state that is detrimental to the animal.

Experimental Procedures

Materials

Type I collagenase was from Worthington Biochemical Corporation. [2-^{14}C]Pyruvic acid, [1-^{14}C]oleic acid, and [9,10-^{3}H]oleic acid were purchased from PerkinElmer Life Sciences. Silica G gel plates were from Whatman. Tissue culture plates were from BD Biosciences, and media were obtained from Invitrogen. Sigma was the source of all other chemicals, unless otherwise indicated.

Animal care

Animal protocols were approved by the University of North Carolina at Chapel Hill Institutional Animal Care and Use Committee. Mice were housed in a pathogen-free barrier facility on a 12-h light/dark cycle with free access to water and food (Prolab 5P76 Isopro 3000; 5.4% fat by weight). *Gpat4*$^{-/-}$ mice have been backcrossed at least eight times onto a C57BL6/J background. *Gpat4*$^{-/-}$ mice were compared to littermate controls, all born to heterozygous dams since homozygous females produce milk that is deficient in TAG (5). Unless noted in the figure legends, female mice were used. At 8 weeks of age, littermate controls and *Gpat4*$^{-/-}$ mice were either fed a control diet containing 10% kcal from fat or a matched high fat diet containing 45% kcal from fat, for either 4 or 8 weeks (Research Diets D12450H and D12451, respectively). Body weights were measured weekly. Using a BAT10 thermometer with rectal probe attachment (Physitemp Instruments, Inc.), rectal temperature was measured between 10AM-12PM. To determine fecal TAG content, control and *Gpat4*$^{-/-}$ mice of both sexes were housed individually and fed a diet containing 60% kcal from fat (Research Diets, D12452).

Before collection of blood or tissues, food was removed from mouse cages for 4 hours, and mice were anesthetized with 250 mg/kg Avertin unless otherwise stated. Body composition was determined with a 7T Bruker PharmaScan MRI system (Bruker BioSpin Corporation). After the MRI, mice were placed in individual TSE Lab Systems metabolic cages (TSE Systems International Group) for 72 h to measure metabolic performance by indirect calorimetry. To allow mice to acclimate, data were collected after the first 24 h in the metabolic cages. Using the Weir equation (REE=[3.9(VO_2) + 1.1(VCO_2)]1.44]), energy expenditure was calculated and normalized to the lean body mass of each mouse. Before cold tolerance tests, 12 week old control and *Gpat4*$^{-/-}$ mice fed a 10% fat diet for 4 weeks were fasted for 4h. Mice were placed into individual cages without food or bedding in a 4^{o}C cold room. Rectal temperatures were measured at 0, 1, 2, 3 and 4 h. To measure VO_2 in response to β-adrenergic stimulation, 12 week old control and *Gpat4*$^{-/-}$ mice fed a 10% fat diet for 4 weeks were placed into metabolic cages (TSE Systems International Group). Mice were transferred to TSE cages at 7AM and acclimated until 10AM. Baseline O_2 consumption measurements were collected from 10AM-1PM. Mice were injected intraperitoneal with 5 mg/kg CL316243 at 1PM with measurements collected until 4PM.

GPAT Activity

After the diet challenge, tissues from control and *Gpat4*$^{-/-}$ mice were excised and frozen in liquid N_2, and stored at -80^{o}C until further use. To obtain intestinal mucosa, intestines were resected, flushed with ice-cold phosphate-buffered saline (PBS), divided into four equal sections, and longitudinally dissected to expose the mucosa which was

scraped using a clean microscope slide. One hundred milligrams of tissue was homogenized in ice-cold Medium I buffer (250 mM sucrose, 10 mM Tris, pH 7.4, 1 mM EDTA, 1 mM dithiothreitol) using 10 up-and-down strokes of a Potter-Elvehjem homogenizer. Total membranes were isolated by centrifuging the homogenate at 100,000 x g for 1 h. GPAT initial rates were measured with 800 μM [^{3}H]glycerol-3-phosphate, and 82.5 μM palmitoyl-CoA (109). The reaction was initiated by adding 10 μg (cells) or 5-50 μg (tissue) of membrane protein after incubating the membrane protein on ice for 15 min in the presence or absence of 2 mM *N*-ethylmaleimide (NEM), which inactivates GPAT isoforms 2, 3, and 4. NEM-resistant activity was calculated by subtracting NEM-sensitive activity from total activity. The reaction products were extracted into $CHCl_3$, dried under N_2, resuspended in 4 mLs Cytoscint and counted on scintillation counter. NEM-resistant activity (GPAT1) was calculated by subtracting NEM-sensitive activity from total activity.

Measurement of Acute Lipid Absorption

Twelve-week old control and *Gpat4*$^{-/-}$ mice were fasted for 4 h, anesthetized with isoflurane gas after which 200 μL of 15% Tyloxapol was injected into the retroorbital plexus to inhibit lipoprotein lipase activity and prevent TAG clearance by peripheral tissues (110). Fifteen minutes after the Tyloxapol injection, blood was collected for baseline TAG measurement, and mice were gavaged with 200 μL olive oil. Blood was collected via tail nick at 1, 2, 4, and 6 h after gavage. Plasma TAG was measured colorimetrically (Stanbio).

Lipid Extraction and TAG Measurement in Feces and Brown Adipose tissue and cells

Feces were collected, pulverized under liquid nitrogen, and extracted by the Folch method (111). Lysates from brown adipose and primary brown adipocytes were extracted similarly. Chloroform extracts were dried under N_2 gas and resuspended in 200 µL tert-butanol:methanol:Triton X-100 (3:1:1, v:v:v). TAG was determined as described above.

Osmium Tetroxide Staining in Small Intestine

The small intestine was resected, flushed with ice-cold PBS and divided into 3 equal sections. Sections were fixed in 1.5% glutaraldehyde, neutral lipids were stained in 2% osmium tetroxide (112), and visualized using light microscopy.

2-Br-[1-^{14}C]palmitate and 2-Deoxy[1-^{14}C]glucose Uptake

To determine 2-Br-[1-^{14}C]palmitate uptake, anesthetized mice were injected retroorbitally with 200 µL of 1% FA-free BSA solution containing 2 µCi 2-Br-[1-^{14}C]palmitate. To determine 2-deoxy[1-^{14}C]glucose uptake, 200 µL of sterile PBS containing 2 µCi 2-deoxy[1-^{14}C]glucose was injected intraperitoneal. For both experiments, blood was collected via tail nick 5 min after injection. Thirty minutes after injection, tissues were excised, weights recorded, and snap-frozen in liquid N_2. Tissues were homogenized in 1 mL water with a blade homogenizer. Aliquots of 250 µL tissue homogenates and 3 mL Ecolite were mixed in scintillation vials with radioactivity counted by a scintillation counter. All measurements were performed in duplicate, and data were expressed as DPM/g tissue/DPM in 5 µL plasma 5 min after injection/30 min.

RNA Extraction and RT-PCR

Extraction of total RNA, cDNA synthesis, and RT-PCR were performed using primer sequences and data normalization as described (113).

Mitochondrial Isolation, and Fatty Acid and Pyruvate Oxidation

BAT from control and *Gpat4*$^{-/-}$ mice fed a 45% fat diet were excised and mitochondria were isolated (113) and resuspended in mitochondrial isolation buffer containing 1 mM EDTA, 250 mM sucrose, 10 mM Tris-HCl pH7.8 and Complete protease inhibitor (Roche Biosciences). Forty micrograms of mitochondrial protein was incubated at 37°C with 200 μM [1-^{14}C]oleic acid or [2-^{14}C]pyruvic acid in a sealed tube. Note that use of [2-^{14}C]pyruvate (rather than [1-^{14}C]), permits the measurement of CO_2 release after a complete cycle through the TCA cycle. After 30 min, the reaction was stopped with 100 μL 70% perchloric acid and CO_2 was liberated. CO_2 was trapped in 250 μL microcentrifuge tubes containing 1M NaOH by incubating the tubes at RT for 1 h with shaking. The acidified media were incubated overnight with 15% BSA and then centrifuged at 14,000 x g for 20 min. Aliquots of the supernatant were counted for radiolabeled acid soluble metabolites (ASM), a measure of incomplete FA oxidation. Use of [2-^{14}C]pyruvate (rather than [1-^{14}C]), permits measurement of the release of [$^{14}CO_2$] after a complete cycle through the TCA cycle.

[1-^{14}C]Oleate and [9,10-^{3}H]Oleate Incorporation, Oxidation, and Lipid Extraction in Primary Brown Adipocytes

Primary brown adipocyte precursors were isolated, cultured, and differentiated as described previously (114). After isolation, cells were split twice to increase cell number and all experiments were performed at passage 2. Sixteen hours before labeling, differentiation media was changed to pre-labeling media (DMEM, 1 g/L glucose, 10 mM HEPES, 10 % FBS). Cells were incubated for 3 h with 1 mL of labeling media (DMEM, 10 mM HEPES, 1 g/L glucose, 0.25% FA-free BSA, 1 mM carnitine) containing 500 μM [1-^{14}C]oleic acid. To distinguish between exogenous and endogenous FA oxidation, cells were incubated for 1.5 h with labeling media containing 500 μM [9,10-^{3}H]oleic acid. Specific activity of brown adipocyte TAG stores was determined by dividing the radioactive counts in TAG by the nmol of TAG in brown adipocytes (DPM/nmol TAG). In parallel plates, media containing 500 μM oleic acid or 500 μM [9,10-^{3}H]oleic acid was replaced for an additional 1.5 h. In media from cells that were given media that containing unlabeled oleic acid, the oxidation metabolites recovered were from endogenous TAG stores (endogenous FA). In the media of cells given labeling buffer containing [9,10-^{3}H]oleic acid, radioactive oxidation metabolites were considered to represent total FA oxidation. The amount of exogenous FA oxidation was calculated by subtracting the amount of endogenous FA oxidation from total FA oxidation. Radioactive oxidation metabolites in the media were extracted and measured as described above. Cells were washed with pre-warmed PBS containing 1% BSA before lipids were extracted (84). Lipid extracts and standards were separated by thin layer chromatography on Partisil LK5D Silica gel plates in a two-phase system: chloroform:

methanol: ammonium hydroxide (65:25:4, v/v/v) run to 50% of the plate, then air dried and run in heptane: isopropyl ether: acetic acid (60:40:4) to the top of the plate. Authentic lipid standards were visualized by iodine staining. ^{14}C-labeled lipids were quantified with a Bioscan AR-2000 Imaging Scanner. [^{3}H]Labeled lipids were scraped from thin-layer chromatography plates, transferred to scintillation vials and counted.

Statistics

Data represent means ± standard error of the mean of at least three independent experiments performed in triplicate unless otherwise indicated. *In vitro* models were analyzed by Student's t-test comparing each genotype to controls. *In vivo* models were analyzed by two-way analysis of variance and post-hoc comparisons of diet conditions within each genotype. Data were considered significant with $p < 0.05$.

Additional Contributions

We thank Vicky Madden (UNC Microscopy Core) for her assistance with intestinal staining and imaging and Kunjie Hua (UNC Animal Phenotyping Core) for operation of indirect calorimetry cages. We appreciate the thoughtful advice of Dr. P. Kay Lund, Dr. Kimberley Buhman, and Ms. Amanda Mah.

This work was supported by National Institutes of Health Grants DK56598 (RAC), K08DK090141 (ELK), and DK56350 (University of North Carolina Nutrition Obesity Research Center), and by a predoctoral grant from the American Heart Association 13PRE16910109 (TJG).

Figures

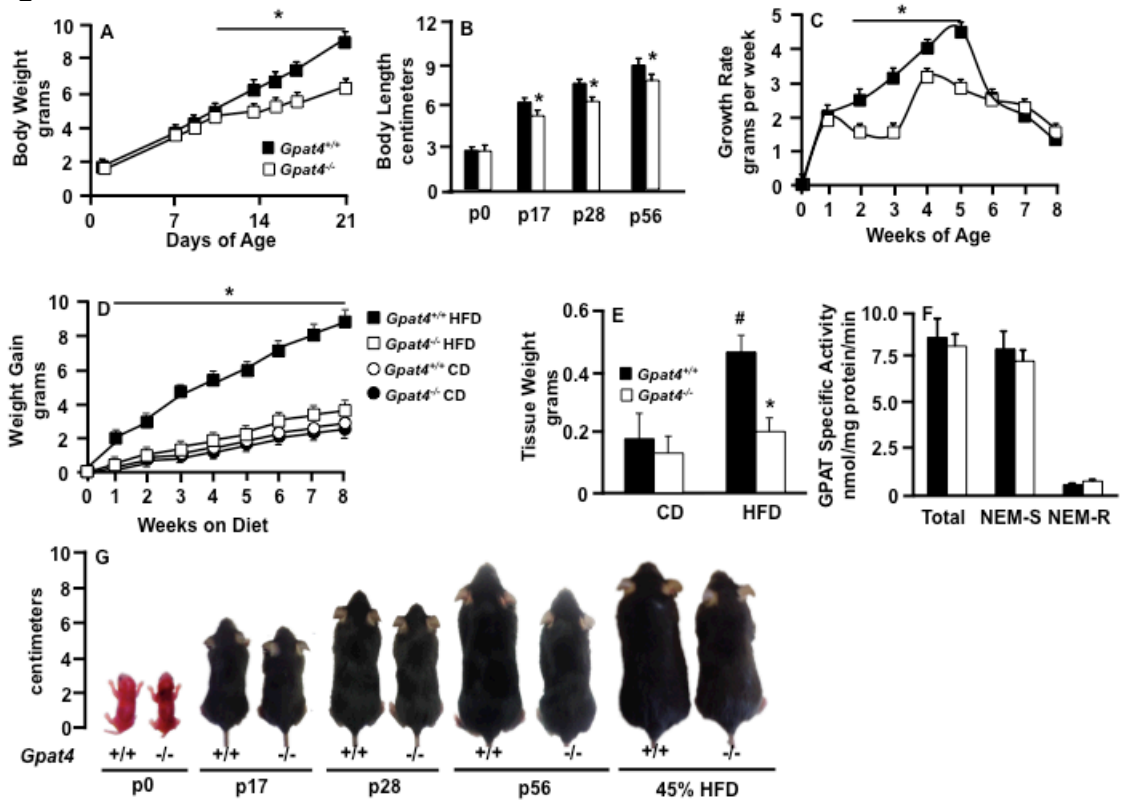

Figure 4.1: When dietary fat was the predominant macronutrient in the diet, *Gpat4*$^{-/-}$ mice gained less weight and were shorter than controls. *A-C,* Growth and weight gain of control littermate and *Gpat4*$^{-/-}$ male mice were characterized from birth until 8 weeks of age. *A,* Weight gain during nursing, *B*, total body length at birth (p0), postnatal day 17 (p17), postnatal day 28 (p28), and 8 weeks of age (p56). *C*, Weekly growth rates of control littermate and *Gpat4*$^{-/-}$ male mice from birth to 8 weeks of age, n=20-35. *D-F,* Control and *Gpat4*$^{-/-}$ male mice were fed a 10% fat (CD) or 45% fat diet (HFD) for 8 weeks. *D,* Weight gain and *(E)* inguinal adipose tissue mass, n=6 per genotype, diet. *F,* Total, *N*-ethylmaleimide sensitive, and *N*-ethylmaleimide resistant GPAT specific activity, n=6 per genotype. *G,* Representative photographs of control littermate and *Gpat4*$^{-/-}$ male mice at p17, p28, 8 wks old and when fed a HFD for 8 wks. Data are presented ± SEM. *p<.05, ANOVA

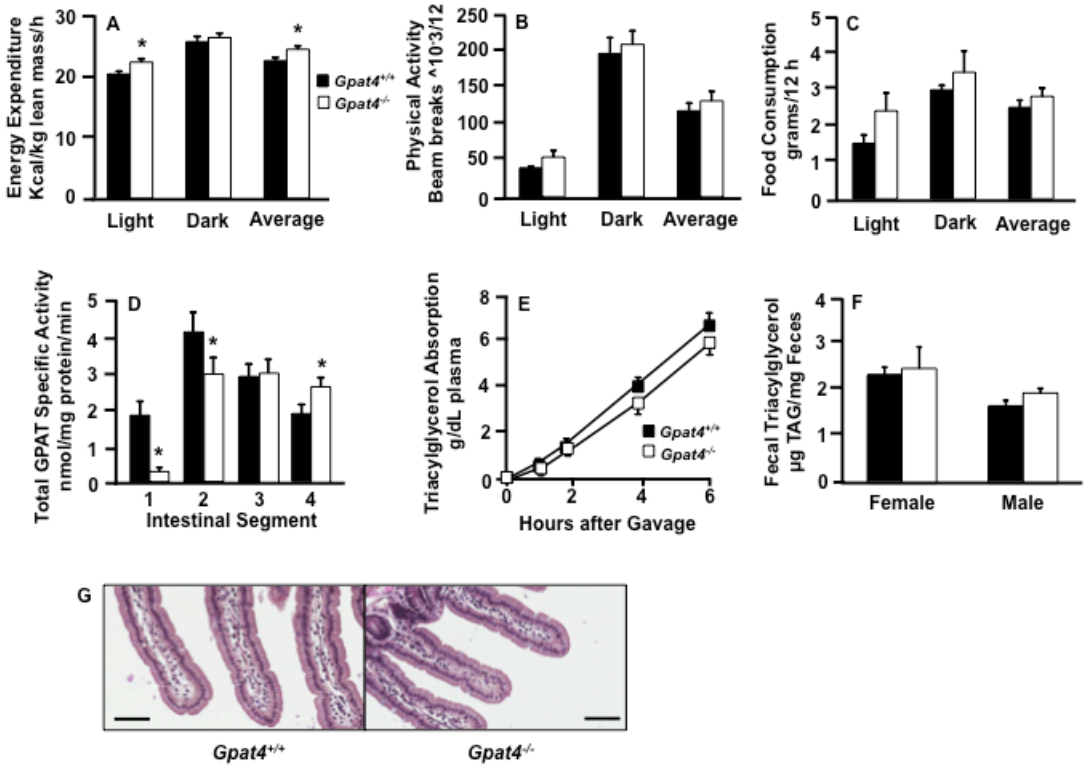

Figure 4.2: When fed a high-fat diet, *Gpat4*$^{-/-}$ mice were hypermetabolic. *A-C*, Energy expenditure, physical activity, and food consumption in female control and *Gpat4*$^{-/-}$ mice fed a 45% fat diet for 4 weeks, n=6. *D,* Total membrane preparations were obtained from littermate control and *Gpat4*$^{-/-}$ female mice fed a 10% fat diet for 4 weeks. Total GPAT specific activities were reported in four equal sections of the small intestine. *E,* Female control and *Gpat4*$^{-/-}$ mice fed a 10% fat diet for 4 weeks were gavaged with 200 µL olive oil. Fifteen minutes prior to gavage, 500 mg/kg Tyloxapol was injected into the retroorbital plexus (to inhibit triacylglycerol clearance by peripheral tissues). Blood was collected at 0, 1, 2, 4, and 6 h after gavage and plasma TAG were measured, n=5. *F,* Fecal TAG content of littermate control and *Gpat4*$^{-/-}$ mice of both sexes. Mice were individually housed and fed a diet containing 60% kcal from fat for 7 days, n=5. *G,* Intestines from control and *Gpat4*$^{-/-}$ female mice fed a 45% HFD were cut into three equal sections, fixed in 1.5% glutaraldehyde, stained in 2% osmium tetroxide and visualized by light microscopy, n=4. Data are presented ± SEM. *p<.05, ANOVA.

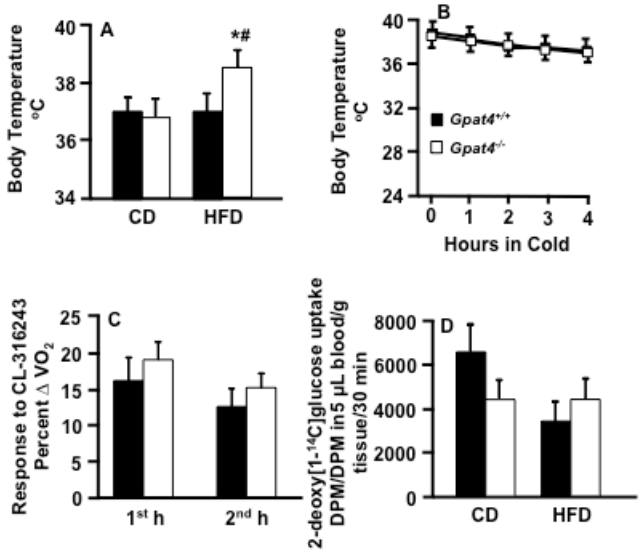

Figure 4.3: GPAT4-deficient mice produce excess heat without constitutive heat loss. GPAT4-deficient mice release excess heat without constitutive heat loss. *A,* Daytime body temperature of female *Gpat4*$^{-/-}$ mice fed a 10% fat (CD) or 45% fat diet (HFD) for 4 weeks. Rectal temperature was measured between 10AM and 12PM, n=6 per diet/genotype*. B,* Body temperature of fasted control and *Gpat4*$^{-/-}$ female mice exposed to 4^{o}C for 4 h, n=5*. C,* Oxygen consumption rate in control and *Gpat4*$^{-/-}$ female mice after injection of CL-316243 (5 mg/kg), n=5*. D,* 2-Deoxy[1-^{14}C]glucose uptake in BAT from control and *Gpat4*$^{-/-}$ female mice fed a 10% or 45% fat diet for 4 weeks, n=5-6. Data are normalized to tissue weight and radioactive counts in 5 µL plasma 5 min after i.p. injection. Data are presented ± SEM. *p<.05 genotype, #p<.05 diet, ANOVA.

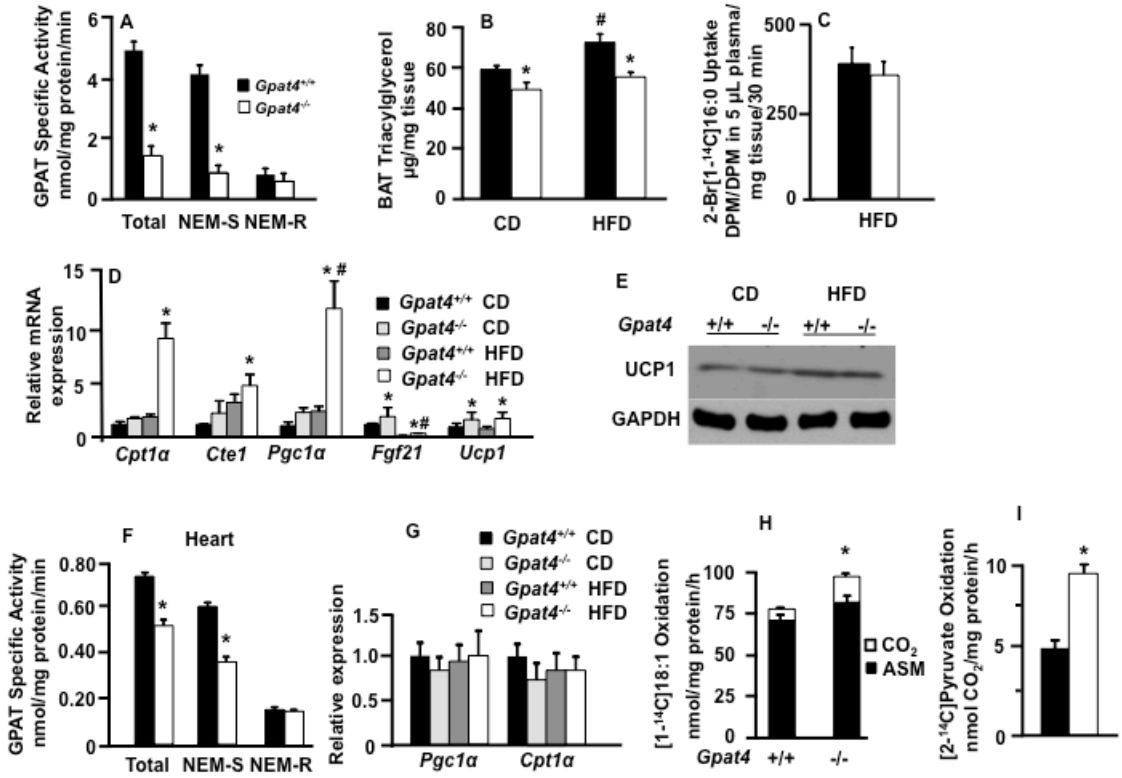

Figure 4.4: BAT in *Gpat4*$^{-/-}$ mice had an increased oxidative capacity. *A-F,* Control littermate and *Gpat4*$^{-/-}$ female mice were fed a 10% fat (CD) or 45% fat diet (HFD) for 4 weeks. *A,* Total, *N*-ethylmaleimide sensitive and *N*-ethylmaleimide resistant GPAT specific activity in BAT, n=6 per genotype. *B,* BAT triacylglycerol content, n=6 per diet/genotype. Thirty minutes after retroorbital injection of 2 µCi 2Br-[1-^{14}C]palmitate, *(C)* 2Br-[1-^{14}C]palmitate uptake into BAT was measured, n=5-6. Data are normalized to tissue weight and radioactive counts in 5 µL plasma 5 min after retroorbital injection. *D,* mRNA expression of oxidation-related genes, n=6. Data are normalized to the expression of 36B4. *E,* Ucp1 protein levels. *F and G,* GPAT specific activity and mRNA expression of oxidation-related genes in heart. *H)* BAT mitochondrial [1-^{14}C]oleic acid oxidation to acid soluble metabolites (ASM) and carbon dioxide (CO_2) and *(I)* [2-^{14}C]pyruvic acid oxidation to CO_2, n=4. Data are presented ± SEM. *p<.05 genotype, #p<.05 diet, ANOVA.

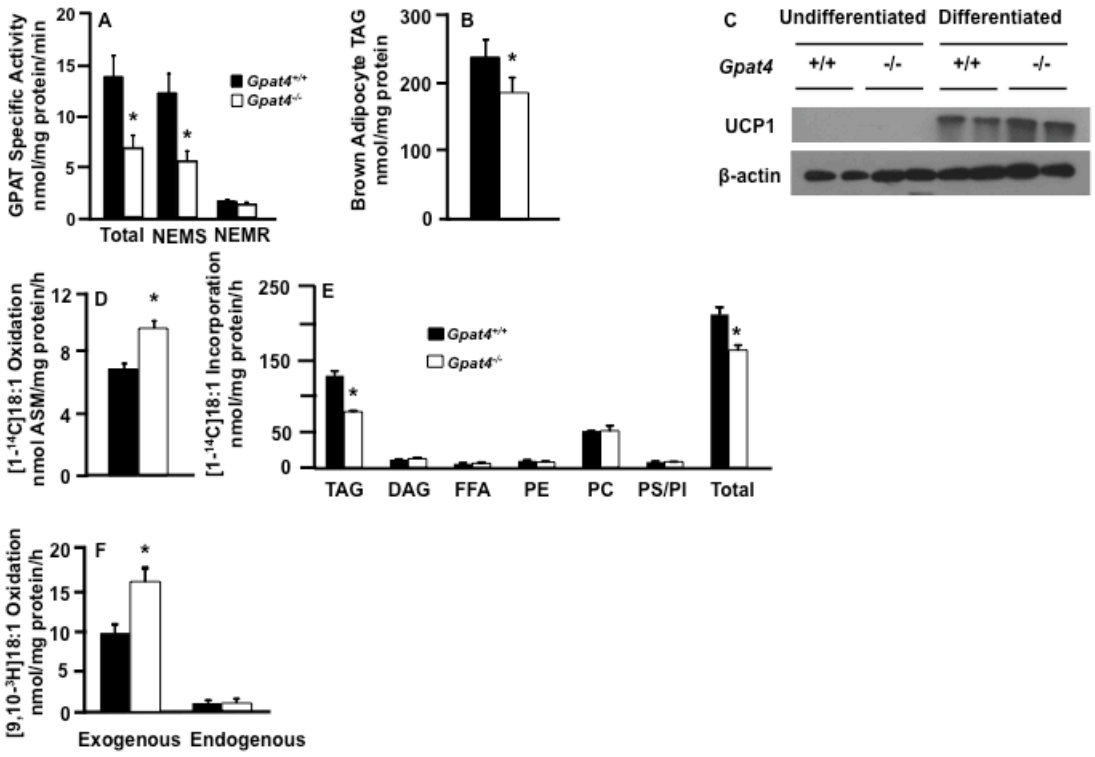

Figure 4.5: Primary Brown Adipocytes lacking GPAT4 oxidize 46% more fatty acid than controls. *A-F,* Brown adipocyte precursors were isolated from littermate control and *Gpat4*$^{-/-}$ neonates, cultured, and differentiated to mature brown adipocytes. *A,* GPAT specific activity *and (B)* TAG content, n=3-6. *C,* Ucp1 protein levels in undifferentiated and differentiated brown adipocytes. *D and E,* Differentiated brown adipocyte precursors from control and *Gpat4*$^{-/-}$ neonates were labeled with 500 μM [1-^{14}C]oleic acid for 3 hours. Media were collected and *(D)* acid soluble metabolites (ASM) were extracted. Cellular lipids were extracted in CHCl3:MeOH and separated by TLC to quantify [1-^{14}C]oleic acid incorporation into *(E)* glycerolipids. Differentiated brown adipocytes from control and *Gpat4*$^{-/-}$ neonates were incubated in the presence of *(F)* 500 μM [9,10-^{3}H]oleic acid for 1.5 h (total fatty acid oxidation) or 500 μM [9,10-^{3}H]oleic acid for 1.5 h followed by 500 μM oleate for 1.5 h (endogenous fatty acid oxidation). Exogenous fatty acid oxidation rate was calculated by subtracting the endogenous fatty acid oxidation rate from the total fatty acid oxidation rate, n=4-6 animals per genotype across 3 independent experiments. Data are presented ± SEM. *p<.05, student's T-test.

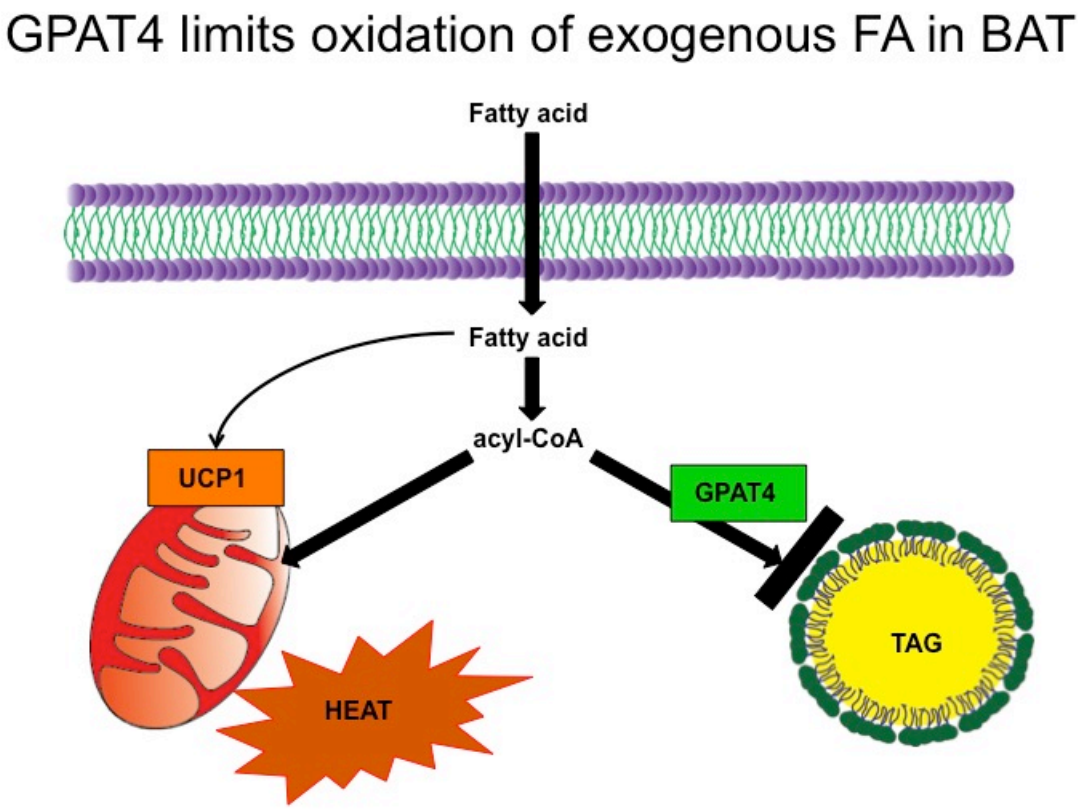

Figure 4.6: GPAT4 limits the oxidation of exogenous fatty acids in brown adipocytes. Under normal conditions, GPAT4 diverts exogenous fatty acids toward triacylglycerol (TAG) storage. In the absence of GPAT4, those fatty acids are available for oxidation and to activate UCP1 to produce heat.

Chapter V: SEIPIN IS AN EVOLUTIONARILY CONSERVED REGULATOR OF GLYCEROL-3-PHOSPHATE ACYLTRANSFERASE (GPAT) – IN PROGRESS

Summary

Loss-of-function mutations of Seipin (also known as Berardinelli-Seip Congenital Lipodystrophy 2/BSCL2) cause the most severe form of human lipodystrophy. Seipin can also regulate the formation and/or expansion of lipid droplets (LDs). Recent studies have implicated Seipin in the metabolism of phosphatidic acid, however, the molecular function of Seipin has remained obscure. Here, we identify physical and functional interactions between Seipin and glycerol-3-phosphate acyltransferase (GPAT) isoforms that are located on the endoplasmic reticulum (Gat1 in yeast and GPAT3/4 in mammals); this interaction is evolutionarily conserved. In Seipin-deficient yeast, mammalian cells, and in tissues from *Bscl2*$^{-/-}$ mice GPAT specific activity is significantly increased. The lack of Seipin changed GPAT kinetics by increasing Vmax and decreasing Km, suggesting an increased affinity for GPATs substrates, glycerol-3-phosphate and 16:0-CoA. During the first 12 h of differentiation, Seipin's regulation of GPAT kinetics was essential to prevent an increase in intracellular PA levels. Because Seipin deficiency impairs adipogenesis and alters lipid droplet morphology, we investigated the role of GPAT in mediating these functions. When GPAT was overexpressed in yeast or mammalian cells, lipid droplets were larger and fewer in number than control cells, suggesting that increased GPAT activity was sufficient to recapitulate the effects of Seipin deficiency on LD morphology. In contrast, although the

overexpression of GPAT1 and GPAT4 increased NEM-R and NEM-S GPAT activity, respectively, the overexpression of these isoforms did not block adipogenesis. We hypothesize that the overexpression of GPAT3 will block adipogenesis (Experiments will be completed at time of dissertation defense). Taken as a whole, these results identify Seipin as an evolutionally conserved regulator of microsomal GPAT and suggest that inhibition of GPAT activity might be a viable therapeutic strategy for restoring adipogenesis in lipodystrophic patients.

Introduction

Congenital generalized lipodystrophy (CGL, also known as Berardinelli-Seip congenital lipodystrophy/BSCL), is an autosomal recessive disorder characterized by a near total loss of adipose tissue, severe hypertriglyceridemia, insulin resistance and fatty liver (69,115). To date, four genes have been linked to CGL/BSCL: 1-acylglycerol-3-phosphate-O-acyl transferase-2 (*AGPAT2*)/CGL1; *SEIPIN*/CGL2; *CAVEOLIN*/CGL3 and *CAVIN*/CGL4 (75). The most severe form of human CGL/BSCL is caused by loss-of-function mutations in *SEIPIN*/*BSCL2*, which encodes an integral membrane protein of the endoplasmic reticulum (ER) with no recognizable functional domains (75,116,117). *Seipin* knockout mice (*Bscl2*$^{-/-}$) suffer from severe lipodystrophy and insulin resistance (118-120), demonstrating *in vivo* an essential role of *Seipin* for adipogenesis. Importantly, Seipin and its orthologs also control the expansion of lipid droplets (LDs), as *Bscl2*$^{-/-}$cells produce “supersized” LDs (71,73,74,121). Therefore, Seipin has a unique role in regulating both systemic (adipogenesis) and cellular (LD expansion) lipid storage.

Little is known about how the ER-localized Seipin may regulate both LD formation and adipogenesis. Recent studies have implicated Seipin and its yeast ortholog Fld1 in regulating phospholipid metabolism (74). In particular, an increase in the level of phosphatidic acid (PA) has been detected in a number of Seipin deficient cells/tissues (73,74). Based on these findings, we have postulated that the increased PA may block PPARγ function and thus, preadipocyte differentiation. Thus, intracellular PA may possess two distinct roles in serving as a PPARγ antagonist (77)

and promoting LD expansion in other cell types because of its fusogenic biophysical property (71,122). However, because functional or catalytic domains in Seipin and its ortholog are not apparent, it is unlikely that Seipin itself functions as a glycerolipid synthetic enzyme.

Through affinity isolation and tandem mass spectrometry analysis, we have identified a number of proteins that specifically co-precipitate with Fld1-GFP in the yeast *Saccharomyces cerevisiae*. The most prominent of these proteins was a yeast glycerol-3-phosphate acyltransferase (GPAT), Gat1. We further demonstrate that mammalian Seipin specifically interacts with the corresponding mammalian glycerol-3-phosphate acyltransferase (GPAT) orthologs, GPAT3 and -4). Seipin deficiency in yeast, mammalian cells, and tissues was associated with increased GPAT specific activity due to an increased affinity of GPAT for one of its substrates, glycerol-3-phosphate. Furthermore, overexpression of GPAT3 and GPAT4 was sufficient to induce the formation of “supersized” LDs. In contrast, although the overexpression of GPAT1 and GPAT4 increased NEM-R and NEM-S GPAT activity, respectively, the overexpression of these isoforms did not block adipogenesis. We hypothesize that the overexpression of GPAT3 will block adipogenesis.

Results

Fld1 and Gat1 interact physically and functionally.[3]

To identify potential Fld1p/Seipin interacting proteins, we expressed GFP alone, or a functional Fld1-GFP fusion protein using *FLD1*'s native promoter on a low copy plasmid in wild type or *fld1*Δ yeast cells (74). Cell membranes were isolated and solubilized under three different buffer conditions (see Materials and Methods). The extracts were then subjected to affinity purification using a GFP-Trap (123), and the final eluate was resolved by SDS-PAGE and stained with silver (**Fig 5.S1**). Proteins were digested in-gel with trypsin, and the sequences of the resultant peptides were determined by tandem mass spectrometry.

We identified 19 proteins that co-precipitated with Fld1-GFP, but not with matrix or GFP alone, in all three buffer/lysis conditions used (**Table 5.S1**). Fifteen additional proteins specifically co-precipitated with Fld1-GFP in two of the three lysis conditions used (**Table 5.S2**). Among the 34 proteins, two stand out: Gat1/Gpt2 and Ldb16. Ldb16 was recently identified to interact with Fld1, and the Fld1-Ldb16 complex was proposed to form the yeast ortholog of Seipin (124). Gat1 and Gpt2 are highly interesting as they each encode one of the two GPATs expressed in yeast and initiate the synthesis of phosphatidic acid which has been proposed as the regulatory molecule controlled by Fld1/Seipin-tagged and overexpressed Fld1 and Gat1 can be specifically co-immunoprecipitated from yeast (**Fig 5.1A, 5.S1B)**. Importantly, this specific interaction was retained when both proteins were expressed at close to endogenous

[3] Data in this section contributed by Martin Pagac.

levels by adding tags at the C-termini of their respective genomic loci (**Fig 5.1B**). As recently reported (74), we were also able to co-immunoprecipitate Fld1 and Ldb16 expressed at close to endogenous levels (**Fig 5.1B**) and to co-immunoprecipitate Ldb16 and Gat1 (**Fig 5.1C**). Fld1 can also be co-immunoprecipitated with Gat2, a yeast GPAT that shares ~38% sequence identity and ~58% sequence similarity with Gat1 (**Fig 5.1D**). We then examined the physical relationships among Fld1, Ldb16 and Gat1 and -2. The Fld1-Gat1 interaction was not affected in *ldb16* null cells (**Fig 5.1E**). Thus, it appears that Fld1, Ldb16 and Gat1/2 form a ternary complex, but that Ldb16 is not required for the Fld1-Gat1/2 interaction. We were not able to test whether the Ldb16 and Gat1/2 interaction requires Fld1 because Ldb16 is extremely unstable in the absence of Fld1.

Mammalian Seipin and GPAT3/4 physically interact[4]

We wondered if the Seipin-GPAT interaction was conserved in mammals. To date, four mammalian GPATs have been identified; GPAT1 and GPAT2 localize to mitochondria outer membrane, and GPAT3 and GPAT4 are present on the ER (28). GPAT1 is resistant to sulfhydryl reagents like *N*-ethylmaleimide (NEM), whereas GPAT2, 3 and 4 are sensitive. Seipin can be co-immunoprecipitated with both GPAT3 and GPAT4 in 3T3 L1 cells (**Fig 5.2A, 5.S2A,B**). Notably, the interaction between GPAT3/4 and a *Seipin* missense mutant (T78A) that is linked to human lipodystrophy was significantly weakened (**Fig 5.2B,C**). The C-terminal cytoplasmic region of Seipin does not seem to be required for this interaction (**Fig 5.2D**). Importantly, endogenous

[4] Data in this section contributed by Martin Pagac.

GPAT3/4 can be immunoprecipitated by overexpressed Seipin (**Fig 5.2E,F**). Finally, we employed the proximity ligation assay to further examine the Seipin-GPAT3/4 interaction. GPAT3 and GPAT4 are much closer to Seipin than AGPAT2 (**Fig 5.2G**) and, consistent with Fig. 2D, full length, but not the carboxy terminus of Seipin, interacts strongly with GPAT3/4 (**Fig 5.2F**).

In SEIPIN-deficient cells and tissues, GPAT activity was higher than controls

Because Seipin and GPAT physically interact, we hypothesized that Seipin regulates GPAT activity. In order to test this hypothesis, we measured GPAT activity in control and *fld1 null* yeast cells. Consistent with our hypothesis, microsomal GPAT activity in *fld1 null* yeast cells was ~35% higher than controls (**Fig 5.3A**). To determine whether Seipin also regulates GPAT activity in mammalian cells, we compared microsomal GPAT activity in control and *Bscl2*$^{-/-}$/*Seipin*$^{-/-}$ mouse embryonic fibroblasts (MEFs). Consistent with our observations in yeast, compared to controls, GPAT specific activity in *Bscl2*$^{-/-}$ mEFs was approximately 2.5-fold higher (**Fig 5.3B**). Surprisingly, when Seipin was replaced by retroviral overexpression in *Bscl2*$^{-/-}$ mEFs GPAT specific activity remained 2.5-fold higher than controls, suggesting that microsomal GPAT was no longer accessible to Seipin. Next, we used shRNA to knock down *Seipin* in 3T3L1 preadipocytes and measured GPAT specific activity in the presence and absence of NEM, which inhibits GPAT2, 3, and 4. With each shRNA, Seipin was knocked down by ~70%, and total GPAT activity in these cells was two-fold higher than in control cells (**Fig 6.5D**). In both control and Seipin knockdown cells, NEM-resistant GPAT activity was only 10% of the total activity, thus, the higher GPAT

activity in Seipin knockdown cells was largely due to NEM-sensitive GPAT activity (**Fig 5.3C**). Finally, to determine whether the absence of SEIPIN would also alter GPAT activity under more complex physiological conditions, in control and *Bscl2*$^{-/-}$ mouse testis we measured GPAT activity. Compared to controls, in *Bscl2*$^{-/-}$ testes NEM-sensitive GPAT activity was 67% higher (**Fig 5.3D**). Importantly, Seipin knockdown did not increase the mRNA or protein expression of any GPAT isoforms, confirming that the higher GPAT activity in the absence of Seipin was not due to increases in GPAT mRNA expression or protein levels (**Fig 5.S3A-H**). Taken together, these data demonstrate that Seipin regulates GPAT activity and that this regulatory role is conserved from yeast to mammals.

Seipin deficiency altered GPAT kinetics

In the absence of compensatory GPAT expression, the higher GPAT activity in Seipin-deficient cells and tissues suggested that Seipin might regulate GPAT enzyme kinetics. In order to test the effect of Seipin deficiency on GPAT enzyme kinetics, we characterized the affinity of GPAT for its two substrates, glycerol-3-phosphate and long-chain acyl-CoA. Acyl-CoA is an amphipathic molecule and a detergent that, at higher concentrations, disrupts membranes (125). Thus, because GPAT activity is inhibited at palmitoyl-CoA concentrations higher than 82.5 μM, the apparent Km values for acyl-CoA cannot be calculated in cells or tissues (**Fig 5.4I-P**). In control mEFs GPAT showed an apparent Km for glycerol-3-phosphate of 241.3 μM (**Fig 5.4C, D**); however in *Bscl2*$^{-/-}$ mEFs, the apparent Km for glycerol-3-P was 517.9 μM, suggesting that Seipin-deficiency increases GPATs affinity for glycerol-3-P. Despite the fact that Seipin

overexpression in *Bscl2*$^{-/-}$ mEFs did not inhibit steady state GPAT activity (**Fig 5.3B**), in these cells the apparent Km was 249.8 μM, suggesting that the replacement of Seipin was sufficient restore GPAT substrate affinity to control levels. Compared to that in yeast and mEFs, in 3T3L1 preadipocytes, Seipin regulated GPAT kinetics in a similar manner. In control preadipocytes, the apparent Km for G3P was 216.6 μM and in shRNA-*Seipin* preadipocytes the apparent Km for G3P was 117.6 μM (**Fig 5.4E,F**). Because Seipin is most highly expressed in the testis, we also characterized GPAT enzyme kinetics in that tissue. Similar to the yeast and mammalian cells, the apparent Km for glycerol-3-P in *Bscl2*$^{-/-}$ testes was 454.2 μM whereas in control testis the apparent Km for G3P was 578.1 μM (**Fig 5.4G,H**). Therefore, because the absence of *Seipin* increased GPAT activity and shifted its apparent Km for glycerol-3-P in yeast, preadipocytes, mEFs, and testis we concluded that Seipin is an evolutionarily conserved regulator of GPAT.

Increased GPAT activity underpins the change in LD morphology in Seipin-deficient cells[5]

Increased GPAT activity may also cause the formation of "supersized" LDs and increased PA in *fld1* null cells. Indeed, overexpressing wild type, but not catalytic-dead *GAT1* and *GAT2* in yeast cells leads to the formation of supersized LDs (**Fig. 5.5A, 5.S5A**), phenocopying *fld1* null cells. The level of PA in the ER was similarly increased in these cells, as in *fld1* null cells, as indicated by increased *INO1* expression (**Fig 5.5B**). Despite the presence of large LDs, the total amount of TAG was not significantly

[5] Data in this section contributed by Martin Pagac.

increased in these cells (**Fig 5.S5B**), and Importantly, when either *GAT1* or *GAT2* was co-expressed with *FLD1*, few supersized LDs were detected.

Seipin deficiency in mammals is associated with clustered LDs in fibroblasts and cell lines, and with supersized LDs in the testes where Seipin is normally highly expressed. By increasing GPAT activity, these changes can be recapitulated. When GPAT3/4 are overexpressed in 3T3-L1 cells, LDs appear enlarged and clustered (**Fig 5.5C**).

During adipogenesis, Seipin regulates GPAT kinetics and increased GPAT1 and GPAT4 activity did not impair differentiation.

Because Seipin deficiency is associated with increased GPAT activity and altered GPAT kinetics we hypothesized that Seipin would regulate GPAT kinetics during differentiation. To test this hypothesis, control and shBSCL2 3T3L1 cells were differentiated for 0, 4, 8, and 12 h and GPAT kinetics were measured. Consistent with this hypothesis, Seipin deficiency altered GPAT kinetics at 0 and 4 h of differentiation. In differentiating control cells, the apparent Km for glycerol-3-phosphate was 175.6, 267.1, 176.2, and 153.1 μM, respectively (**Fig 5.6A,C**). In contrast, in Seipin knockdown cells, the apparent Km for glycerol-3-phosphate was 113.3, 146.7, 141.8, 138.4 μM, respectively (**Fig 5.6B, C**). Because the differences in GPAT kinetics were transient and occurred within the first 4 h of differentiation, suggests that the regulation of GPAT by Seipin is required for an early step in adipogenesis. To test the effect of Seipin deficiency throughout differentiation, we used lentivirus expressing GFP or

shRNA targeting BSCL2 to construct stable 3T3L1 cells and differentiated them for 0 h, 12 h, 24 h, 48 h, and 8 d. Compared to controls, in shBSCL2-expressing cells Seipin mRNA was reduced by ~70% at 0 h and remained low throughout differentiation (**Fig 5.6D**). Consistent with the role for Seipin in differentiation, shBSCL2-expressing cells were unable to differentiate and Seipin deficiency virtually abolished PPARγ expression (**Fig 5.6E**). These findings are consistent with previous reports that Seipin deficiency blocks PPARγ activation early in differentiation (126) and provide evidence to suggest that the regulation of GPAT by Seipin is required for normal adipogenesis.

Because Seipin deficiency impairs adipogenesis and increased GPAT activity, we investigated whether increased GPAT activity would be sufficient to block adipogenesis. To do so, 3T3L1ΔCar cells were infected with adenovirus overexpressing eGFP, GPAT1, or GPAT4 and tested their ability to differentiate. First, we confirmed that overexpression of GPAT1 and GPAT4 increased GPAT activity. Compared to eGFP expressing cells, the overexpression of GPAT1 and GPAT4 increased NEM-R and NEM-S GPAT activity ~3-fold, respectively (**Fig 5.6F**). In contrast to our hypothesis that increased GPAT activity was sufficient to block adipogenesis, neither the overexpression of GPAT1 nor GPAT4 prevented PPARγ activation (**Fig 5.6G**). That GPAT1 overexpression did not block adipogenesis is unsurprising because GPAT1 overexpression did not increase NEM-S GPAT activity to levels seen in Seipin-deficient 3T3L1 cells (**Fig 5.3C**). However, because Seipin physically interacted with GPAT4 and GPAT4 overexpression increased GPAT activity to a similar level to that in Seipin-deficient cells, these findings are perplexing. Either

our hypothesis about GPAT activity and adipogenesis is incorrect or the increased GPAT activity in Seipin-deficient cells is not due to increased GPAT4 activity, but possibly increased GPAT3 activity. To test this possibility, we have overexpressed GPAT3 in this system and plan to measure the ability of GPAT3-overexpressing cells to differentiate. These data will be complete by the date of my defense.

Discussion

Seipin's role is unique role in mammalian lipid storage because it regulates both cellular (LDs) and systemic (adipogenesis) lipid storage. However, as an integral membrane protein of the ER without any known functional domains, Seipin's function has been difficulty to understand. Here, we demonstrate that Seipin orthologs can interact specifically with the ER-located GPAT isoforms, and that this evolutionarily-conserved interaction inhibits both the specific activity of GPAT and its affinity for glycerol-3-P. Our data provide additional evidence that enhanced GPAT activity in the ER of Seipin-deficient cells increases the level of PA, inhibits adipogenesis in preadipocytes, and modulates LD formation and growth in other cell types.

GPAT catalyzes the acylation of glycerol-3-P and initiates the pathway of TAG and phospholipid synthesis. There are four GPAT isoforms in mammalian cells, each encoded by a separate gene. Both GPAT1 and GPAT2 localize to mitochondria but GPAT1 is resistant to NEM whereas GPAT2 sensitive. The microsomal, NEM-sensitive GPAT is encoded by two closely related genes, GPAT3 and GPAT4. The ER (microsomal) GPAT activity is conserved from yeast to humans as both GPAT isoforms in yeast are integral membrane proteins of the ER. Although GPAT controls the rate-limiting step in the synthesis of both TAG and phospholipids, the regulation of microsomal GPAT activity remains largely unknown, and to our knowledge, no GPAT interacting proteins have been identified.

Here, we show Seipin interacts with GPAT3/4 in an evolutionarily conserved manner to regulate GPAT enzyme kinetics. This interaction and regulation is highly conserved from yeast to mammalian cells and tissues. Furthermore, we provide evidence that increased GPAT activity is the underlying cause of the aberrant lipid droplet morphology in Seipin deficient yeast and mammalian cells. Finally, we are working to determine whether increased GPAT activity is sufficient to block adipogenesis. If this hypothesis were true, then GPAT might be a suitable therapeutic target for the treatment of type 2 CGL.

Experimental Procedures

Isolation of Fld1 interacting proteins using GFP-Trap

Yeast wild type cells transformed with plasmid pLacYCP-GFP and fld1Δ cells transformed with pLacYCP-Fld1-GFP were grown to early stationary phase and then lysed using bead beater in the following buffers: buffer #1 (25 mM Tris-HCl pH 8.0, 150 mM NaCl, 0.5% Triton X-100, 0.2 mM EDTA, 0.2 mM DTT); buffer #2 (20 mM K-HEPES pH 7.4, 110 mM KOAc, 150 mM NaCl, 0.1% Triton X-100, 0.1% Tween 20, 2 mM $MgCl_2$); buffer #3 (20 mM K-HEPES pH 7.4, 110 mM KOAc, 150 mM NaCl, 0.1% Triton X-100, 0.1% Tween 20, 46 mM n-octyl-B-D-glucopyranoside, 2 mM MgCl2, 5% glycerol). Each lysis buffers also contained a mixture of protease (1 mg/mL PMSF, 1 mg/mL phenanthroline, 3 µg/mL leupeptin, 15 µg/mL Pepstatin) and phosphatase (2 mM NaF, 2 mM Na_3VO_4) inhibitors except that buffer #2 did not contain phenanthroline. Cell lysates were initially incubated with Sepharose CL-4B (GE Healthcare) to pull down proteins interacting with beads, and the supernatants were subjected to affinity purification using a GFP-Trap (ChromoTek GmbH, Martinsried, Germany) to pull down proteins interacting with GFP and Fld1-GFP, respectively.

Identification of Fld1 interacting candidates using mass spectrometry

Proteins were eluted from the Sepharose and GFP-Trap beads with a low pH buffer (pH2) containing 100 mM glycine, neutralized and separated on 4-15% Tris-HCl gels (Bio-Rad). After staining with Coomassie Brilliant Blue R-250 (Sigma), protein bands were digested in-gel with trypsin [Shevchenko, A., Wilm, M., Vorm, O., and Mann, M. (1996) Mass spectrometric sequencing of proteins silver-stained

polyacrylamide gels. Anal Chem 68, 850-858] and the sequences of the resultant peptides were determined by liquid chromatography tandem mass spectrometry using LTQ-Orbitrap Velos Pro (Thermo Fisher Scientific) coupled to UltiMate 3000 RSLC (Dionex). Mass spectra were acquired in data-dependent mode with one 30,000 resolution MS survey scan in the Orbitrap (350-1750 m/z) followed by up to 10 MS/MS scans triggered above intensity of 2500 using CID (normalized collision energy 35) in ion trap. The raw files were processed in Proteome Discoverer software (Thermo Scientific) using default parameters. The fragmentation spectra were searched against the SwissProt protein database using the Mascot search engine (Matrix Science). One missed tryptic cleavage was allowed, carbamidomethylation of cysteines was set as a fixed modification, and methionine oxidation, protein N-terminal acetylation, glutamine and asparagine deamidation were used as variable modifications. The precursor and fragment mass tolerances were set to 5 ppm and 0.5 Da, respectively. Both peptide and protein identifications were filtered at 1% false discovery rate. The list of candidate interactors was created from proteins identified in at least two FLD-GFP pull-downs and not present in any of the controls (Sepharose and GFP alone pull-downs).

Cell culture

HeLa and NIH3T3 cells were grown in Dulbecco's Minimum Essential Medium (DMEM) supplemented with 10% FBS (Invitrogen). Transient transfections of plasmids were performed using the calcium phosphate method. Small interfering RNA (siRNA) oligos were transfected using the Lipofectamine RNAiMAX reagent (Invitrogen). SiRNAs (SiBscl2-1 and siBscl2-2 against murine Bscl2, siBSCL2-1, and siBSCL2-2 against

human BSCL2) were from Sigma; their sequences are shown in Supplementary Table I. To induce TAG synthesis and LD formation, cells were treated with 200 μM BSA-conjugated oleate (molar ratio of oleate to BSA ~8:1) 48 h after transfections and incubated for 16 h.

Lentivirus Production and Stable Cell Line Generation

One control and two shBSCL2 lentiviral constructs were used to generate 10 mL of lentivirus in HEK293 cells using a 2nd generation lentivirus packaging system and Roche X-tremeGENE HP Transfection Reagent. To generate stable 3T3-L1 cells with each lentivirus, cells were incubated overnight with 1 mL of lentivirus containing 8 μg/mL polybrene. After selecting stable cell lines with 4 μg/mL puromycin for 1 wk, cells were used for experiments or stored in liquid N_2.

3T3-L1 Cell Culture and Differentiation Time course

Cells stably expressing lentivirus empty vector, shBSCL2-1, or shBSCL2-2 were grown to confluence in DMEM, 10% calf serum, 4 mM glutamine and 100 U/ml penicillin/streptomycin. After reaching confluence, cells were grown for an additional 2 d in fresh growth media. Differentiation was initiated by culturing cells in DMEM, 10% FBS, 4 mM glutamine, antibiotics and 1 μM dexamethasone, 250 nM IBMX, and 1 μg/ml insulin for 2 days. Two days later fresh DMEM and 10% FBS with 1 μg/ml insulin was added and refreshed every 2 days. Cells were rinsed with room temperature PBS and frozen in plates at 0, 12, 24, 48 h, and 8 days of differentiation. For GPAT activity and PA measurements, plates were frozen after 0, 4, 8 and 12 h of differentiation.

Phosphatidic Acid Measurement

Total cell lipid was extracted (84) and PA content was analyzed by LC/MS (127). The amount of each PA species in the biological samples was calculated from the peak areas obtained using software that controls the LC/MS system (Analyst 1.5, Applied Biosystems). Raw peak areas were corrected for recovery and sample loading, and transformed into amounts of analyte, using standard curves made with commercially obtained glycerolipids. Glycerolipids were quantified with 0.1 nmol 17:0 LPA as an internal standard to correct for recovery. PA was quantified and normalized to protein concentrations of the cellular lysates.

Adenoviral Overexpression of GPAT in 3T3L1ΔCar cells

3T3L1ΔCar cells were provided by David Orlicky. To enhance their ability to be infected, Dr. Orlicky engineered these cells to overexpress the coxsackie/adenovirus receptor (128). These modifications do not affect normal adipocyte function. Adenovirus expressing eGFP, GPAT1, and GPAT4 were obtained from the UNC Vector Core (14). When cells reached 90% confluence, they were infected with adenovirus in serum-free Optimem containing virus at 25 MOI for 2 hours. After 2 hours, fresh 3T3L1 growth media were replaced and cells were grown for an additional 72 h prior to differentiation. Differentiation protocol was the same as described above.

GPAT Activity Assay

One hundred milligrams of tissue or cells from 10 cm plates were homogenized in cold Medium I (250 mM sucrose, 10 mM Tris, pH 7.4, 1 mM EDTA, 1 mM

dithiothreitol) using 10 up-and-down strokes with a Teflon-glass motor-driven homogenizer. Total membranes were isolated by centrifuging the homogenate at 100,000 x g for 1 h. GPAT specific activity (initial rate) was assayed for 10 min at RT in a 200 µl reaction mixture containing 75 mM Tris-HCl, pH 7.5, 4 mM $MgCl_2$, 1 mg/ml BSA (essentially fatty acid–free), 1 mM dithiothreitol, 8 mM NaF, 800 µM [^{3}H]glycerol-3-phosphate, and 82.5 µM palmitoyl-CoA (109). The reaction was initiated by adding 25-50 µg of testis membrane protein or 5-10 µg of cellular membrane protein after incubating the membrane protein on ice for 15 min in the presence or absence of 2 mM NEM, which inactivates GPAT isoforms 2, 3, and 4 (109). The reaction products were extracted into 2 mL $CHCl_3$ and measured as described (109). NEM-resistant activity (GPAT1) was calculated by subtracting NEM-sensitive activity from total activity. To determine the reaction products, 1 mL $CHCl_3$ was dried under N_2, resuspended in 30 µL $CHCl_3$:CH_3OH (2:1; v/v), and separated by TLC ($CHCl_3$:pyridine:88% formic acid, 50:30:7; v/v). Greater than 90% of the reaction product was PA; the remainder was lysophosphatidic acid.

GPAT Activity Enzyme Kinetics

Total particulate protein (5 µg) from control and *Bscl2*$^{-/-}$ mEFs and 3T3L1 cells stably expressing lentivirus empty vector or shBSCL2 was used to determine enzyme kinetics. To measure enzyme dependence on [^{3}H]glycerol-3-P, the palmitoyl-CoA concentration was held at 82.5 µM and [^{3}H]glycerol-3-P concentrations were varied (40-400 µM). Palmitoyl-CoA concentrations above 82.5 µM inhibited the reaction.

Plasmid constructions

Strains, primers and plasmids are listed in Table S1.

Co-immunoprecipitations

The following antibodies were used: mouse and rabbit anti-V5 (Santa Cruz Biotechnology, 1:2'000), mouse anti-FLAG (Clontech, 1:1'000), mouse anti-Dpm1 (Life Technologies, 1:250), rabbit anti-Ldb16, rabbit anti-Erg1, rabbit anti-Are2 (kind gifts from Dr. C.W. Wang, 1:500; 1:8'000; 1:2'000), mouse anti-HA (Covance, 1:1'000), rabbit anti-HA (Cell Signaling, 1:1'000), rabbit anti-Calnexin (Cell Signaling, 1:1'000), rabbit anti-Calreticulin (Abcam, 1:1'000), rabbit anti-Actin (Sigma, 1:1'000), rabbit anti-AGPAT6/GPAT4 (Origene, 1:1'000).

Yeast cells were grown at 30°C in defined media containing glucose or galactose as the carbon source and amino acids as required. Cells were washed with ice-cold PBS, frozen at -80°C for at least 2 h. Cells were lysed in IP Lysis/Wash buffer [0.5% (w/v) CHAPS, 150 mM $NaCl_2$, 2 mM EDTA, 25 mM HEPES, pH 7.4, 1 mM DTT, 5% Glycerol, Sigma Protease Inhibitor Cocktail, 1 mM PMSF] by vortexing 6 x 1 min with glass beads, and cooling the tubes on ice between each cycle. Cell lysates were incubated for 30 min on ice, then centrifuged at 1,000 x rcf for 5 min at 4°C to remove intact cells and debris. The supernatant was further centrifuged at 17,000 x rcf for 45 min at 4°C to pellet insoluble material. Protein concentration in the supernatant was determined by the BCA method, and 2 mg of protein were used for each co-immunoprecipitation condition. For mouse anti-FLAG antibody and mouse anti-V5

antibody immunoprecipitations, each antibody was immobilized on magnetic Dynabeads® according to the Dynabeads® Co-Immunoprecipitation Kit manual. After 30 min of incubation with the cell lysates containing over-expressed protein at room temperature, or after overnight incubation with the cell lysates containing low-levels of recombinant protein at 4°C, the beads were washed 5 times with IP Lysis/Wash buffer and eluted in 2 x non-reducing SDS PAGE sample buffer at 37°C for 20 min for western blotting. Proteins were transferred onto PVDF membranes in CAPS buffer, pH 11.0, followed by immunodetection.

Transiently or stably transfected mammalian cells, mouse embryonic fibroblasts (MEF), mouse preadipocytes (3T3-L1), and HeLa cells, were washed three times with ice-cold PBS and lysed in IP Lysis/Wash buffer (see above) containing either 0.5% (w/v) CHAPS or 1% (w/v) n-dodecyl-β-D-maltopyranoside (DDM) by forcing the cells 30 times through a 0.8 mm needle. Cell lysates were incubated for 60 min at 4°C on the wheel to solubilize membrane proteins, then the lysate was centrifuged at 17,000 rcf for 60 min at 4°C to pellet insoluble material. Protein concentration in the supernatant was determined by the BCA method, and 2 mg of protein were used for each coimmunoprecipitation condition.

Cell lysates were pre-cleared for 2 h at 4°C with agarose beads, or with mouse or rabbit IgG-Dynabeads®. After 60 min of incubation with the cell lysates containing over-expressed recombinant protein at room temperature, or after overnight incubation with the cell lysates containing endogenous GPAT3 and GPAT4 at 4°C, the beads were

washed 3 times with IP Lysis/Wash buffer, then eluted in 2 x non-reducing SDS PAGE sample buffer at 37°C for 20 min for western blotting. Proteins were transferred onto PVDF membranes in CAPS buffer, pH 11.0, followed by immunodetection.

Antibodies, immunoprecipitation, immunofluorescence, and immunoblot

DsRed polyclonal antibody to detect mCherry and fusion proteins (Clontech), Flag monoclonal antibody (Sigma), actin monoclonal antibody (Abcam), and HA and Myc monoclonal antibodies (Covance) were purchased. For immunoprecipitation, cells were lysed with Lysis buffer B, 50 mM Hepes-KOH, pH 7.4/100 mM NaCl/1.5 mM $MgCl_2$/0.5% (v/v) CHAPSO containing protease inhibitors (27). Cell lysates were passed through a 22-gauge needle 5 times, extracted by rotating for 1 h at 4°C, and clarified by centrifuging at 100,000 x g for 15 min. The lysates were precleared by incubation for 1 h at 4°C with 50 µl of protein G sepharose beads (Sigma). Precleared lysates were rotated overnight at 4°C with 10 µg of monoclonal anti-Flag together with 50 µl of protein G sepharose beads. Pelleted beads were washed three times (10 min at 4°C) with 1 ml of Lysis buffer B containing protease inhibitors, resuspended in 80 µl of 2× SDS sample buffer, boiled for 5 min, and subjected to SDS/10% PAGE and immunoblot analysis.

For immunofluorescence, cells were fixed with 4% paraformaldehyde and permeabilized with 0.1% saponin/PBS for 30 min, then blocked with 3% BSA/0.05% saponin in PBS for 1 h. Cells were incubated with primary antibodies diluted in 1%

BSA/PBS for 1 h, then incubated with Alexa Fluor 568 conjugated secondary antibodies for 1 h.

For immunoblot analysis, cells were lysed with Lysis buffer A and passed through a 22-gauge needle 5 times and clarified by centrifugation at 3,000 x g for 5 min. Samples were subjected to SDS/10% PAGE, transferred to nitrocellulose filters, and subjected to immunoblot analysis. Bound antibodies were visualized by chemiluminescence using ECL Western blotting detection reagents (GE Healthcare). For Blue Native PAGE, HeLa cells transfected with wild-type or mutant forms of mCherry- or Flag-tagged Seipin were lysed with Lysis buffer B. After clearing unsolubilized debris by centrifugation at 13,000 x g for 10 min, lysates were loaded onto 4-16% NativePAGE gels (Invitrogen) for protein separation. Flag- and mCherry-tagged seipin were probed with anti-Flag and anti-mCherry, respectively.

Statistics

For statistics, experiments were performed in triplicates. The results are presented as mean ± SD. Two-tailed Student's t-test was used for comparison.

Contributions

Martin Pagac[1*], Daniel E. Cooper[2*], Ivan Lukmantara[1], Mona Lei[1], Hoi Yin Mak[1], Tamar Kapterian[1], Damian Kotevski[1], Pawel Sadowski[1, &], Weiqin Chen[3], George Liu[4], Rosalind A. Coleman[2] and Hongyuan Yang[1, #]

[1]School of Biotechnology and Biomolecular Sciences, the University of New South Wales, Sydney, NSW, 2052, Australia

[2]Department of Nutrition, University of North Carolina, Chapel Hill, North Carolina 27599, USA

[3]Department of Physiology, Medical College of Georgia Regents University, Augusta, GA 30912, USA

[4]Institute of Cardiovascular Sciences and Key Laboratory of Molecular Cardiovascular Sciences, Ministry of Education, Peking University Health Science Center, Beijing, China

*These authors contributed equally to this manuscript.

#Address correspondence to: Hongyuan Yang, School of Biotechnology and Biomolecular Sciences, The University of New South Wales, Sydney, NSW, 2052, Australia

Running Title: SEIPIN regulates glycerol-3-phosphate acyltransferase

[&]Current address: Institute for Future Environments, Queensland University of Technology, Brisbane, Australia.

Mass spectrometric analysis for this work was carried out at the Bioanalytical Mass Spectrometry Facility, UNSW and was supported in part by infrastructure funding

from the New South Wales Government as part of its co-investment in the National Collaborative Research Infrastructure Strategy. RAC was supported by NIH DK56598.

Figures

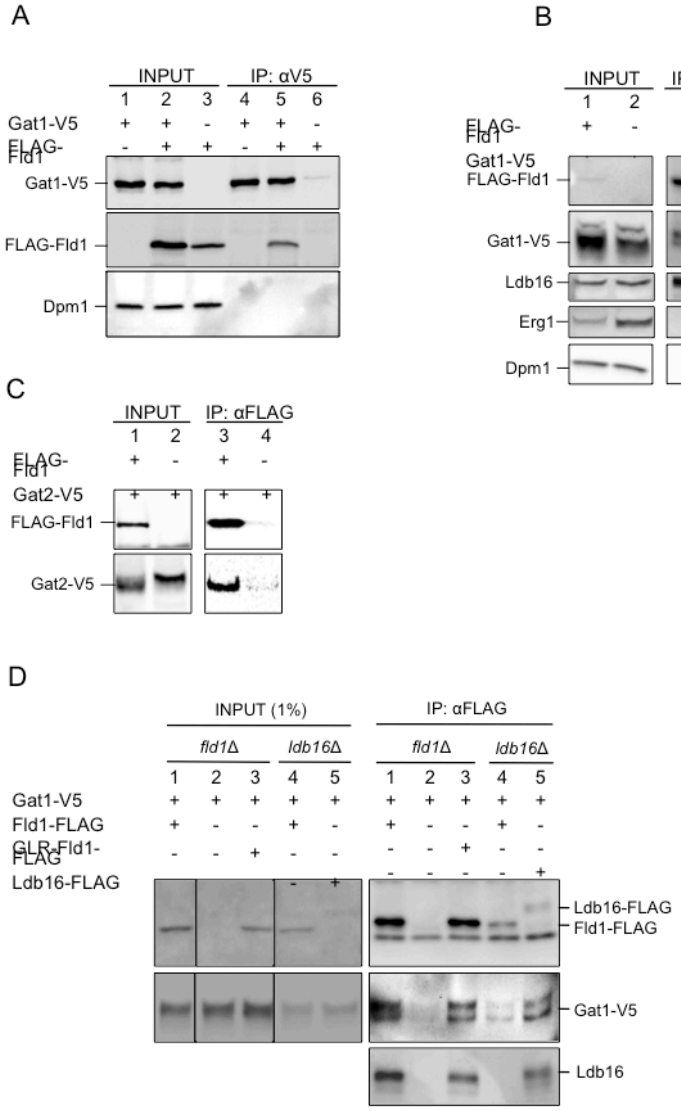

Figure 5.1: Fld1, Ldb16 AND Gat1/2 form a ternary complex in yeast.[6] A) Coimmunoprecipitation of overexpressed Gat1-V5 and FLAG-Fld1 by V5 antibody from yeast lysates. (V5 antibody does not immunoprecipitate FLAG-Fld1 in absence of Gat1-V5. Dpm1 can only be detected in the input). B) Using FLAG antibody, endogenous levels of Gat1-V5 and Ldb16 coimmunoprecipitate with FLAG-Fld1 from yeast cell lysates. (FLAG antibody does not immunoprecipitate Gat1-V5 or Ldb16 in absence of FLAG-Fld1. Dpm1 and Erg1 can only be detected in the input). C) Coimmunoprecipitation of endogenous levels of Gat2-V5 and FLAG-Fld1 by FLAG antibody from yeast lysates. (FLAG antibody does not immunoprecipitate Gat2-V5 in absence of FLAG-Fld1. D) Using FLAG antibody, endogenous levels of Gat1-V5 and Ldb16 coimmunoprecipitate with FLAG-Fld1 and mutant GLR-Fld1-FLAG from *fld1Δ* or *ldb16Δ* yeast cell lysates. (FLAG antibody does not immunoprecipitate Gat1-V5 or

[6] Results from Martin Pagac.

Ldb16 in absence of FLAG-Fld1. Coimmunoprecipitation of Gat1-V5 and Ldb16 with mutant GLR-Fld1-FLAG is weakened).

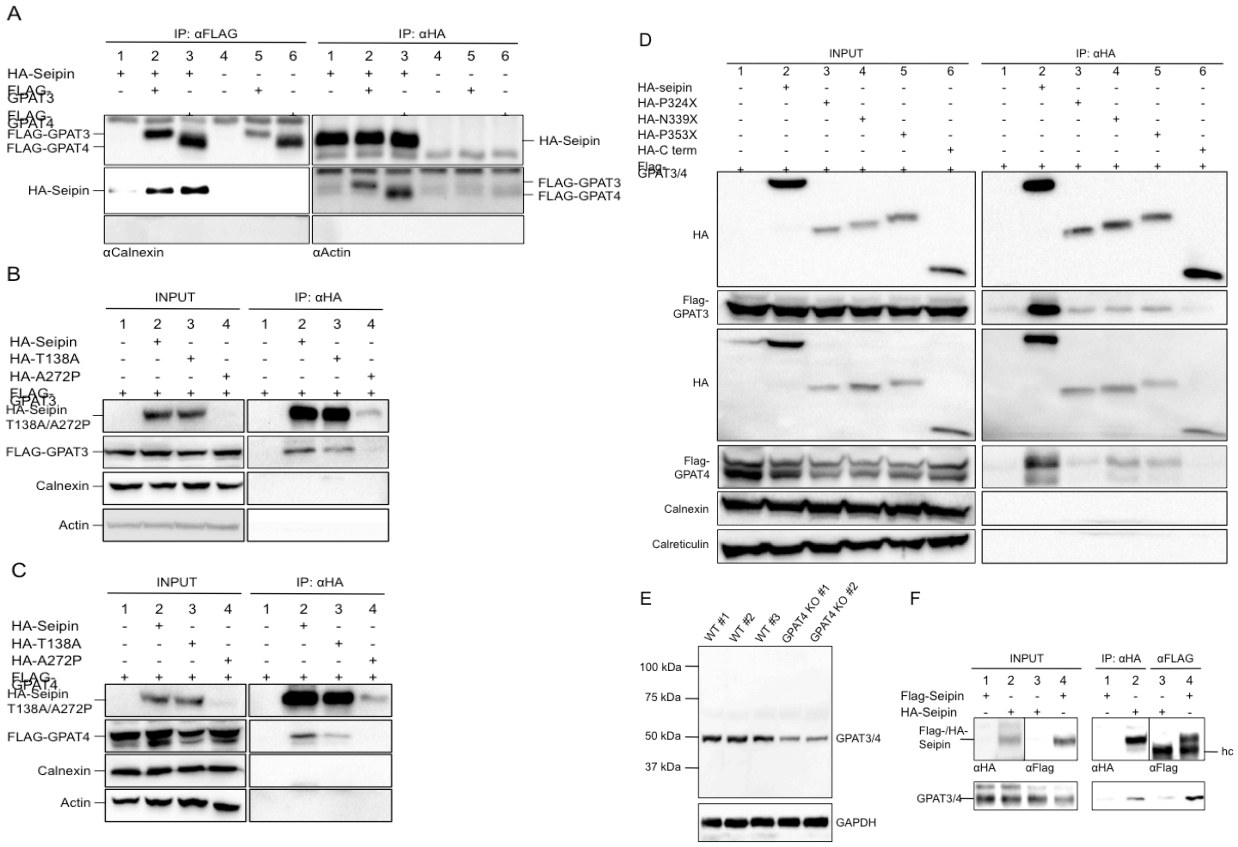

Figure 5.2: Mammalian Seipin and GPAT3/4 physically interact.[7]

A) Coimmunoprecipitation by FLAG and HA antibody of overexpressed FLAG-tagged GPAT3 or GPAT4 and HA-tagged Seipin, respectively, from transfected mEF cell lysates. (FLAG-GPAT3 and -GPAT4 and HA-Seipin do not immunoprecipitate in absence of the bait. Calnexin and Actin can only be detected in the input, see Figure S. A). B) and C) Coimmunoprecipitation by HA antibody of overexpressed HA-tagged mutant or wild-type Seipin forms from stably FLAG-GPAT3 and -GPAT4 transfected 3T3-L1 cell lysates. (Coimmunoprecipitation of FLAG-GPAT3 and FLAG-GPAT4 with mutant HA-T138A-Seipin is weakened. The mutant HA-A272P-Seipin form is not stable in 3T3-L1 cells. Calnexin and Actin can only be detected in the input). D) Using HA antibody, FLAG-tagged GPAT3 and -GPAT4 coimmunoprecipitate with a series of overexpressed HA-tagged C-terminal Seipin truncations, but not with the HA-tagged Seipin C-terminus. (Calnexin and Calnectin can only be detected in the input). E) GPAT4 antibody detects a specific band of ~50 kDa in lysates from three different mouse liver tissue homogenates, but also from lysates isolated from two different GPAT4$^{-/-}$ mouse liver tissues. (The band detected in GPAT4$^{-/-}$ mouse liver tissue lysates derives likely from GPAT3, as the peptide used to raise the GPAT4 antibody in rabbit is 96% identical to the corresponding GPAT3 sequence). F) Using HA and FLAG antibody, endogenous GPAT4 and GPAT3 coimmunoprecipitate from lysates prepared from stably HA- and FLAG-Seipin transfected 3T3-L1 adipocytes. (HA and FLAG

[7] Courtesy of Martin Pagac.

antibodies do not immunoprecipitate GPAT4 and GPAT3 in the presence of FLAG-Seipin and HA-Seipin, respectively).

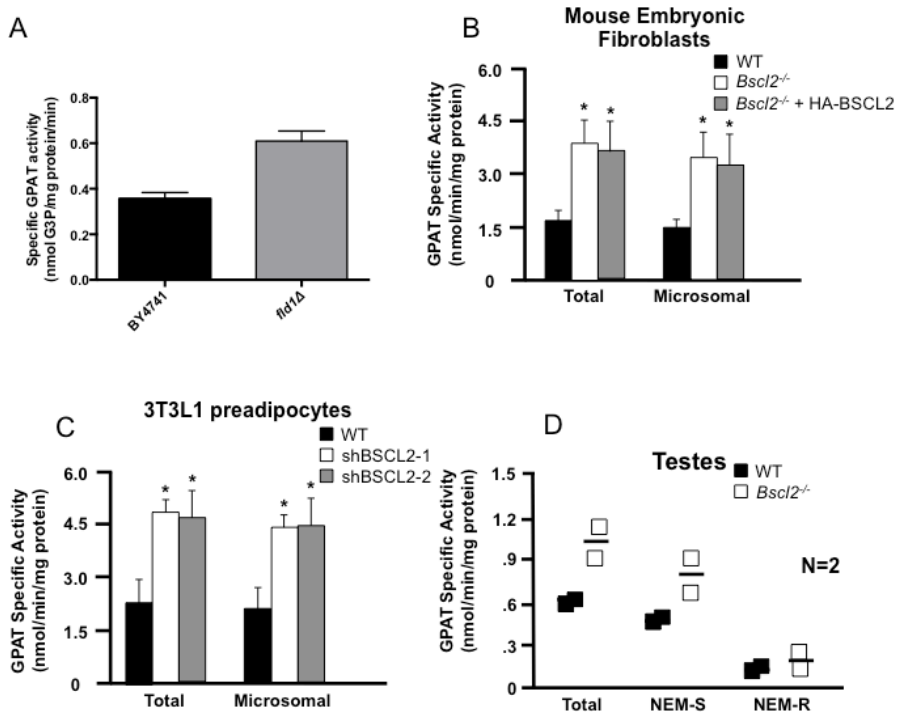

Figure 5.3: GPAT activity is significantly increased in Fld1/Seipin-deficient cells and tissues.

A) GPAT specific activity in control and fld1Δ yeast microsomes. GPAT activity was measured by adding 7.1 mM [^{14}C]glycerol-3-P and 50 µM acyl-CoA (1:1, C16:0- and C18:1-CoA) to 100 µg microsomes and reactions were allowed to proceed for 10 mins. Lipids were extracted and incorporation of [^{14}C]glycerol-3-P into lipids quantified by scintillation counting. B-D) GPAT activity was measured by adding 5, 10, or 15 ug of total particulate protein, in the presence or absence of 2 mM *N*-ethylmaleimide (NEM) for 15 mins, to a reaction mixture containing 800 µM [1,2,3-H]glycerol-3-phosphate and 82.5 µM 16:0-CoA. Reactions were terminated after 10 mins and lipids were extracted into $CHCl_3$, dried and quantified by scintillation counting. NEM-Sensitive (NEM-S) GPAT activity was calculated by subtracting NEM-resistant (NEM-R) GPAT activity from total GPAT activity. B) GPAT specific activity in control and *Bscl2*$^{-/-}$ mEF cells, and *Bscl2*$^{-/-}$ cells containing overexpressed HA-tagged Seipin. C) GPAT specific in control and shBSCL2-expressing 3T3-L1 cells. D) GPAT specific activity in control and *Bscl2*$^{-/-}$ testis. N=2-3, Results are shown as mean ± S.E.M. *p<.05, student's T-test.

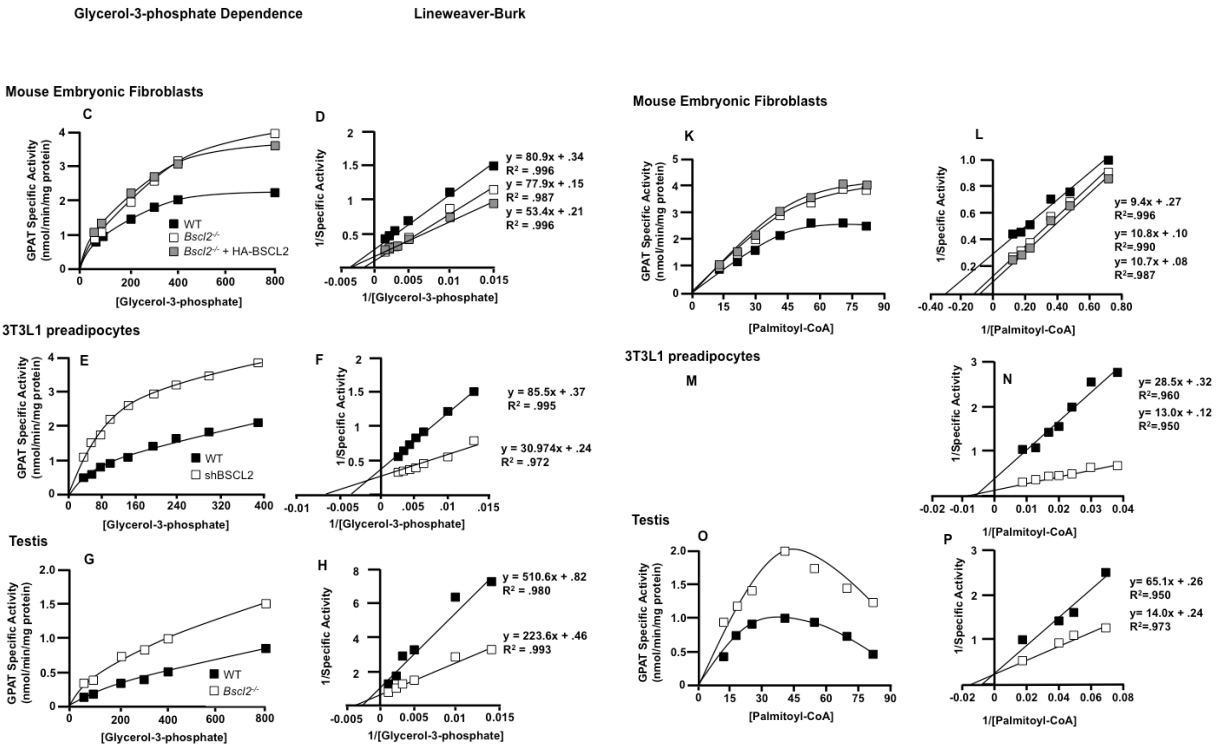

Q Enzyme Kinetics Summary

Tissue/Cells		Substrate: G-3-P Km[1]	G-3-P Vmax[2]	16:0-CoA Km[1]	16:0-CoA Vmax[2]
yeast	Wildtype	xxx.x μM	x.x	xx.X μM	x.x
	Δfld1	xxx.x μM	x.x	xxx.x μM	xx.x
mouse embryonic fibroblasts	Wildtype	241.3 ± 45.1	3.0 ± 0.5	34.8 ± 16.6	3.7 ± 1.7
	Bscl2$^{-/-}$	517.9 ± 26.8*	6.8 ± 0.6*	107.8 ± 31.4*	10.0 ± 3.0*
	Bscl2$^{-/-}$ + HA-BSCL2	249.8 ± 20.3	4.7 ± 0.7*	129.8 ± 16.3*	12.1 ± 3.1*
3T3L1 preadipocytes	Control	216.6 ± 46.2	3.1 ± 1.6	205.0 μM	3.1
	shBSCL2	117.6 ± 08.9*	5.4 ± 1.8*	107.8 μM	8.3 ± 0.65
Testis	Wildtype	578.1 ± 34.0	1.2 ± 0.2	111.5 μM	3.9
	Bscl2$^{-/-}$	454.2 ± 25.3*	2.2 ± 0.3*	58.4 μM	4.2

[1]μM

[2]nmol/min/mg protein

Figure 5.4: GPAT kinetics were altered in Seipin-deficient cells and tissues.

A-H) Glycerol-3-phosphate dependence and Lineweaver-Burk plots. A and B) BY and fld1 yeast. C and D) Control and *Bscl2*$^{-/-}$ mouse embryonice fibroblasts. E and F) Control and shRNA knockdown of Seipin in 3T3L1 cells. G and H) Control and *Bscl2*$^{-/-}$ testis. Five micrograms of membrane proteins were incubated in the presence of increasing amounts of [1,2,3-H]glycerol-3-phosphate (50-800 μM). I-P) Palmitoyl-CoA dependence and Lineweaver-Burk plots. I and J) BY and fld1 yeast. K and L) Control and *Bscl2*$^{-/-}$ mouse embryonic fibroblasts. M and N) Control and shRNA knockdown of Seipin in 3T3L1 cells. O and P) Control and *Bscl2*$^{-/-}$ testis. Palmitoyl-CoA

concentrations were varied from 11.25-82.5 μM. Q) Summary table for kinetics. Reactions were terminated after 10 mins, lipids extracted into $CHCl_3$, dried and quantified by scintillation counting. N=2-3 for each group represents cells from 3 different cell passages. Results are shown as means ± S.E.M.

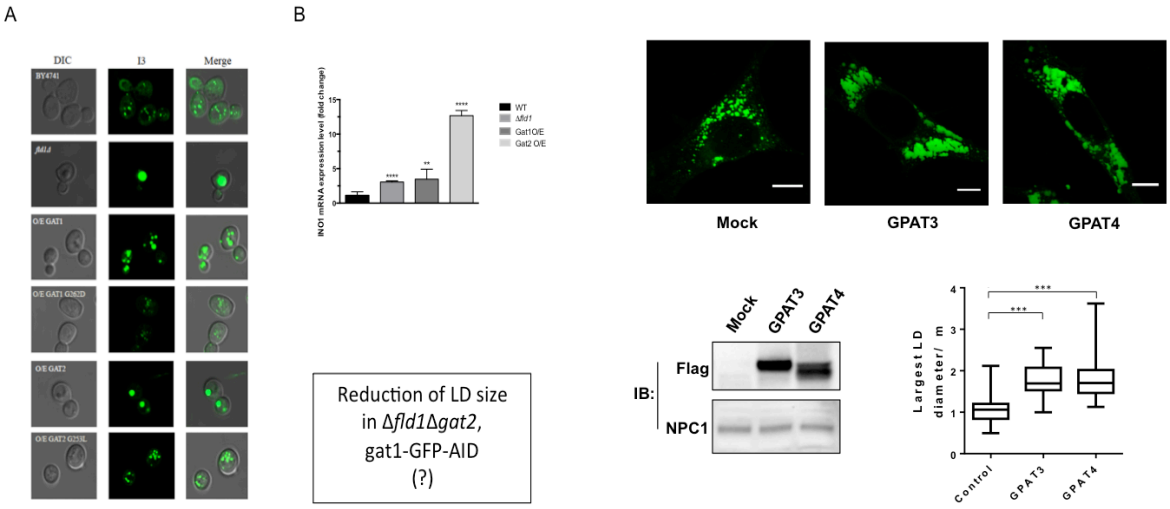

Figure 5.5: Activation of GPAT drives the formation of supersized LDs in yeast and mammalian cells.[8]

A) LDs of BY4741 wild-type (WT), SLD-forming yeast strains (O/E Gat1 and O/E Gat2) and mutants (O/E Gat1 G262D and O/E Gat2 G253L) grown in SC media until early stationary phase. Cells were stained with Nile red and immediately observed for LDs under a fluorescence microscope. B) INO1 mRNA levels in WT, *fld1*Δ, Gat1 O/E and Gat2 O/E yeast strains. Increased INO1 mRNA levels indicate increased PA levels in the ER membrane. C) 3T3-L1 control cells (mock) or stably expressing Flag-tagged GPAT3 or GPAT4 were treated with oleate-BSA complexes for 16 h, fixed, and then stained with BODIPY 493/503 for lipid droplets. Representative confocal images are shown. Immunoblotting analysis of total cell lysates with anti-Flag or anti-NPC1. Diameters of top 3 largest lipid droplets in each cell. Data represent mean ± SD (***p < 0.001).

[8] Contributed by Martin Pagac.

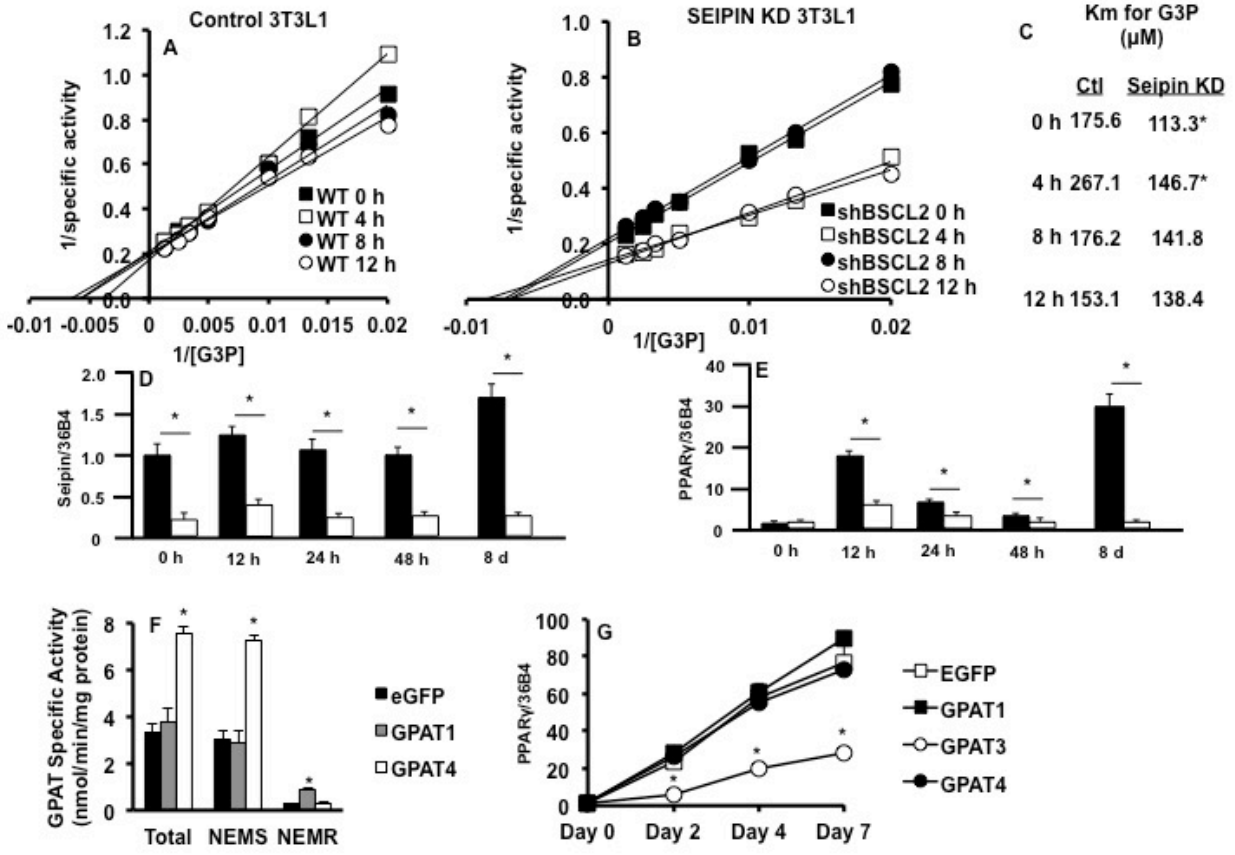

Figure 5.6: During differentiation, Seipin regulates GPAT kinetics and increased GPAT1 or GPAT4 activity does not block adipogenesis. A-C) GPAT kinetics in control and shBSCL2 3T3L1 preadipocytes at 0, 4, 8, and 12 h of differentiation. Results shown are Lineweaver-Burk plots with 1/specific activity in y-axis and 1/[glycerol-3-phosphate] in the x-axis. Five micrograms of membrane protein was incubated in the presence of increasing amounts of [1,2,3H]-glycerol-3-phosphate (50-800 μM) for 10 mins. D) In 3T3L1 cells, lentiviral knockdown reduces Seipin mRNA by 70% at 0 h and it remains low throughout differentiation. E) During differentiation, lentiviral knockdown of Seipin prevents normal PPARγ expression. F) In 3T3L1ΔCar cells, adenoviral overexpression of GPAT1 and GPAT4 increases *N*-ethylmaleimide resistant (NEM-R) and sensitive (NEM-S) GPAT activity, respectively. G) During differentiation, GPAT3 overexpression, but not that of GPAT1 or GPAT4, blocks PPARγ expression. mRNA expression was normalized to 36B4 expression. The expression of this gene does not change with differentiation status. Results shown are from 3 different cell passages or 3 independent infections and are presented as the mean ± S.E.M.

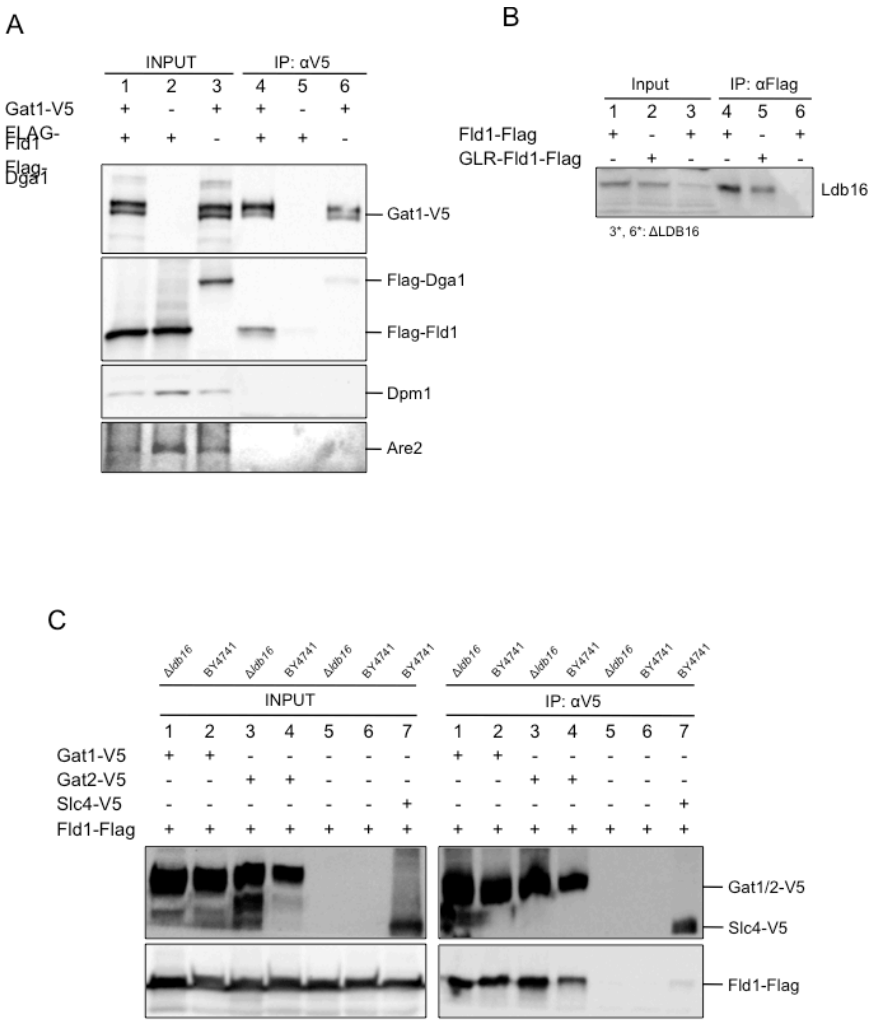

Figure 5.S1: Fld1, Ldb16 AND Gat1/2 form a ternary complex in yeast.[9]

A,B) Coimmunoprecipitation of overexpressed Gat1-V5 and FLAG-Fld1 by V5 antibody from yeast lysates. (FLAG-Dga1 does not coimmunoprecipitate with Gat1-V5. V5 antibody does not immunoprecipitate FLAG-Fld1 in absence of Gat1-V5. Dpm1 and Are2 can only be detected in the input). C) Coimmunoprecipitation of Ldb16 with mutant GLR-Fld1-FLAG, compared to wild-type Fld1-FLAG, is weakened.

[9] Contributed by Martin Pagac.

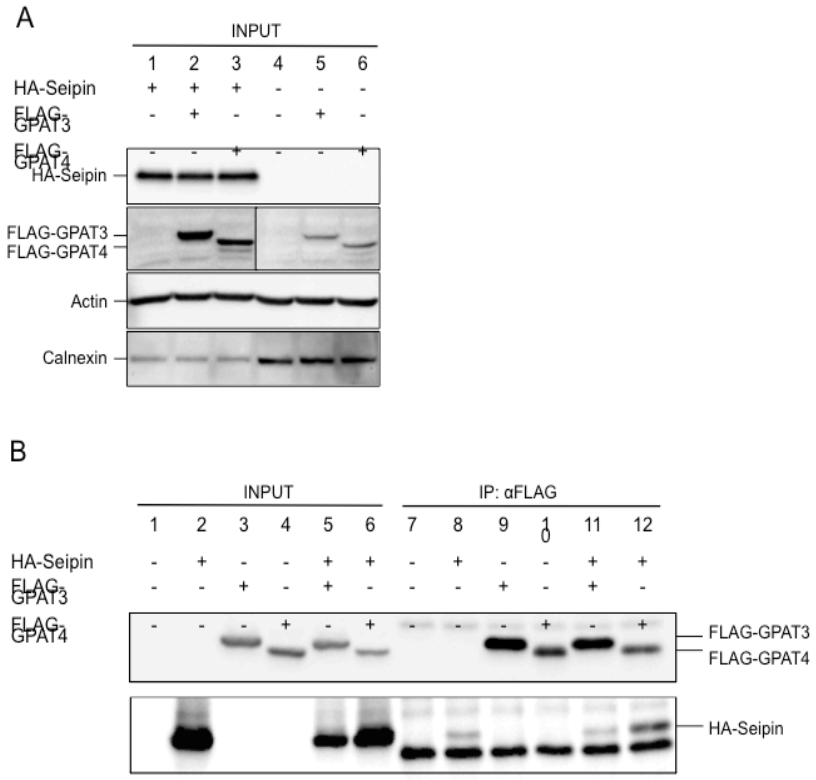

Figure 5.S2: Mammalian Seipin and GPAT3/4 physically interact.[10]

A) Inputs used for the coimmunoprecipitation experiment described in Figure 2 A). B) Coimmunoprecipitation by FLAG antibody of overexpressed FLAG-tagged GPAT3 or GPAT4 and HA-tagged Seipin, respectively, from transfected HeLa cell lysates. (HA-Seipin immunoprecipitates equally in the presence or absence of FLAG-GPAT3).

[10] Contributed by Martin Pagac.

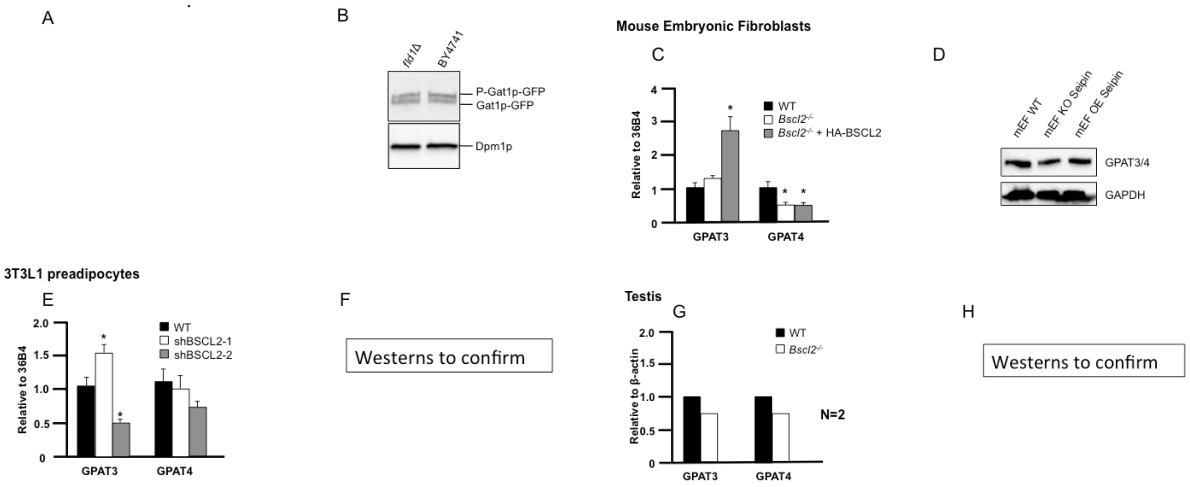

Figure 5.S3: GPAT activity is significantly increased in Fld1/Seipin-deficient cells and tissues.

A,B) Gat1 mRNA and protein expression in control and *fld1*Δ yeast microsomes. Dpm1p is used as loading control. C,D) GPAT3/4 mRNA and protein expression in control and *Bscl2*$^{-/-}$ mEFs or *Bscl2*$^{-/-}$ cells containing overexpressed HA-tagged Seipin (OE Seipin). mRNA expression was normalized to 36B4 and GAPDH was used as protein loading control. E,F) GPAT3 and GPAT4 mRNA levels in control and shBSCL2-expressing 3T3L1 cells. mRNA expression was normalized to 36B4. Western blots are in progress. G,H) GPAT3/4 mRNA expression in control and *Bscl2*$^{-/-}$ testis. mRNA expression was normalized to β-actin. Western blots are in progress.

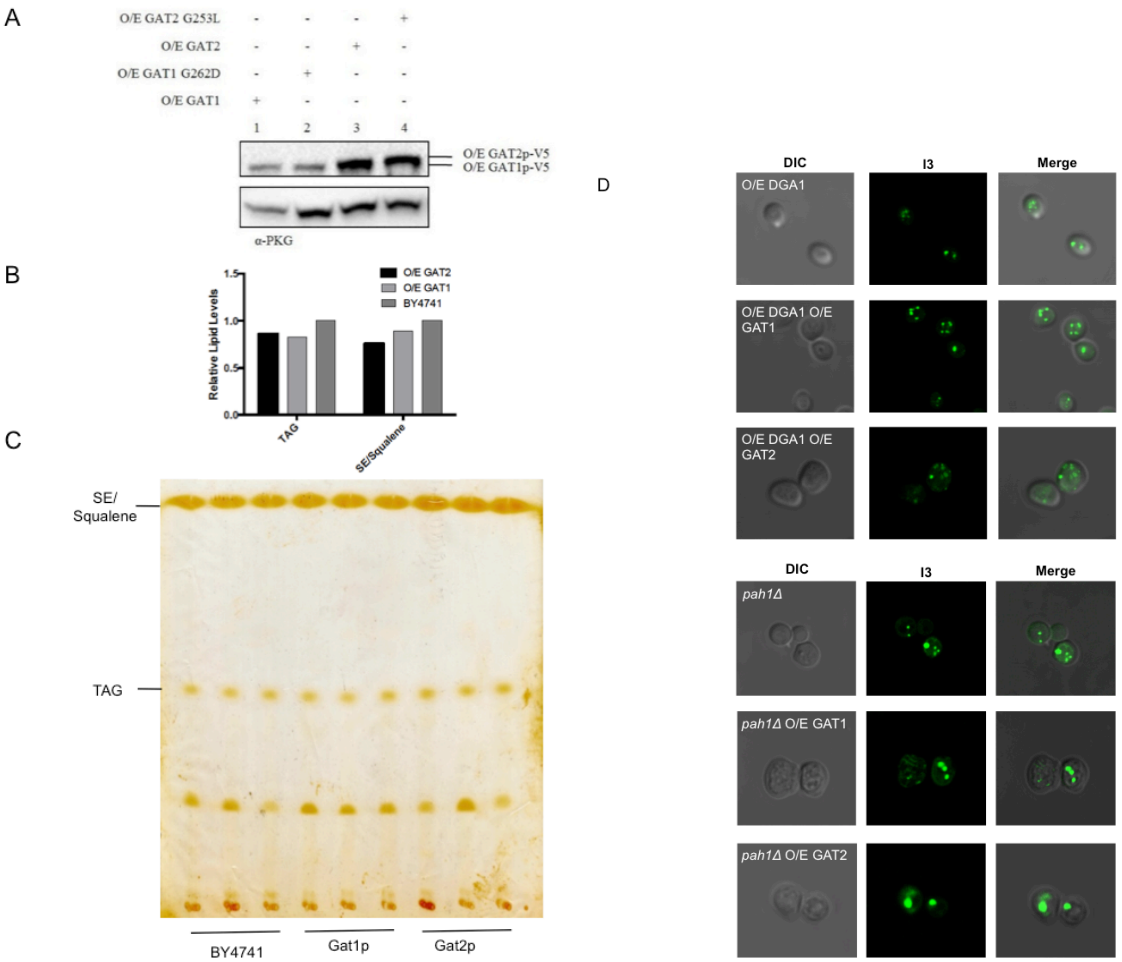

Fig 5.S5: Activation of GPAT drives the formation of "supersized" LDs in yeast and mammalian cells.[11]

A) Protein levels of O/E Gat1-V5 and G262D, O/E Gat2-V5 and G253L are similar. Normal LD size in yeast containing O/E catalytically dead Gat1 and Gat2 is not due to lower enzyme levels. B) Relative neutral lipid level quantification by thin layer chromatography. C) Thin layer chromatography separation of neutral lipids (TAG) and stearoyl ester (SE). Used for quantifications in Figure 5.S5B). D) Cells were grown until early stationary phase in SC media, stained with Nile red, and examined by fluorescence microscopy. LDs of mutant strains O/E Dga1 and *pah1Δ*. SLDs were present in *pah1Δ* strains but not in the O/E Dga1 strain.

[11] Contributed by Martin Pagac.

Chapter VI: SYNTHESIS

The focus of this dissertation was to elucidate independent functions of GPAT isoforms. Hepatic GPAT1, but not GPAT4, was required for the incorporation of *de novo* synthesized fatty acids into TAG and to divert fatty acids away from β-oxidation (**Ch. III**). Thus, despite catalyzing a similar amount of GPAT activity in the liver, GPAT1 and GPAT4 perform distinct and non-redundant functions. The differences in the functions of hepatic GPAT1 and GPAT4 are likely due to variations in subcellular location, acyl-CoA preference, or nutritional regulation. In contrast to its role in liver, GPAT4 limits the oxidation of exogenous fatty acids in brown adipocytes (**Ch. IV**). The disparate functions of GPAT4 in liver and BAT suggests that compartmentalization of glycerolipid synthesis is tissue-dependent. Finally, (**Ch. V**) we provide preliminary data suggesting a novel role for Seipin as an evolutionarily conserved regulator of microsomal GPAT activity. In both yeast and mammalian cells, Seipin physically interacted with microsomal GPAT, and the loss of Seipin increased GPAT activity. The activity of GPAT was increased because GPAT had a higher affinity for one of its substrates, glycerol-3-phosphate. Taken together, the work in this dissertation provides strong evidence that the flux of acyl-CoAs toward glycerolipid synthesis is compartmentalized and that each GPAT isoform performs a specific function within a physiological context.

Directions for Future Research

How do cells compartmentalize glycerolipid synthesis?

Enzyme complexes

Little work has been done to examine the interactions of membrane-bound metabolic enzyme complexes, but some examples are available. In the intestinal lumen, dietary TAG is hydrolyzed to 2 fatty acid constituents and a 2-monoacylglycerol. Once these components are transported into the intestinal epithelium, fatty acids are reesterified to the 2-monoacylglycerol, packed into chylomicrons and secreted into the lymph. The rate-limiting enzyme in intestinal TAG resynthesis is catalyzed by monoacylglycerol acyltransferase isoform-2 (MGAT2). MGAT2 esterifies an acyl-CoA to the *sn*-1 position of the 2-MAG to produce PA, and subsequent acyl-CoA esterification is catalyzed by DGAT1 to produce TAG. To enhance the efficiency of these reactions, it seems likely that these proteins might interact. Interestingly, in Cos-7 cells, MGAT2 heterodimerizes with DGAT1 and in McArdle rat hepatoma cells, it heterodimerizes with DGAT2 (129,130). The fact that these interactions differ in a cell type-dependent manner suggests that MGAT2 may have additional interacting partners in other tissues. Because these enzymes are found in complexes, it is likely that GPAT and other lipid metabolism enzymes interact in a similar manner.

In the Coleman lab, experiments are underway to identify protein-protein interactions of the acyl-CoA synthetase isoform-1 (ACSL1). ACSLs activate fatty acids to fatty acyl-CoAs before their use in downstream metabolic reactions, including complex lipid synthesis. Pamela Young has generated stable cell lines that

overexpress ACSL1 tagged with BirA. This BirA tag biotinylates enzymes that come into close contact with ACSL1 and, once biotinylated, these proteins can be purified with streptavidin, and identified with an unbiased proteomics approach. Once protein-protein interacting partners are identified, the interactions can be confirmed using co-immunoprecipitation. By performing these experiments in different cell-types and examining interactions with different physiological stimuli, these studies will provide direct evidence of cell type-dependent interactions that vary in response to physiological stimuli. A similar approach can be undertaken to identify interacting proteins with GPAT proteins.

Reorganization of organelles

Located on the outer mitochondrial membrane, GPAT1 and 2 produce LPA that is incorporated into TAG. However, the second enzyme, AGPAT, is thought to be exclusively located on the ER. Thus, how the GPAT-derived LPA on the outer mitochondrial membrane is accessible to ER-bound AGPAT enzymes remains unclear. Because GPAT1 does not move from the mitochondria (37), it is possible that certain physiological conditions result in the association of the mitochondria and ER and permit GPAT1-derived LPA to be accessible to the downstream metabolic enzymes in TAG synthesis. Studies using confocal microscopy might be best suited to reveal interactions between metabolic enzymes on distinct organelles. Alternatively, mitochondrial-derived LPA may be bound to an intracellular fatty acid binding protein (FABP) that directs its transport toward the enzymes on the ER (131). Acetate-labeling studies similar to those completed in Chapter III could be performed in various FABP-

null hepatocyte models and determine if deletion of FABP produces a similar result to GPAT1 deficiency.

Movement of enzymes to different intracellular compartments

Recent evidence demonstrates that the full complement of TAG synthetic enzymes moves from the bilayer of the ER onto the outer leaflet of LDs, and this movement is required for LD expansion (37). Incubation with oleate induces relocation of GPAT4, AGPAT2, and DGAT2. The overexpression of these proteins increases the size of lipid droplets within cells. It remains unclear how this movement is controlled, however, recent studies have identified the ER protein Seipin as essential for controlling LD biogenesis. Loss of Seipin results in increased LD size, likely mediated via its interaction with GPAT3 or GPAT4. How this interaction regulates GPAT4 and LD size remains obscure. It is possible that Seipin restricts the movement of GPAT4 or that Seipin controls the production of the fusogenic lipid, PA. This possibility would suggest that release of Seipin from GPAT4 increases local PA production and induces fusion of LDs and ER, permitting movement of TAG synthetic enzymes onto LDs. Further studies using confocal microscopy and an intracellular probe for PA will be useful in elucidating these mechanisms.

A second question relates to the activity of membrane-bound enzymes on the monolayer of LDs. All of the TAG synthetic enzymes are predicted to have at least two strongly hydrophobic domains, suggesting that they traverse the ER bilayer. Their movement onto the outer leaflet of LDs would likely alter their conformation, thus,

modifying their enzymatic activities. Whether these enzymes retain their activity on the outer leaflet of the LD has not been confirmed, but is supported by their coordinated movement and LD expansion. It is possible that the conformational change resulting from relocation to LDs alters the kinetics of these enzymes and increases their activity. To confirm this, methods need to be developed to measure enzyme activity on LDs. Purification of LDs is commonly used in proteomic screens that identify LD-associated proteins, however, the close association of LDs and ER prohibits entirely pure fractions and may contaminate LD fractions and obscure results. Further, the amount of protein found on the LDs is low and requires an excess of material to permit measurement of enzymatic activity. Additionally, the amount of lipid within the droplet fractions may confound enzymatic assay measurements. Nonetheless, development of adequate techniques to measure LD-associated enzyme activity would provide valuable information with regard to LD biogenesis.

Do lipid droplets segregate into functional pools?

Lipid droplets and the "athletes paradox"

The overexpression of GPAT1 and GPAT4 results in dramatic differences in LD size and number. Whereas the overexpression of GPAT1 increases the number of LDs, these droplets are decidedly smaller. In contrast, GPAT4 overexpression increases the size of LDs. These differences in LD dynamics may inform the "athlete's paradox". Although the accumulation of TAG in skeletal muscle of obese individuals is associated with insulin resistance, highly trained athletes also accumulate excess TAG, but remain exquisitely insulin sensitive. However, the mechanisms remain obscure. Based on the

known roles of GPAT1 and GPAT4 in LD biogenesis, it is possible that the GPAT isoform that catalyzes TAG synthesis in muscle from obese individuals and highly trained athletes is different. It is possible that the resulting lipid droplets either contain differences in the complements of proteins, interactions with organelles, or GPAT-derived lipid intermediates that alter distinct signaling pathways that affect larger metabolic pathways. Theoretically, one could obtain muscle biopsies from obese and highly trained individuals and measure the incorporation of radiolabeled fatty acid into lipid. These results would provide preliminary data to begin exploring which GPAT isoform is involved in each process. Alternatively, GPAT assays could be performed on these samples to determine whether GPAT1 or an alternate GPAT isoform catalyzes the predominant amount of GPAT activity in the respective samples.

GPAT-derived lipid droplets in BAT thermogenesis

Similar to the athletes' paradox, TAG accumulation in BAT is observed in obesity and in cold-acclimated rodents. Because GPAT4 limits oxidation of exogenous fatty acids in brown adipocytes and loss of GPAT4 does not affect acute cold tolerance (**Ch. IV**), it is possible that an alternate GPAT isoform is important for BAT TAG accumulation in cold-acclimation. Consistent with differential nutritional regulation of GPAT isoforms, mitochondrial GPAT activity in BAT is upregulated 3-fold with exposure to an acute cold challenge and nearly 7-fold following a 21-day cold exposure. In contrast, microsomal GPAT activity is unchanged in response to an acute cold exposure, and following a 21-day cold challenge, is increased 2 to 3-fold (132). Consistent with the regulation in cold-exposed rodents, β -adrenergic stimulation did not alter microsomal GPAT activity, but

mitochondrial GPAT activity was increased 5-fold (133). To distinguish the role of the mitochondrial and microsomal GPAT isoforms in BAT thermogenesis, direct comparison of GPAT-null mice in response to cold-acclimation is necessary. Furthermore, direct comparison of fatty acid incorporation into GPAT-null primary brown adipocytes will provide valuable information regarding acyl-CoA metabolism in β-adrenergic activated brown adipocyte cells. With the interest in BAT activation as a potential therapeutic target for the treatment of obesity, these studies may prove particularly informative.

GPAT Double-knockout models

Based on the variable phenotypes of GPAT-null mice, curiosity has arisen with respect to the simultaneous deletion of multiple GPAT isoforms. Because GPAT1 and GPAT4 are the predominant GPAT isoforms in liver, deletion of both isoforms would provide valuable information on the ability of other GPAT isoforms to compensate. Deletion of both microsomal GPAT isoforms, GPAT3 and GPAT4, would permit us to determine the necessity of differentially localized GPATs, i.e. Can mitochondrial GPATs fully compensate for the loss of all microsomal GPAT activity. Assuming that the loss of both microsomal GPATs would produce viable offspring, one could potentially identify additional microsomal GPAT isoforms. To avoid the potential for embryonic lethality, one could inducibly delete the second GPAT after birth. Despite our current understanding that GPAT1 is the only NEM-resistant GPAT isoform, GPAT1-deficient hearts retain NEM-resistant GPAT activity, suggesting that an alternate GPAT isoform is present in cardiac tissue. Together, these studies could identify new GPAT isoforms and explain the necessity of GPAT isoforms in different intracellular locations.

How does GPAT subcellular location affect function?

Because our evidence supports the hypothesis that the metabolism of acyl-CoAs through GPAT is highly compartmentalized, it is likely that some of this is due to differences in subcellular location. Zengying Wu, a member of the Coleman Lab, is currently investigating the relationship between GPAT location and function. To do so, Zengying is modifying the signal peptide of microsomal GPAT4 to target this enzyme to the outer mitochondrial membrane. Results from these studies will inform questions related to GPAT location and function. An alternate approach could be used to evaluate the importance of the C-terminus of GPAT1. Using a cloning approach, one could add the C-terminus of GPAT1 to either microsomal GPAT isoform and subsequently measure sensitivity to NEM or the ability to use various acyl-CoA substrates.

Do GPATs possess other enzymatic activities?

GPAT isoforms possess four highly conserved motifs that are essential for their catalytic activity. Leading to their initial identification as AGPATs, the microsomal GPATs possess a fifth motif, present in the AGPAT family of enzymes. Although subsequent studies show that both GPAT3 and GPAT4 possess GPAT activity, some work suggests that GPAT3 may also express AGPAT activity. However, the techniques used to isolate membranes for AGPAT activity assays limit this conclusion. Furthermore, plant GPAT enzymes are bifunctional enzymes that possess *sn*-2 acyltransferase activity and phosphatase activity, suggesting the potential for mammalian GPATs to exhibit dual functions. When William Lands first identified the *sn*-1 specificity of GPAT (134), the discovery of four distinct GPAT isoforms had not been

made. Thus, further biochemical characterization of the GPAT enzyme substrate preference and positional specificity is necessary. Determining the potential for AGPAT or other enzymatic activities in GPATs would provide valuable insights into the flux of acyl-CoAs towards specific glycerolipid fates and lipid intermediate signals.

Seipin and GPAT: impact on lipodystrophy and LD biogenesis

Does the overexpression of GPAT block adipogenesis?

Based on our preliminary findings (see manuscript 3), we hypothesize that in Seipin-deficient cells, increased GPAT activity underpins the block of adipogenesis. To test this, we plan to overexpress GPAT3 and GPAT4 in 3T3L1 preadipocytes and measure their ability to differentiate. Differentiation will be determined by measuring the mRNA expression of PPARγ and Oil Red O staining of neutral lipids to confirm lipid accumulation. We will confirm that GPAT activity is increased with overexpression and send samples to our collaborator Thurl Harris at the University of Virginia for mass spectrometric identification of PA species. These experiments are currently underway.

How does increased GPAT activity in Seipin-deficient cells impair adipogenesis?

With the discovery that Seipin is an evolutionarily conserved regulator of microsomal GPAT activity and the observation that Seipin deficiency increased GPAT activity, our next step is to determine the mechanism for how GPAT activity impairs adipogenesis. Our collaborator on this project, Hongyuan (Rob) Yang at the University of New South Wales has proposed a theory that links the increased intracellular PA levels in lipodystrophic tissues to the inhibition of PPARγ activation. This theory posits

that increased GPAT activity leads to increased intracellular PA and that PA acts as an antagonist to PPARγ activation (77). Based on our previous studies on the action of di-16:0-PA in the insulin-signaling pathway, it is possible that microsomal GPAT generates a PA specie with an acyl-chain composition that acts as a potent antagonist to PPARγ. To address this question, we have overexpressed GPAT3 and GPAT4 in 3T3L1 cells and will use mass spectrometric studies, with our collaborator Thurl Harris at the University of Virginia, to compare the PA species that are elevated in both Seipin-deficient and GPAT overexpressing cells. If our hypothesis is correct, we would expect that the PA species in Seipin-deficient tissues and cells overexpressing GPAT would be similar to those lacking Seipin. By identifying those PA species that were specifically increased in these cells, but not in GPAT4 overexpressing cells, we could test the potential of the identified PA species as antagonists of PPARγ. Although it has been proposed that PPARγ is modulated by naturally occurring lipid, no endogenous ligands have been identified. Results from these studies would reveal the molecular mechanism for Seipin-deficient lipodystrophy and identify the first endogenous ligand for the master regulator of adipogenesis, PPARγ.

Does the lack of Seipin alter AGPAT activity?

Because the lack of Seipin increases GPAT activity and intracellular PA levels, it is possible that AGPAT, the enzyme that synthesizes PA from LPA, activity is also increased. My preliminary data suggests that in Seipin-deficient cells, AGPAT activity is increased when 16:0-CoA, but not 18:1-CoA, is used as an acyl-donor. If we are able to confirm these findings then we will proceed with characterization of the enzymatic

kinetics and substrate preference of this activity. Whether this activity is catalyzed by an AGPAT isoform or by one of the microsomal GPAT isoforms will also require further investigation.

How does Seipin regulate LD biogenesis through GPAT?

Current evidence supports that Seipin's interaction with GPAT4 is required to control the movement of GPAT4 on to the outer leaflet of growing LDs. Studies to identify how this interaction modulates LD biogenesis are currently underway in our lab and in several labs within our field. Whether Seipin restricts the movement of GPAT4 onto the droplet or mediates the fusion of LDs with the ER membrane remains unclear. Alternatively, it is possible that Seipin modifies the potential for microsomal GPATs to catalyze AGPAT activity. Identifying these mechanisms would provide valuable insights in our understanding of LD biogenesis and the accumulation of TAG in the context of obesity.

Would GPAT inhibition rescue Seipin-deficient lipodystrophy?

Based on our hypothesis that in Seipin-deficient cells increased GPAT activity underpins the block on adipogenesis, GPAT inhibition may correct Seipin-deficient lipodystrophy. We recently obtained a GPAT inhibitor, of similar structure to those described in **Background 5**, which possess potent GPAT inhibitory activity in our in vitro activity assays. Because Craig Townsend's group at Yale University reported that these compounds also possess inhibitory activity in 3T3L1 cells, we are currently evaluating whether the GPAT inhibitor can treat Seipin-deficient lipodystrophy.

Zengying Wu and I are currently performing these assays. If GPAT inhibition rescues adipogenesis in 3T3L1 cells, we plan to treat Seipin-deficient mice with the compound and evaluate its efficacy in vivo. These studies will provide proof-of-concept that GPAT inhibition can restore adipogenesis in individuals with Seipin-deficient lipodystrophy. Additionally, we have discussed making a double knockout mouse of Seipin and GPAT3, however, this approach will require a significant amount of time. Whether microsomal GPAT is involved in the etiology of the acquired lipodystrophies also is an intriguing possibility.

Public Health Significance

Despite the significant resources and human capital invested in understanding the etiology of obesity and the metabolic syndrome, relatively little progress has been made in developing therapeutic treatments. Clearly, the complex nature of metabolism has slowed our progress. However, results from this dissertation highlighting that important aspects of nutrient metabolism are compartmentalized provide valuable insights toward our shared treatment goals. Improving our basic understandings of glycerolipid synthesis in this way will strengthen the approaches of research focused on the pharmacological inhibition of glycerolipid synthetic enzymes. These studies will inform potential treatment strategies and drug delivery techniques. Furthermore, these discoveries will improve current approaches and inform the work of others in the field. Our work revealing the relationship between Seipin and GPAT, suggests that GPAT inhibition might be a suitable strategy for treating type 2 congenital generalized lipodystrophy. Although this lipodystrophy only affects a small proportion of people, the insights gained from understanding the basic biology of adipose tissue can be applied in other areas of research related to obesity.

REFERENCES

1. Ogden, C. L., Carroll, M. D., Kit, B. K., and Flegal, K. M. (2014) Prevalence of childhood and adult obesity in the United States, 2011-2012. *Jama* **311**, 806-814

2. Trogdon, J. G., Finkelstein, E. A., Feagan, C. W., and Cohen, J. W. (2012) State- and payer-specific estimates of annual medical expenditures attributable to obesity. *Obesity* **20**, 214-220

3. Finkelstein, E. A., Trogdon, J. G., Cohen, J. W., and Dietz, W. (2009) Annual medical spending attributable to obesity: payer-and service-specific estimates. *Health affairs* **28**, w822-831

4. Muoio, D. M., and Newgard, C. B. (2006) Obesity-related derangements in metabolic regulation. *Annual review of biochemistry* **75**, 367-401

5. Hammond, L. E., Gallagher, P. A., Wang, S., Posey-Marcos, E., Hiller, S., Kluckman, K., Maeda, N., and Coleman, R. A. (2002) Mitochondrial glycerol-3-phosphate acyltransferase-deficient mice have reduced weight and liver triacylglycerol content and altered glycerolipid fatty acid composition. *Mol. Cell. Biol.* **22**, 8204-8214

6. Neschen, S., Morino, K., Hammond, L. E., Zhang, D., Liu, Z. X., Romanelli, A. J., Cline, G. W., Pongratz, R. L., Zhang, X. M., Choi, C. S., Coleman, R. A., and Shulman, G. I. (2005) Prevention of hepatic steatosis and hepatic insulin resistance in mitochondrial acyl-CoA:glycerol-sn-3-phosphate acyltransferase 1 knock out mice. *Cell Metab.* **2**, 55-65

7. Hammond, L. E., Albright, C. D., He, L., Rusyn, I., Watkins, S. W., Doughman, S. D., Lemasters, J. J., and Coleman, R. A. (2007) Increased oxidative stress is associated with balanced increases in hepatocyte apoptosis and proliferation in glycerol-3-phosphate acyltransferase-1 deficient mice. *Exper. Molec. Pathol.* **82**, 210-219

8. Ellis, J. M., Paul, D. S., Depetrillo, M. A., Singh, B. P., Malarkey, D. E., and Coleman, R. A. (2012) Mice deficient in glycerol-3-phosphate acyltransferase-1 have a reduced susceptibility to liver cancer. *Toxicologic pathology* **doi:10.1177/0192623311432298**

9. Cattaneo, E. R., Pellon-Maison, M., Rabassa, M. E., Lacunza, E., Coleman, R. A., and Gonzalez-Baro, M. R. (2012) Glycerol-3-phosphate acyltransferase-2 is

expressed in spermatic germ cells and incorporates arachidonic acid into triacylglycerols. *PloS one* **7**, e42986

10. Cao, J., Li, J. L., Li, D., Tobin, J. F., and Gimeno, R. E. (2006) Molecular identification of microsomal acyl-CoA:glycerol-3-phosphate acyltransferase, a key enzyme in de novo triacylglycerol synthesis. *Proceedings of the National Academy of Sciences of the United States of America* **103**, 19695-19700

11. Cao, J., Perez, S., Goodwin, B., Lin, Q., Peng, H., Qadri, A., Zhou, Y., Clark, R. W., Perreault, M., Tobin, J. F., and Gimeno, R. E. (2014) Mice deleted for GPAT3 have reduced GPAT activity in white adipose tissue and altered energy and cholesterol homeostasis in diet-induced obesity. *American journal of physiology. Endocrinology and metabolism* **306**, E1176-1187

12. Nagle, C. A., Verges, L., Wang, S., deJong, H., Wang, S., Lewin, T. M., Reue, K., and Coleman, R. A. (2008) Identification of a novel *sn*-glycerol-3-phosphate acyltransferase isoform, GPAT4 as the enzyme deficient in Agpat6-/- mice. *J. Lipid Res.* **49**, 823-831

13. Beigneux, A. P., Vergnes, L., Qiao, X., Quatela, S., Davis, R., Watkins, S. M., Coleman, R. A., Walzem, R. L., Philips, M., Reue, K., and Young, S. G. (2006) Agpat6--a novel lipid biosynthetic gene required for triacylglycerol production in mammary epithelium. *J. Lipid Res.* **47**, 734-744

14. Zhang, C., Cooper, D. E., Grevengoed, T. J., Li, L. O., Klett, E. L., Eaton, J. M., Harris, T. E., and Coleman, R. A. (2014) Glycerol-3-phosphate acyltransferase-4-deficient mice are protected from diet-induced insulin resistance by the enhanced association of mTOR and rictor. *American journal of physiology. Endocrinology and metabolism* **307**, E305-315

15. Vergnes, L., Beigneux, A. P., Davis, R. G., Watkins, S. M., Young, S. G., and Reue, K. (2006) Agpat6 deficiency causes subdermal lipodystrophy and resistance to obesity. *J. Lipid Res.* **47**, 745-754

16. Ovadi, J., and Saks, V. (2004) On the origin of intracellular compartmentation and organized metabolic systems. *Mol. Cell. Biochem.* **256-257**, 5-12

17. Kornberg, A., and Pricer, W. E., Jr. (1953) Enzymatic esterification of alpha-glycerophosphate by long chain fatty acids. *The Journal of biological chemistry* **204**, 345-357

18. Bell, R. M., and Coleman, R. A. (1980) Enzymes of glycerolipid synthesis in eukaryotes. *Annual review of biochemistry* **49**, 459-487

19. Coleman, R. A., and Lee, D. P. (2004) Enzymes of triacylglycerol synthesis and their regulation. *Progress in lipid research* **43**, 134-176

20. Lewin, T. M., Wang, P., and Coleman, R. A. (1999) Analysis of amino acid motifs diagnostic for the sn-glycerol-3-phosphate acyltransferase reaction. *Biochemistry* **38**, 5764-5771

21. Dircks, L. K., Ke, J., and Sul, H. S. (1999) A conserved seven amino acid stretch important for murine mitochondrial glycerol-3-phosphate acyltransferase activity. Significance of arginine 318 in catalysis. *The Journal of biological chemistry* **274**, 34728-34734

22. Chen, Y., Kuo, M. S., Li, S., Bui, H. H., Peake, D. A., Sanders, P. E., Thibodeaux, S. J., Chu, S., Qian, Y. W., Zhao, Y., Bredt, D. S., Moller, D. E., Konrad, R. J., Beigneux, A. P., Young, S. G., and Cao, G. (2008) AGPAT6 Is a novel microsomal glycerol-3-phosphate acyltransferase (GPAT). *J. Biol. Chem.* **283**, 10048-10057

23. Smart, H. C., Mast, F. D., Chilije, M. F., Tavassoli, M., Dacks, J. B., and Zaremberg, V. (2014) Phylogenetic analysis of glycerol 3-phosphate acyltransferases in opisthokonts reveals unexpected ancestral complexity and novel modern biosynthetic components. *PloS one* **9**, e110684

24. Fares, M. A., Keane, O. M., Toft, C., Carretero-Paulet, L., and Jones, G. W. (2013) The roles of whole-genome and small-scale duplications in the functional specialization of Saccharomyces cerevisiae genes. *PLoS genetics* **9**, e1003176

25. Gonzalez-Baro, M. R., Granger, D. A., and Coleman, R. A. (2001) Mitochondrial glycerol phosphate acyltransferase contains two transmembrane domains with the active site in the N-terminal domain facing the cytosol. *The Journal of biological chemistry* **276**, 43182-43188

26. Coleman, R., and Bell, R. M. (1978) Evidence that biosynthesis of phosphatidylethanolamine, phosphatidylcholine, and triacylglycerol occurs on the cytoplasmic side of microsomal vesicles. *The Journal of cell biology* **76**, 245-253

27. Pellon-Maison, M., Coleman, R. A., and Gonzalez-Baro, M. R. (2006) The C-terminal region of mitochondrial glycerol-3-phosphate acyltransferase-1 interacts with the active site region and is required for activity. *Archives of biochemistry and biophysics* **450**, 157-166

28. Coleman, R. A., and Mashek, D. G. (2011) Mammalian triacylglycerol metabolism: synthesis, lipolysis, and signaling. *Chemical reviews* **111**, 6359-6386

29. Lewin, T. M., Granger, D. A., Kim, J. H., and Coleman, R. A. (2001) Regulation of mitochondrial sn-glycerol-3-phosphate acyltransferase activity: response to feeding status is unique in various rat tissues and is discordant with protein expression. *Archives of biochemistry and biophysics* **396**, 119-127

30. Muoio, D. M., Seefeld, K., Witters, L. A., and Coleman, R. A. (1999) AMP-activated kinase reciprocally regulates triacylglycerol synthesis and fatty acid oxidation in liver and muscle: evidence that sn-glycerol-3-phosphate acyltransferase is a novel target. *The Biochemical journal* **338 (Pt 3)**, 783-791

31. Bremer, J., Bjerve, K. S., Borrebaek, B., and Christiansen, R. (1976) The glycerolphosphate acyltransferases and their function in the metabolism of fatty acids. *Mol. Cell Biochem.* **12**, 113-125

32. Wendel, A. A., Li, L. O., Li, Y., Cline, G. W., Shulman, G. I., and Coleman, R. A. (2010) Glycerol-3-phosphate acyltransferase 1 deficiency in ob/ob mice diminishes hepatic steatosis but does not protect against insulin resistance or obesity. *Diabetes* **59**, 1321-1329

33. Harada, N., Fujimoto, E., Okuyama, M., Sakaue, H., and Nakaya, Y. (2012) Identification and functional characterization of human glycerol-3-phosphate acyltransferase 1 gene promoters. *Biochem Biophys Res Commun* **423**, 128-133

34. Nakagawa, T., Harada, N., Miyamoto, A., Kawanishi, Y., Yoshida, M., Shono, M., Mawatari, K., Takahashi, A., Sakaue, H., and Nakaya, Y. (2012) Membrane topology of murine glycerol-3-phosphate acyltransferase 2. *Biochem Biophys Res Commun* **418**, 506-511

35. Pellon-Maison, M., Montanaro, M. A., Lacunza, E., Garcia-Fabiani, M. B., Soler-Gerino, M. C., Cattaneo, E. R., Quiroga, I. Y., Abba, M. C., Coleman, R. A., and Gonzalez-Baro, M. R. (2014) Glycerol-3-phosphate acyltranferase-2 behaves as

a cancer testis gene and promotes growth and tumorigenicity of the breast cancer MDA-MB-231 cell line. *PloS one* **9**, e100896

36. Shan, D., Li, J. L., Wu, L., Li, D., Hurov, J., Tobin, J. F., Gimeno, R. E., and Cao, J. (2010) GPAT3 and GPAT4 are regulated by insulin-stimulated phosphorylation and play distinct roles in adipogenesis. *Journal of lipid research* **51**, 1971-1981

37. Wilfling, F., Wang, H., Haas, J. T., Krahmer, N., Gould, T. J., Uchida, A., Cheng, J. X., Graham, M., Christiano, R., Frohlich, F., Liu, X., Buhman, K. K., Coleman, R. A., Bewersdorf, J., Farese, R. V., Jr., and Walther, T. C. (2013) Triacylglycerol synthesis enzymes mediate lipid droplet growth by relocalizing from the ER to lipid droplets. *Developmental cell* **24**, 384-399

38. Nagle, C. A., Vergnes, L., Dejong, H., Wang, S., Lewin, T. M., Reue, K., and Coleman, R. A. (2008) Identification of a novel sn-glycerol-3-phosphate acyltransferase isoform, GPAT4, as the enzyme deficient in Agpat6-/- mice. *Journal of lipid research* **49**, 823-831

39. Hammond, L. E., Neschen, S., Romanelli, A. J., Cline, G. W., Ilkayeva, O. R., Shulman, G. I., Muoio, D. M., and Coleman, R. A. (2005) Mitochondrial glycerol-3-phosphate acyltransferase-1 is essential in liver for the metabolism of excess acyl-CoAs. *The Journal of biological chemistry* **280**, 25629-25636

40. Vergnes, L., Beigneux, A. P., Davis, R., Watkins, S. M., Young, S. G., and Reue, K. (2006) Agpat6 deficiency causes subdermal lipodystrophy and resistance to obesity. *Journal of lipid research* **47**, 745-754

41. Banh, T., Nelson, D. W., Gao, Y., Huang, T. N., Yen, M. I., and Yen, C. L. (2015) Adult-onset deficiency of acyl CoA:monoacylglycerol acyltransferase 2 protects mice from diet-induced obesity and glucose intolerance. *Journal of lipid research* **56**, 379-389

42. Yen, C. L., Cheong, M. L., Grueter, C., Zhou, P., Moriwaki, J., Wong, J. S., Hubbard, B., Marmor, S., and Farese, R. V., Jr. (2009) Deficiency of the intestinal enzyme acyl CoA:monoacylglycerol acyltransferase-2 protects mice from metabolic disorders induced by high-fat feeding. *Nat. Med.* **15**, 442-446

43. Smith, S. J., Cases, S., Jensen, D. R., Chen, H. C., Sande, E., Tow, B., Sanan, D. A., Raber, J., Eckel, R. H., and Farese, R. V., Jr. (2000) Obesity resistance and multiple mechanisms of triglyceride synthesis in mice lacking Dgat. *Nature genetics* **25**, 87-90

44. Cao, J., Hawkins, E., Brozinick, J., Liu, X., Zhang, H., Burn, P., and Shi, Y. (2004) A predominant role of acyl-CoA:monoacylglycerol acyltransferase-2 in dietary fat absorption implicated by tissue distribution, subcellular localization, and up-regulation by high fat diet. *The Journal of biological chemistry* **279**, 18878-18886

45. Yen, C. L., and Farese, R. V., Jr. (2003) MGAT2, a monoacylglycerol acyltransferase expressed in the small intestine. *The Journal of biological chemistry* **278**, 18532-18537

46. Nelson, D. W., Gao, Y., Spencer, N. M., Banh, T., and Yen, C. L. (2011) Deficiency of MGAT2 increases energy expenditure without high-fat feeding and protects genetically obese mice from excessive weight gain. *Journal of lipid research* **52**, 1723-1732

47. Stone, S. J., Myers, H. M., Watkins, S. M., Brown, B. E., Feingold, K. R., Elias, P. M., and Farese, R. V., Jr. (2004) Lipopenia and skin barrier abnormalities in DGAT2-deficient mice. *The Journal of biological chemistry* **279**, 11767-11776

48. Nagle, C. A., An, J., Shiota, M., Torres, T. P., Cline, G. W., Liu, Z.-X., Wang, S., Catlin, R. L., Shulman, G. I., Newgard, C. B., and Coleman, R. A. (2007) Hepatic overexpression of glycerol-sn-3-phosphate acyltransferase 1 in rats causes insulin resistance. *J. Biol. Chem.* **282**, 14807-14815

49. Zhang, C., Klett, E. L., and Coleman, R. A. (2013) Lipid signals and insulin resistance. *Clinical lipidology* **8**, 659-667

50. Perry, R. J., Samuel, V. T., Petersen, K. F., and Shulman, G. I. (2014) The role of hepatic lipids in hepatic insulin resistance and type 2 diabetes. *Nature* **510**, 84-91

51. Cantley, J. L., Yoshimura, T., Camporez, J. P., Zhang, D., Jornayvaz, F. R., Kumashiro, N., Guebre-Egziabher, F., Jurczak, M. J., Kahn, M., Guigni, B. A., Serr, J., Hankin, J., Murphy, R. C., Cline, G. W., Bhanot, S., Manchem, V. P., Brown, J. M., Samuel, V. T., and Shulman, G. I. (2013) CGI-58 knockdown sequesters diacylglycerols in lipid droplets/ER-preventing diacylglycerol-mediated hepatic insulin resistance. *Proc Natl Acad Sci U S A* **110**, 1869-1874

52. Zhang, C., Wendel, A. A., Keogh, M. R., Harris, T. E., Chen, J., and Coleman, R. A. (2012) Glycerolipid signals alter mTOR complex 2 (mTORC2) to diminish insulin signaling. *Proc Natl Acad Sci U S A* **109**, 1667-1672

53. Jornayvaz, F. R., Birkenfeld, A. L., Jurczak, M. J., Kanda, S., Guigni, B. A., Jiang, D. C., Zhang, D., Lee, H. Y., Samuel, V. T., and Shulman, G. I. (2011) Hepatic insulin resistance in mice with hepatic overexpression of diacylglycerol acyltransferase 2. *Proc Natl Acad Sci U S A* **108**, 5748-5752

54. Kumashiro, N., Erion, D. M., Zhang, D., Kahn, M., Beddow, S. A., Chu, X., Still, C. D., Gerhard, G. S., Han, X., Dziura, J., Petersen, K. F., Samuel, V. T., and Shulman, G. I. (2011) Cellular mechanism of insulin resistance in nonalcoholic fatty liver disease. *Proc Natl Acad Sci U S A* **108**, 16381-16385

55. Szendroedi, J., Yoshimura, T., Phielix, E., Koliaki, C., Marcucci, M., Zhang, D., Jelenik, T., Muller, J., Herder, C., Nowotny, P., Shulman, G. I., and Roden, M. (2014) Role of diacylglycerol activation of PKCtheta in lipid-induced muscle insulin resistance in humans. *Proc Natl Acad Sci U S A* **111**, 9597-9602

56. Zhang, C., Hwarng, G., Cooper, D. E., Grevengoed, T. J., Eaton, J. M., Natarajan, V., Harris, T. E., and Coleman, R. A. (2015) Inhibited insulin signaling in mouse hepatocytes is associated with increased phosphatidic Acid but not diacylglycerol. *The Journal of biological chemistry* **290**, 3519-3528

57. Madani, S., Hichami, A., Legrand, A., Belleville, J., and Khan, N. A. (2001) Implication of acyl chain of diacylglycerols in activation of different isoforms of protein kinase C. *FASEB journal : official publication of the Federation of American Societies for Experimental Biology* **15**, 2595-2601

58. Wilfling, F., Haas, J. T., Walther, T. C., and Farese, R. V., Jr. (2014) Lipid droplet biogenesis. *Current opinion in cell biology* **29**, 39-45

59. Farese, R. V., Jr., and Walther, T. C. (2009) Lipid droplets finally get a little R-E-S-P-E-C-T. *Cell* **139**, 855-860

60. Cao, G., Konrad, R. J., Li, S. D., and Hammond, C. (2012) Glycerolipid acyltransferases in triglyceride metabolism and energy homeostasis-potential as drug targets. *Endocrine, metabolic & immune disorders drug targets* **12**, 197-206

61. Shi, Y., and Burn, P. (2004) Lipid metabolic enzymes: emerging drug targets for the treatment of obesity. *Nature reviews. Drug discovery* **3**, 695-710

62. Guerciolini, R. (1997) Mode of action of orlistat. *Int J Obes Relat Metab Disord* **21 Suppl 3**, S12-23

63. Wydysh, E. A., Medghalchi, S. M., Vadlamudi, A., and Townsend, C. A. (2009) Design and synthesis of small molecule glycerol 3-phosphate acyltransferase inhibitors. *Journal of medicinal chemistry* **52**, 3317-3327

64. Wydysh, E. A., Vadlamudi, A., Medghalchi, S. M., and Townsend, C. A. (2010) Design, synthesis, and biological evaluation of conformationally constrained glycerol 3-phosphate acyltransferase inhibitors. *Bioorganic & medicinal chemistry* **18**, 6470-6479

65. Kuhajda, F. P., Aja, S., Tu, Y., Han, W. F., Medghalchi, S. M., El Meskini, R., Landree, L. E., Peterson, J. M., Daniels, K., Wong, K., Wydysh, E. A., Townsend, C. A., and Ronnett, G. V. (2011) Pharmacological glycerol-3-phosphate acyltransferase inhibition decreases food intake and adiposity and increases insulin sensitivity in diet-induced obesity. *Am J Physiol Regul Integr Comp Physiol* **301**, R116-130

66. Garg, A., and Agarwal, A. K. (2009) Lipodystrophies: disorders of adipose tissue biology. *Biochimica et biophysica acta* **1791**, 507-513

67. Carr, A., Samaras, K., Burton, S., Law, M., Freund, J., Chisholm, D. J., and Cooper, D. A. (1998) A syndrome of peripheral lipodystrophy, hyperlipidaemia and insulin resistance in patients receiving HIV protease inhibitors. *Aids* **12**, F51-58

68. Simha, V., and Garg, A. (2009) Inherited lipodystrophies and hypertriglyceridemia. *Current opinion in lipidology* **20**, 300-308

69. Agarwal, A. K., and Garg, A. (2006) Genetic basis of lipodystrophies and management of metabolic complications. *Annu Rev Med* **57**, 297-311

70. Agarwal, A. K., and Garg, A. (2003) Congenital generalized lipodystrophy: significance of triglyceride biosynthetic pathways. *Trends in endocrinology and metabolism: TEM* **14**, 214-221

71. Szymanski, K. M., Binns, D., Bartz, R., Grishin, N. V., Li, W. P., Agarwal, A. K., Garg, A., Anderson, R. G., and Goodman, J. M. (2007) The lipodystrophy protein seipin is found at endoplasmic reticulum lipid droplet junctions and is important for droplet morphology. *Proc Natl Acad Sci U S A* **104**, 20890-20895

72. Payne, V. A., Grimsey, N., Tuthill, A., Virtue, S., Gray, S. L., Dalla Nora, E., Semple, R. K., O'Rahilly, S., and Rochford, J. J. (2008) The human lipodystrophy gene BSCL2/seipin may be essential for normal adipocyte differentiation. *Diabetes* **57**, 2055-2060

73. Fei, W., Li, H., Shui, G., Kapterian, T. S., Bielby, C., Du, X., Brown, A. J., Li, P., Wenk, M. R., Liu, P., and Yang, H. (2011) Molecular characterization of seipin and its mutants: implications for seipin in triacylglycerol synthesis. *Journal of lipid research* **52**, 2136-2147

74. Fei, W., Shui, G., Gaeta, B., Du, X., Kuerschner, L., Li, P., Brown, A. J., Wenk, M. R., Parton, R. G., and Yang, H. (2008) Fld1p, a functional homologue of human seipin, regulates the size of lipid droplets in yeast. *The Journal of cell biology* **180**, 473-482

75. Fei, W., Du, X., and Yang, H. (2011) Seipin, adipogenesis and lipid droplets. *Trends in endocrinology and metabolism: TEM* **22**, 204-210

76. Tontonoz, P., and Spiegelman, B. M. (2008) Fat and beyond: the diverse biology of PPARgamma. *Annual review of biochemistry* **77**, 289-312

77. Stapleton, C. M., Mashek, D. G., Wang, S., Nagle, C. A., Cline, G. W., Thuillier, P., Leesnitzer, L. M., Li, L. O., Stimmel, J. B., Shulman, G. I., and Coleman, R. A. (2011) Lysophosphatidic acid activates peroxisome proliferator activated receptor-gamma in CHO cells that over-express glycerol 3-phosphate acyltransferase-1. *PloS one* **6**, e18932

78. Hammond, L. E., Gallagher, P. A., Wang, S., Hiller, S., Kluckman, K. D., Posey-Marcos, E. L., Maeda, N., and Coleman, R. A. (2002) Mitochondrial Glycerol-3-Phosphate Acyltransferase-Deficient Mice Have Reduced Weight and Liver Triacylglycerol Content and Altered Glycerolipid Fatty Acid Composition. *Molecular and Cellular Biology* **22**, 8204-8214

79. Wang, S., Lee, D. P., Gong, N., Schwerbrock, N. M., Mashek, D. G., Gonzalez-Baro, M. R., Stapleton, C., Li, L. O., Lewin, T. M., and Coleman, R. A. (2007) Cloning and functional characterization of a novel mitochondrial N-ethylmaleimide-sensitive glycerol-3-phosphate acyltransferase (GPAT2). *Archives of biochemistry and biophysics* **465**, 347-358

80. Pellon-Maison, M., Montanaro, M. A., Coleman, R. A., and Gonzalez-Baro, M. R. (2007) Mitochondrial glycerol-3-P acyltransferase 1 is most active in outer

mitochondrial membrane but not in mitochondrial associated vesicles (MAV). *Biochimica et biophysica acta* **1771**, 830-838

81. Horton, J. D., Goldstein, J. L., and Brown, M. S. (2002) SREBPs: activators of the complete program of cholesterol and fatty acid synthesis in the liver. *The Journal of clinical investigation* **109**, 1125-1131

82. Moon, Y. A., Liang, G., Xie, X., Frank-Kamenetsky, M., Fitzgerald, K., Koteliansky, V., Brown, M. S., Goldstein, J. L., and Horton, J. D. (2012) The Scap/SREBP pathway is essential for developing diabetic fatty liver and carbohydrate-induced hypertriglyceridemia in animals. *Cell metabolism* **15**, 240-246

83. Chen, Y. Q., Kuo, M. S., Li, S., Bui, H. H., Peake, D. A., Sanders, P. E., Thibodeaux, S. J., Chu, S., Qian, Y. W., Zhao, Y., Bredt, D. S., Moller, D. E., Konrad, R. J., Beigneux, A. P., Young, S. G., and Cao, G. (2008) AGPAT6 is a novel microsomal glycerol-3-phosphate acyltransferase. *The Journal of biological chemistry* **283**, 10048-10057

84. Folch, J., Lees, M., and Stanley, G. H. S. (1957) A simple method for the isolation and purification of total lipides from animal tissues. *J. Biol. Chem.* **226**, 497-

85. An, J., Muoio, D. M., Shiota, M., Fujimoto, Y., Cline, G. W., Shulman, G. I., Koves, T. R., Stevens, R., Millington, D. S., and Newgard, C. B. (2004) Hepatic expression of malonyl-CoA decarboxylase reverses muscle, liver and whole-animal insulin resistance. *Nat. Med.* **10**, 268-274

86. McDevitt, R. M., Bott, S. J., Harding, M., Coward, W. A., Bluck, L. J., and Prentice, A. M. (2001) De novo lipogenesis during controlled overfeeding with sucrose or glucose in lean and obese women. *The American journal of clinical nutrition* **74**, 737-746

87. Harada, N., Hara, S., Yoshida, M., Zenitani, T., Mawatari, K., Nakano, M., Takahashi, A., Hosaka, T., Yoshimoto, K., and Nakaya, Y. (2007) Molecular cloning of a murine glycerol-3-phosphate acyltransferase-like protein 1 (xGPAT1). *Molecular and cellular biochemistry* **297**, 41-51

88. Lu, B., Jiang, Y. J., Kim, P., Moser, A., Elias, P. M., Grunfeld, C., and Feingold, K. R. (2010) Expression and regulation of GPAT isoforms in cultured human keratinocytes and rodent epidermis. *Journal of lipid research* **51**, 3207-3216

89. Kelker, H. C., and Pullman, M. E. (1979) Phospholipid requirement of acyl coenzyme A:sn-glycerol-3-phosphate acyltransferase from rat liver mitochondria. *The Journal of biological chemistry* **254**, 5364-5371

90. Monroy, G., Kelker, H. C., and Pullman, M. E. (1973) Partial purification and properties of an acyl coenzyme A:sn-glycerol 3-phosphate acyltransferase from rat liver mitochondria. *The Journal of biological chemistry* **248**, 2845-2852

91. Yet, S.-F., Moon, Y. K., and Sul, H. S. (1995) Purification and reconstitution of murine mitochondrial glycerol-3-phosphate acyltransferase. Functional expression in baculovirus-infected insect cells. *Biochemistry* **34**, 7303-7310

92. Qi, J., Lang, W., Geisler, J. G., Wang, P., Petrounia, I., Mai, S., Smith, C., Askari, H., Struble, G. T., Williams, R., Bhanot, S., Monia, B. P., Bayoumy, S., Grant, E., Caldwell, G. W., Todd, M. J., Liang, Y., Gaul, M. D., Demarest, K. T., and Connelly, M. A. (2012) The use of stable isotope-labeled glycerol and oleic acid to differentiate the hepatic functions of DGAT1 and -2. *Journal of lipid research* **53**, 1106-1116

93. Timlin, M. T., Barrows, B. R., and Parks, E. J. (2005) Increased dietary substrate delivery alters hepatic fatty acid recycling in healthy men. *Diabetes* **54**, 2694-2701

94. Parks, E. J., Skokan, L. E., Timlin, M. T., and Dingfelder, C. S. (2008) Dietary sugars stimulate fatty acid synthesis in adults. *The Journal of nutrition* **138**, 1039-1046

95. Lewin, T. M., de Jong, H., Schwerbrock, N. J., Hammond, L. E., Watkins, S. M., Combs, T. P., and Coleman, R. A. (2008) Mice deficient in mitochondrial glycerol-3-phosphate acyltransferase-1 have diminished myocardial triacylglycerol accumulation during lipogenic diet and altered phospholipid fatty acid composition. *Biochimica et biophysica acta* **1781**, 352-358

96. Aoki, N., Yamaguchi, Y., Ohira, S., and Matsuda, T. (1999) High fat feeding of lactating mice causing a drastic reduction in fat and energy content in milk without affecting the apparent growth of their pups and the production of major milk fat globule membrane components MFG-E8 and butyrophilin. *Bioscience, biotechnology, and biochemistry* **63**, 1749-1755

97. Cannon, B., and Nedergaard, J. (2004) Brown adipose tissue: function and physiological significance. *Physiological reviews* **84**, 277-359

98. Cannon, B., and Nedergaard, J. (2010) Metabolic consequences of the presence or absence of the thermogenic capacity of brown adipose tissue in mice (and probably in humans). *International journal of obesity* **34 Suppl 1**, S7-16

99. Lindberg, O., Prusiner, S. B., Cannon, B., Ching, T. M., and Eisenhardt, R. H. (1970) Metabolic control in isolated brown fat cells. *Lipids* **5**, 204-209

100. Matthias, A., Ohlson, K. B., Fredriksson, J. M., Jacobsson, A., Nedergaard, J., and Cannon, B. (2000) Thermogenic responses in brown fat cells are fully UCP1-dependent. UCP2 or UCP3 do not substitute for UCP1 in adrenergically or fatty scid-induced thermogenesis. *J. Biol. Chem.* **275**, 25073-25081

101. Klingenberg, M., Echtay, K. S., Bienengraeber, M., Winkler, E., and Huang, S. G. (1999) Structure-function relationship in UCP1. *International journal of obesity and related metabolic disorders : journal of the International Association for the Study of Obesity* **23 Suppl 6**, S24-29

102. Khedoe, P. P., Hoeke, G., Kooijman, S., Dijk, W., Buijs, J. T., Kersten, S., Havekes, L. M., Hiemstra, P. S., Berbee, J. F., Boon, M. R., and Rensen, P. C. (2015) Brown adipose tissue takes up plasma triglycerides mostly after lipolysis. *J. Lipid Res.* **56**, 51-59

103. Bartelt, A., Bruns, O. T., Reimer, R., Hohenberg, H., Ittrich, H., Peldschus, K., Kaul, M. G., Tromsdorf, U. I., Weller, H., Waurisch, C., Eychmuller, A., Gordts, P. L., Rinninger, F., Bruegelmann, K., Freund, B., Nielsen, P., Merkel, M., and Heeren, J. (2011) Brown adipose tissue activity controls triglyceride clearance. *Nat. Med.* **17**, 200-205

104. Zechner, R., Zimmermann, R., Eichmann, T. O., Kohlwein, S. D., Haemmerle, G., Lass, A., and Madeo, F. (2012) FAT SIGNALS--lipases and lipolysis in lipid metabolism and signaling. *Cell Metab.* **15**, 279-291

105. Mottillo, E. P., Bloch, A. E., Leff, T., and Granneman, J. G. (2012) Lipolytic products activate peroxisome proliferator-activated receptor (PPAR) alpha and delta in brown adipocytes to match fatty acid oxidation with supply. *J. Biol. Chem.* **287**, 25038-25048

106. Saddik, M., and Lopaschuk, G. D. (1991) Myocardial triglyceride turnover and contribution to energy substrate utilization in isolated working rat hearts. *J. Biol. Chem.* **266**, 8162-8170.

107. Wendel, A. A., Cooper, D. E., Ilkayeva, O. R., Muoio, D. M., and Coleman, R. A. (2013) Glycerol-3-phosphate acyltransferase (GPAT)-1, but not GPAT4, incorporates newly synthesized fatty acids into triacylglycerol and diminishes fatty acid oxidation. *J. Biol. Chem.* **288**, 27299-27306

108. Fromme, T., and Klingenspor, M. (2011) Uncoupling protein 1 expression and high-fat diets. *American journal of physiology. Regulatory, integrative and comparative physiology* **300**, R1-8

109. Lewin, T. M., Schwerbrock, N. M., Lee, D. P., and Coleman, R. A. (2004) Identification of a new glycerol-3-phosphate acyltransferase isoenzyme, mtGPAT2, in mitochondria. *J. Biol. Chem.* **279**, 13488-13495

110. Drover, V. A., Ajmal, M., Nassir, F., Davidson, N. O., Nauli, A. M., Sahoo, D., Tso, P., and Abumrad, N. A. (2005) CD36 deficiency impairs intestinal lipid secretion and clearance of chylomicrons from the blood. *J. Clin. Invest.* **115**, 1290-1297

111. Folch, J., Lees, M., and Sloane Stanley, G. H. (1957) A simple method for the isolation and purification of total lipides from animal tissues. *J. Biol. Chem.* **226**, 497-509

112. Buhman, K. K., Smith, S. J., Stone, S. J., Repa, J. J., Wong, J. S., Knapp, F. F., Jr., Burri, B. J., Hamilton, R. L., Abumrad, N. A., and Farese, R. V., Jr. (2002) DGAT1 is not essential for intestinal triacylglycerol absorption or chylomicron synthesis. *J. Biol. Chem.* **277**, 25474-25479

113. Ellis, J. M., Li, L. O., Wu, P. C., Koves, T. R., Ilkayeva, O., Stevens, R. D., Watkins, S. M., Muoio, D. M., and Coleman, R. A. (2010) Adipose acyl-CoA synthetase-1 directs fatty acids toward beta-oxidation and is required for cold thermogenesis. *Cell Metab.* **12**, 53-64

114. Irie, Y., Asano, A., Canas, X., Nikami, H., Aizawa, S., and Saito, M. (1999) Immortal brown adipocytes from p53-knockout mice: differentiation and expression of uncoupling proteins. *Biochemical and biophysical research communications* **255**, 221-225

115. Magre, J., Delepine, M., Khallouf, E., Gedde-Dahl, T., Jr., Van Maldergem, L., Sobel, E., Papp, J., Meier, M., Megarbane, A., Bachy, A., Verloes, A., d'Abronzo, F. H., Seemanova, E., Assan, R., Baudic, N., Bourut, C., Czernichow, P., Huet, F., Grigorescu, F., de Kerdanet, M., Lacombe, D., Labrune, P., Lanza, M., Loret,

H., Matsuda, F., Navarro, J., Nivelon-Chevalier, A., Polak, M., Robert, J. J., Tric, P., Tubiana-Rufi, N., Vigouroux, C., Weissenbach, J., Savasta, S., Maassen, J. A., Trygstad, O., Bogalho, P., Freitas, P., Medina, J. L., Bonnicci, F., Joffe, B. I., Loyson, G., Panz, V. R., Raal, F. J., O'Rahilly, S., Stephenson, T., Kahn, C. R., Lathrop, M., and Capeau, J. (2001) Identification of the gene altered in Berardinelli-Seip congenital lipodystrophy on chromosome 11q13. *Nature genetics* **28**, 365-370

116. Cartwright, B. R., and Goodman, J. M. (2012) Seipin: from human disease to molecular mechanism. *Journal of lipid research* **53**, 1042-1055

117. Lundin, C., Nordstrom, R., Wagner, K., Windpassinger, C., Andersson, H., von Heijne, G., and Nilsson, I. (2006) Membrane topology of the human seipin protein. *FEBS Lett* **580**, 2281-2284

118. Cui, X., Wang, Y., Tang, Y., Liu, Y., Zhao, L., Deng, J., Xu, G., Peng, X., Ju, S., Liu, G., and Yang, H. (2011) Seipin ablation in mice results in severe generalized lipodystrophy. *Human molecular genetics* **20**, 3022-3030

119. Chen, W., Chang, B., Saha, P., Hartig, S. M., Li, L., Reddy, V. T., Yang, Y., Yechoor, V., Mancini, M. A., and Chan, L. (2012) Berardinelli-seip congenital lipodystrophy 2/seipin is a cell-autonomous regulator of lipolysis essential for adipocyte differentiation. *Mol Cell Biol* **32**, 1099-1111

120. Prieur, X., Dollet, L., Takahashi, M., Nemani, M., Pillot, B., Le May, C., Mounier, C., Takigawa-Imamura, H., Zelenika, D., Matsuda, F., Feve, B., Capeau, J., Lathrop, M., Costet, P., Cariou, B., and Magre, J. (2013) Thiazolidinediones partially reverse the metabolic disturbances observed in Bscl2/seipin-deficient mice. *Diabetologia* **56**, 1813-1825

121. Tian, Y., Bi, J., Shui, G., Liu, Z., Xiang, Y., Liu, Y., Wenk, M. R., Yang, H., and Huang, X. (2011) Tissue-autonomous function of Drosophila seipin in preventing ectopic lipid droplet formation. *PLoS genetics* **7**, e1001364

122. Ohki, S., and Zschornig, O. (1993) Ion-induced fusion of phosphatidic acid vesicles and correlation between surface hydrophobicity and membrane fusion. *Chemistry and physics of lipids* **65**, 193-204

123. Rothbauer, U., Zolghadr, K., Muyldermans, S., Schepers, A., Cardoso, M. C., and Leonhardt, H. (2008) A versatile nanotrap for biochemical and functional

studies with fluorescent fusion proteins. *Molecular & cellular proteomics : MCP* **7**, 282-289

124. Wang, C. W., Miao, Y. H., and Chang, Y. S. (2014) Control of lipid droplet size in budding yeast requires the collaboration between Fld1 and Ldb16. *Journal of cell science* **127**, 1214-1228

125. Polokoff, M. A., and Bell, R. M. (1978) Limited palmitoyl-CoA penetration into microsomal vesicles as evidenced by a highly latent ethanol acyltransferase activity. *The Journal of biological chemistry* **253**, 7173-7178

126. Chen, W., Yechoor, V. K., Chang, B. H., Li, M. V., March, K. L., and Chan, L. (2009) The human lipodystrophy gene product Berardinelli-Seip congenital lipodystrophy 2/seipin plays a key role in adipocyte differentiation. *Endocrinology* **150**, 4552-4561

127. Murphy, R. C., James, P. F., McAnoy, A. M., Krank, J., Duchoslav, E., and Barkley, R. M. (2007) Detection of the abundance of diacylglycerol and triacylglycerol molecular species in cells using neutral loss mass spectrometry. *Anal Biochem* **366**, 59-70

128. Ross, S. A., Song, X., Burney, M. W., Kasai, Y., and Orlicky, D. J. (2003) Efficient adenovirus transduction of 3T3-L1 adipocytes stably expressing coxsackie-adenovirus receptor. *Biochemical and biophysical research communications* **302**, 354-358

129. Jin, Y., McFie, P. J., Banman, S. L., Brandt, C., and Stone, S. J. (2014) Diacylglycerol acyltransferase-2 (DGAT2) and monoacylglycerol acyltransferase-2 (MGAT2) interact to promote triacylglycerol synthesis. *The Journal of biological chemistry* **289**, 28237-28248

130. Zhang, J., Xu, D., Nie, J., Cao, J., Zhai, Y., Tong, D., and Shi, Y. (2014) Monoacylglycerol acyltransferase-2 is a tetrameric enzyme that selectively heterodimerizes with diacylglycerol acyltransferase-1. *The Journal of biological chemistry* **289**, 10909-10918

131. Vancura, A., and Haldar, D. (1992) Regulation of mitochondrial and microsomal phospholipid synthesis by liver fatty acid-binding protein. *The Journal of biological chemistry* **267**, 14353-14359

132. Darnley, A. C., Carpenter, C. A., and Saggerson, E. D. (1988) Changes in activities of some enzymes of glycerolipid synthesis in brown adipose tissue of cold-acclimated rats. *The Biochemical journal* **253**, 351-355

133. Mitchell, J. R., and Saggerson, E. D. (1991) Activities of enzymes of glycerolipid synthesis in brown adipose tissue after treatment of rats with the adrenergic agonists BRL 26830A and phenylephrine, after exposure to cold and in streptozotocin-diabetes. *The Biochemical journal* **277 (Pt 3)**, 665-669

134. Lands, W. E., and Hart, P. (1964) Metabolism of Glycerolipids: V. Metabolism of Phosphatidic Acid. *Journal of lipid research* **5**, 81-87